UiT
THE ARCTIC
UNIVERSITY
OF NORWAY

Faculty of Science and Technology

Department of Geology

Geological controlling parameters on seismic imaging of igneous intrusions on Svalbard

—

Ruud Toonen

Master thesis in marine geology and marine geophysics
May 2017

UNIVERSITY OF TROMSØ

Geological controlling parameters on seismic imaging of igneous intrusions on Svalbard

Ruud Toonen

Master thesis in Marine Geology and Marine Geophysics

May 2017

ARCEx
Research Centre for
Arctic Petroleum Exploration

Abstract

Imaging and mapping igneous intrusions such a sills and dykes has been one of the challenges in recent years. However, igneous intrusions in seismic data have properties that make them good targets for visualization, such as high amplitude and sophisticated shapes. 3D visualization methods are especially well suited for sill reflections. One of the main limitations of tying offshore seismic data to onshore observations and vice versa is a matter of scale. Igneous sills that are exposed onshore might be too thin to consistently map in seismic data, whereas features that are visible in seismic surveys offshore might be too long to be able to view onshore. Understanding the geometry of these intrusions may provide key insights regarding emplacement processes, geological history, and potential for hydrocarbon exploration. The research is based on photogrammetric research, analysis of intrusions and their host rocks, and building 3-D models to use for synthetic seismic generation. Well analysis is also required in order to estimate the properties used for these synthetic seismics. Five different geometries have been tested using different lithologies for the host rocks. Sandstone/shale, organic rich shale, clean sandstone and Paleozoic carbonates. The test cases using organic shale show a high impedance contrast, where the cases using carbonates show a very low contrast, due to the similarities of the Vp and Vs with the doleritic intrusions. The sandstone/shale and shale lithologies have more contrast than the carbonates, but less than the organic rich shale. Most shapes show up fairly well on the synthetic data, however sub-vertical geometries have low visibility regardless of the lithology. There are some seismic properties that are hard to simulate using synthetic seismic, such as seismic attenuation, variance of properties within a lithology, and the presence of other geological features. Regardless, the use of synthetic seismic data may help bridge the data integration gap between onshore and offshore data.

Acknowledgements

I would like to use this opportunity to thank some people who supported me throughout writing this thesis. First of all, I would like to thank my supervisor Kim Senger for the opportunity to work on this project, for support throughout writing this master thesis, and especially for being as patient with me as he was. It must have been hard sometimes. I would also like to thank him and Mark Joseph Mulrooney for letting me use the data they collected during fieldwork. I would also like to thank my supervisor at UiT, Iver Martens for the support he offered. The ARCEx institute also gets my thanks, for providing me with this project, and for providing for me the resources to finish it. The NORSAR software support team deserves a special mention, as they helped me out using their software time and time again. Also, a special thanks to my parents, I would not have been able to finish this project without their support throughout my 2 years of study in Tromsø. It must be hard for them that I live so far away for a long time, but their support never wavered. Last but not least, I would like to thank Anna for supporting me, and being there when I got home after a long day working at university.

Ruud Toonen

Tromsø, May 2017

Contents

List of Figures

List of Tables

1 Introduction

In recent times, interest in the presence of geological formations such as growth faults, igneous intrusions, clinoforms and channels the sedimentary basins has increased. A plausible reason for this is the increased activity and presence of the oil industry in many regions in the world, including the Arctic region. Igneous intrusions have profound effects on the petroleum system, which is why researchers are interested in mapping these intrusions, both onshore and offshore. Imaging and mapping igneous intrusions such a sills and dykes has been one of the challenges in recent years, and 3-D seismic reflection data plays a key role with this challenge. Igneous intrusions are, however, good imaging targets and have some deterministic features that make it possible to interpret them with high confidence in many basins (Planke et al., 2014). A combination of methods is commonly used for interpretation of sill complexes in volcanic basins (Planke et al. 2005): horizon and attribute mapping, interpretation of sill reflections, 3D voxel visualization, seismic facies analyses, and integration with well, geological and other geophysical data. The most characteristic features of sill reflections are the high amplitudes, and the shape, which can be saucer-shaped, transgressive, or different. 3D seismic data is important for increasing the confidence of the seismic interpretation. 3D visualization methods are well suited for sill reflections, as their sophisticated shapes and high amplitude has good visibility in 3D-seismic data. Detailed sill interpretation, attribute analyses, and volume rendering techniques have particularly been applied to 3D seismic data in the Northeast Atlantic to gain a better understanding of sill geometries and emplacement processes (Planke et al., 2014)

One of the main limitations of trying to tie offshore seismic data to onshore observations and vice versa is the scale on which these intrusions occur. Igneous sills that are exposed onshore can be kilometers wide, and somewhere between 1 to 100 meters thick (Figure 1.1). While this scale is perfect for onshore observation of outcrops, in offshore seismic data such features would be near the limits of seismic resolution. In the same way, the opposite might also be true, where some feature can continue for tens of kilometers horizontally in the seismic data, the onshore outcrops might not show this due to a feature dipping below the surface. Many geological features are too large to and lithologically indistinct to view onshore. Figure 1.1 shows the scale on which observation of features is possible.

An understanding of the geometry of these volcanic intrusions might provide key insights concerning different topics. Mapping the extent, geometry and structure of these intrusions might provide more information on the emplacement processes and the geological history of a certain formation. It might also prove interesting for commercial companies, such as the oil industry. Intrusions like volcanic sills or dykes may have a profound impact on the dynamics within a basin, and the related petroleum system. These can be either positive or negative. Sill placement and hydrothermal activity may cause contact metamorphism on the surrounding rock. This in turn may affect the maturation of the source rock or the porosity of the reservoir rock. It may also form a trap for hydrocarbon reservoirs due to forced folding. Therefore, interesting conclusions might be found with regards to hydrocarbon exploration. Furthermore, it can be used to help constrain models for probably magma emplacement pathways by anisotropy of magnetic susceptibility, it can help investigating geochemical variations within the magmatic system, and reveal the relative chronology of igneous emplacement (Senger et al., 2013).

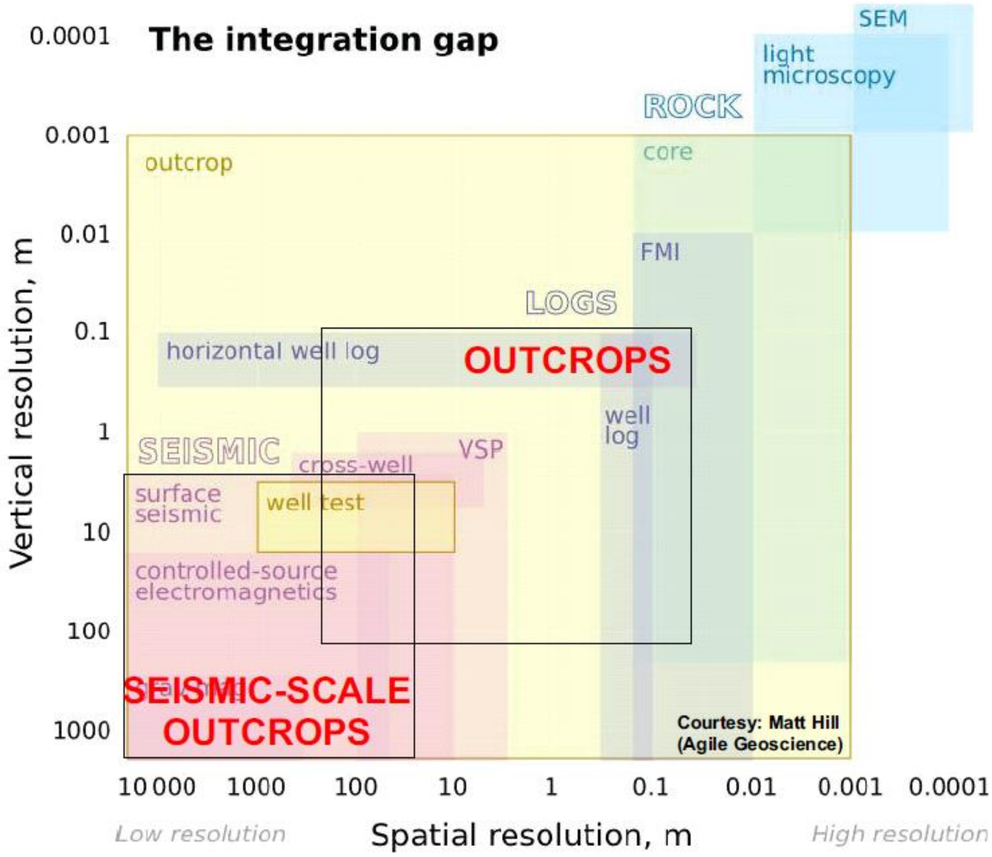

Figure 1.1: The scale on which outcrops can be visible. Onshore outcrops typically have a spatial resolution from 100m to 10 cm, whereas the outcrop has to be between 1000m to 50m to show up on offshore seismic data (Source: https://agilescientific.com/blog/2011/1/5/the-integration-gap.html)

Synthetic seismic modelling can provide a link to understanding the scale, resolution and detail in which onshore sedimentary structures can be visualized, and hence lead to more confident interpretations of seismic data and provide valuable information on survey parameters, potential pit-falls and data limitations (Anell et al., 2016). The focus of this research will be on igneous intrusions within rock formations on Svalbard and in the Barents Sea, and how the geometries of different intrusions (i.e. sills vs dykes) are imaged in different host rocks (i.e. shales, sandstones, carbonates).

For this purpose, synthetic seismic data will be created using the outline of some of the igneous outcrops visible on Svalbard. Different scenarios will be tested in order to collect data on how host rock properties and other factors might affect the imaging of igneous intrusions. The geometries will be constrained using the outcrops viewed in the field.

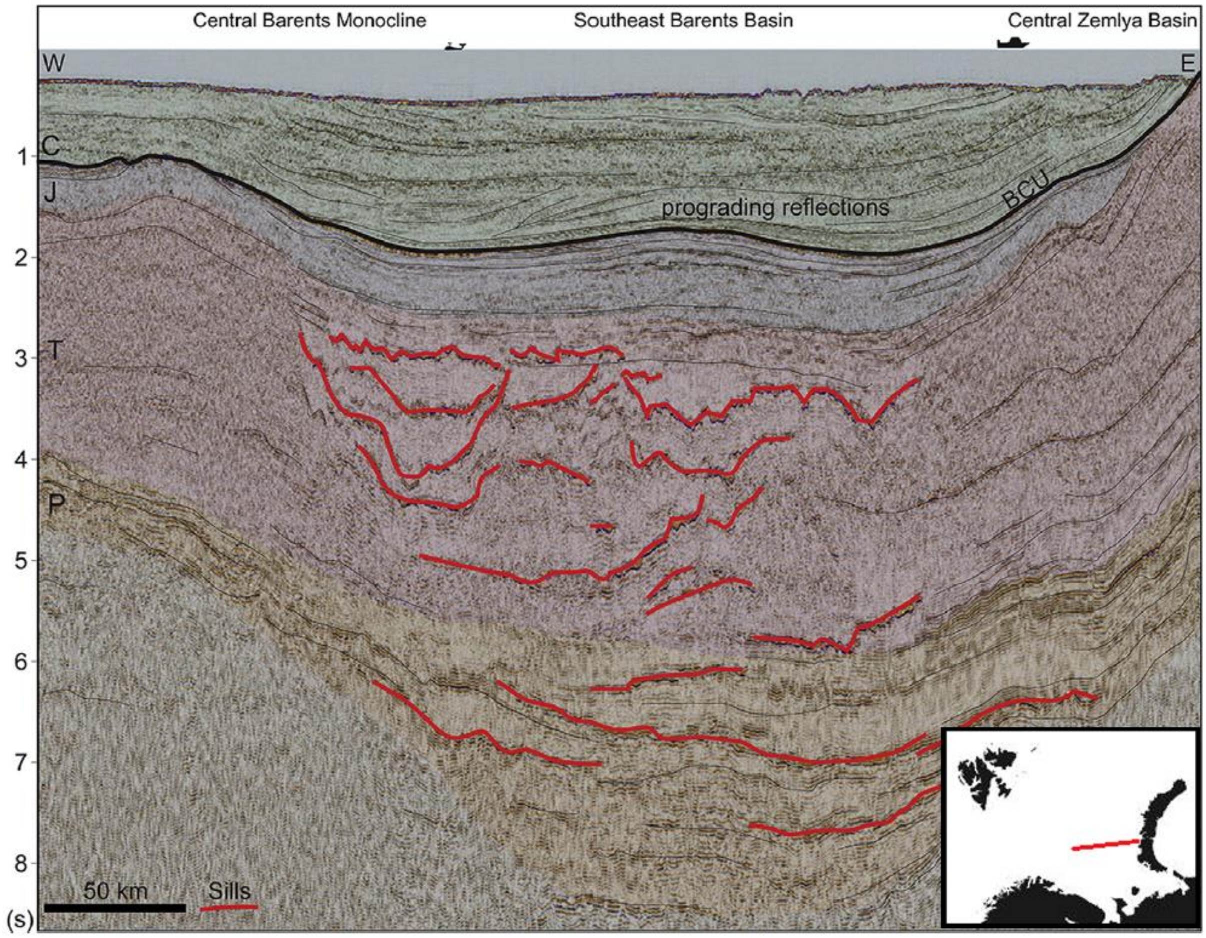

Figure 1.2: Igneous intrusions in offshore data. The reason these intrusions are so well visible on the seismic data is possibly because of the thickness of the intrusions. Field and seismic data suggest that a major port of these sill complexes were formed in a shot time span (Svensen et al., 2004). An explosive release of metamorphic thermogenic methane during this intrusive phase may have caused extraordinary warming during the initial Eocene thermal maximum (Svensen et al., 2004) (Figure modified from Polteau et al., 2016)

The main objective of this research topic concerns the geometry of these sills/intrusions and how they affect the petroleum system.

Three research questions can be derived from the main objective:

- How would different igneous geometries be imaged on seismic data?
- What are the detection thresholds (i.e. size and elastic property contrast) for sills and dykes at typical Barents shelf reservoir depths?
- How do the host rock elastic properties affect the seismic imaging of the igneous intrusions?
- How does the shape of different igneous intrusions affect the petroleum system?

1.1 Study area

Spitsbergen is the largest island of the Svalbard archipelago, and includes the western half of the island group. The study is focused on 3 specific sites around Isfjorden on Spitsbergen. These sites are Tschermakfjellet, Rotundafjellet and Botneheia (Figure 1.3). The reason for choosing these sites is the visibility of the outcrops, scale of the outcrops and data availability. At Tschermakfjellet there are several sills which are very well visible, including a bowl-shaped sill. The main host rock formations are De Geerdalen formation, Tschermakfjellet formation and Botneheia formation. Rotundafjellet was chosen because of the dyke intrusion on the beach next to the mountain. The main host rock formations here are Botneheia formation and Vikinghøyda formation. Botneheia was chosen also because of the high visibility of the sills, which on some locations overlap each other. The main host rock formations on this location are Botneheia formation, Tschermakfjellet formation and De Geerdalen formation.

1.2 Petroleum systems

A working petroleum system includes an active source rock and includes all essential elements and processes needed for oil and gas accumulation to exist. The essential elements which are needed are the source rock, reservoir rock, and seal rock or overburden rock. The processes include formation of traps and the generation, migration and accumulation of petroleum. The source rock generates hydrocarbons, whereas the reservoir rock stores hydrocarbons. The source rock is a sedimentary rock which can be made of limestone or shale. It has the requirements and essential elements of hydrocarbon formation, organic matters which were subjected to high temperatures for a considerable amount of time. The source rock contains the processes that are involved in the formation of hydrocarbons. After their formation, hydrocarbons will migrate upwards until they arrive in a source rock. The source rock is a permeable or porous lithological unit which stores oil and gas after it immigrated from the source rock. Elements will be stored relative to their density, e.g. gas will be the top layer in the reservoir, followed by oil. Below gas and oil the reservoir is filled with water. The seal rock is a lithological unit which has low or no permeability, which causes the hydrocarbons to stay in the reservoir. This can consist of chalk, shale or evaporates. All essential elements must be placed in time and space in such a way that the processes required to form a petroleum accumulation may occur. The petroleum system has a stratigraphic, geographic, and temporal extent (Magoon et al., 1994). The petroleum system can be used as an effective model to investigate discovered hydrocarbon accumulations.

1.3 Effects of igneous intrusions on the petroleum system

Four main effects of intrusives on petroleum systems have been identified. (1) Source rocks can be locally matured due to heat provided by magma intruding into organic rich sediments (Rodriguez Monreal et al., 2009). (2) The host rock can be deformed or uplifted, causing e.g. overlying strata to form "forced folds" or domes which may represent hydrocarbon traps (Polteau et al., 2008; Magee et al., 2014). (3) Migration conduits as well as reservoirs for hydrocarbons may form as a result of intensive fracturing caused by cooling effects and/or tectonic stresses (Polteau et al., 2008; Farooqui et al., 2009; Rodriguez Monreal et al., 2009; Witte et al., 2012). (4) Intrusions may form barriers for fluid flow due to low permeability and thereby they potentially inhibit fluid migration and extraction (Schofield et al., 2015). Figure 1.4 shows some effects that intrusions have on the petroleum system.

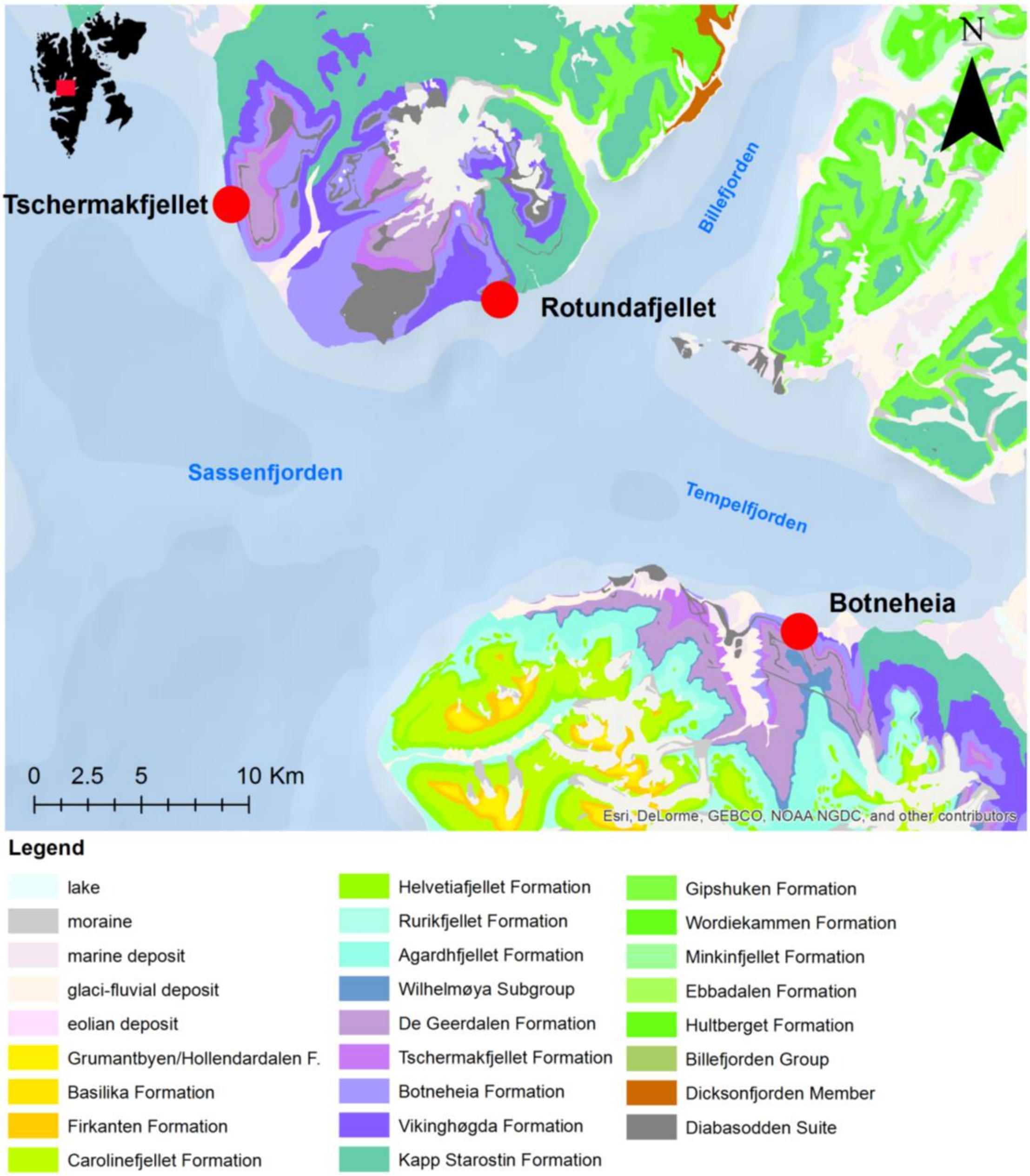

Figure 1.3: The location of the 3 study sites: Tschermakfjellet, Rotundafjellet and Botneheia. Geological data kindly provided by the Norwegian Polar Institute (Dallman, 2015)

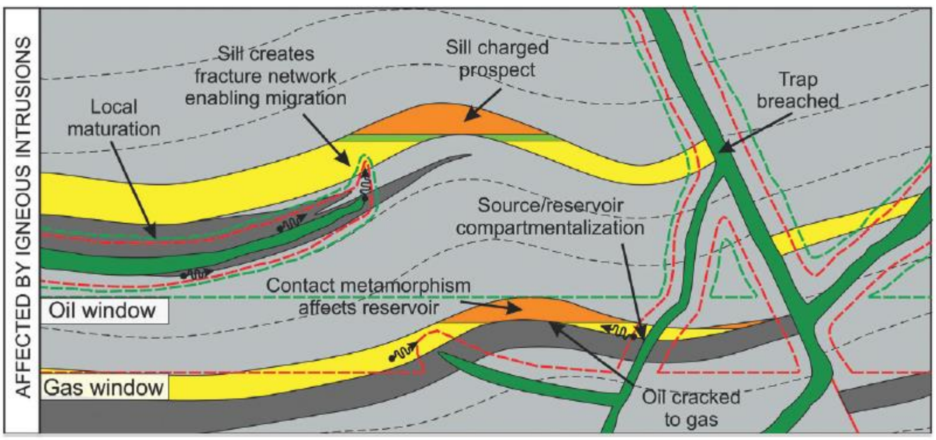

Figure 1.4: Some effects of intrusions on the petroleum system (Senger et al., 2017).

2 Geological setting

Ordovician to Devonian tectonic development was characterized by the formation of NW-trending highs and depressions (Fossum et al. 2001). Ordovician to Devonian strata have not been encountered in the Norwegian part of the Barents Sea. Ordovician marine sediments have been found in Finnmark, however, while some Ordovician limestones are located below the upper Palaeozoic succession on Bjørnøya (Henriksen, 2011). Development of fault-bounded basins commenced on Svalbard and Bjørnøya by the end of Devonian time (Steel & Worsley, 1984). The Barents Sea and Svalbard underwent further rifting during the Carboniferous (Worsley, 2008). The rifts form a fan-shaped array of half-grabens and highs influenced by zones of weakness in the basement, coincident with Caledonian and older trends (Gudlaugsson et al. 1998). Lower Carboniferous strata (Billefjorden Group) comprise of continental siliciclastic deposits to the west, laterally replaced by marine carbonates to the east (Henriksen, 2011). In the central and eastern parts of the western Barents Sea a shift to regional subsidence in the Late Carboniferous happened, coupled with development of a regional sag basin covering the entire Barents Shelf (Gudlaugsson et al. 1998). By the Late Permian, the Uralide Orogeny had closed the marine connection to the south and siliciclastic material eroded from the mountain chain started to fill in the eastern Barents Sea (Henriksen, 2011). A regional unconformity separates the Late Carboniferous– Early Permian strata (Gipsdalen Group) from underlying rocks (Nilsen et al. 1993). The Early Permian palaeogeography consisted of widespread carbonate shelf environments being dissected by a mosaic of shallow basins and highs. During the late Early Permian, the entire Barents Sea saw dramatic changes in the marine circulation systems, with development of a marine seaway between Norway and Greenland causing an abrupt change in oceanic circulation, as cool sea water flowed across the Barents Shelf (Stemmerik et al. 1999; Stemmerik & Worsley 2005).The Triassic was tectonically a quiet period in the western Barents Sea with passive regional subsidence, but minor movements are observed on the Bjarmeland and Finnmark platforms. More active faults are found along the western margin, where the Loppa High was uplifted and eroded in the Early Triassic. (Henriksen, 2011) The Late Triassic–Middle Jurassic succession in the western Barents Sea contains the most important reservoirs in the Norwegian sector and contains four formations (Fruholmen, Tubaen, Nordmela and Stø) currently grouped into the Realgrunnen Subgroup of the Kapp Toscana Group (Henriksen, 2011). Increasing tectonic activity through the Late Jurassic in the western Barents Sea culminated in the Early Cretaceous with the establishment of the present day structural configuration of basins and highs (Gabrielsen et al. 1990). Cenozoic strata are present over significant portions of the Western Barents Sea, but are less widespread than the underlying Cretaceous and older units. Regarding the petroleum system, source rocks ranging in age from Silurian to Cretaceous have been proven in the greater Barents area. Late Permian, Triassic, Late Jurassic and Early Cretaceous marine source rocks are most significant in the Western Barents Sea.

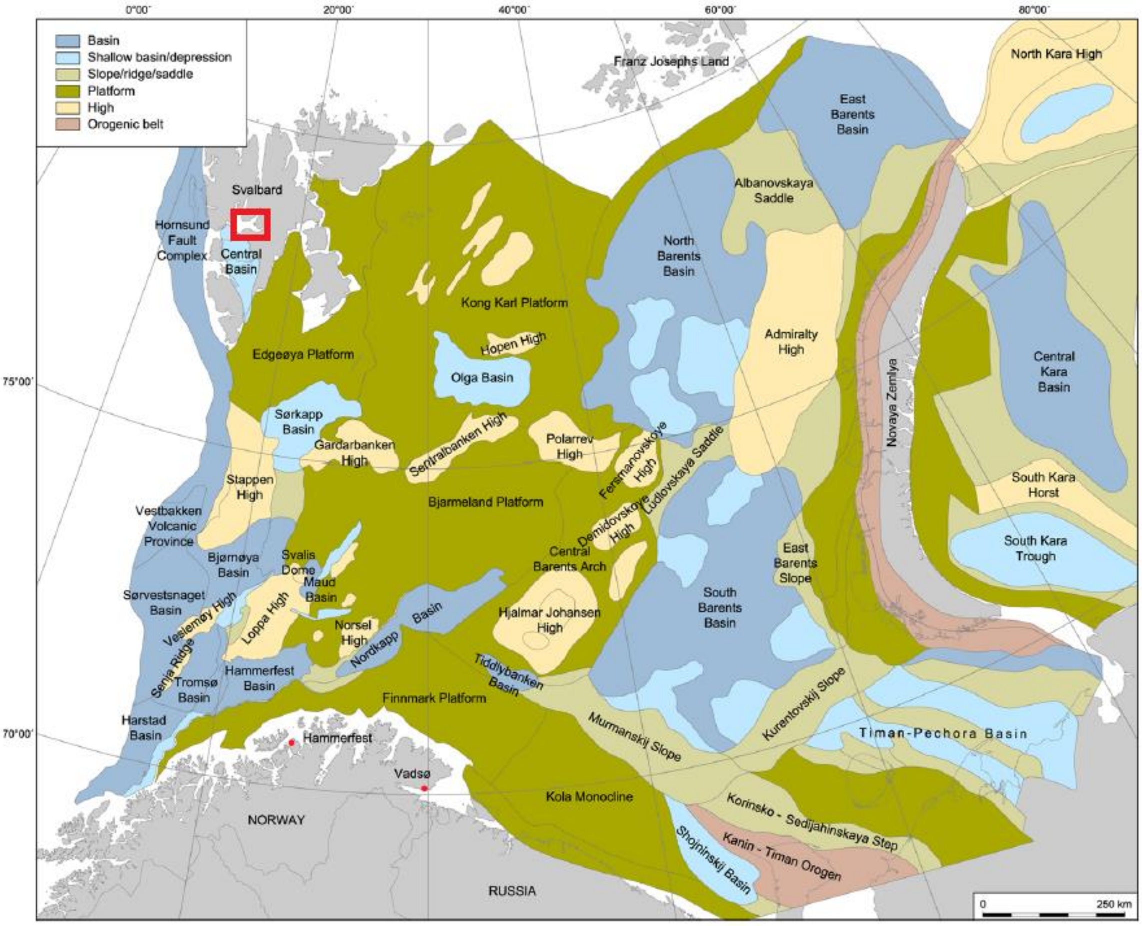

Figure 2.1: The structural elements of the Barents Sea. The red square signifies the study area. Modified from Henriksen et al. (2011).

The Svalbard archipelago contains four large main islands (Spitsbergen, Nordaustlandet, Edgeøya and Barentsøya), and several smaller islands. The Svalbard archipelago, forming the subaerially

exposed north-western margins of the Barents shelf, covers a land area of 63 000 km^2, which is less than 5% of the total area of the Barents Sea, but which displays a comprehensive overview of the geology of the entire region (Steel & Worsley 1984; Worsley et al. 1986; Harland 1997). Its well-exposed Proterozoic–Palaeogene succession serves as an analogue to the hydrocarbon provinces in the Barents Sea (Senger et al., 2013)

Precambrian–Lower Paleozoic basement rocks of Svalbard consist of sediments, metasediments and igneous rocks, ranging in age from the Riphean (1275 Mya) to the Silurian (Worsley, 2008). This succession has a combined maximum thickness of circa 20 km, and is divided into 20 lithostratigraphical groups, also known as the Hecla Hoek. Due to the diversity of groups, a large variety of successions are exposed on the Svalbard islands.

A hypothesis from the late Brian Harland (e.g., Harland & Wright, 1979; Harland, 1997), suggests that Svalbard's basement contains three structural provinces, that through large scale lateral movements were brought together during the Caledonian orogeny. The final phase of the Caledonian deformation on Spitsbergen happened in the Late Devonian, also known as the Svalbardian movements.

The post-Svalbardian evolution of the archipelago can be summed up in five main depositional phases, ranging from the late Devonian to the Neogene. These depositional phases partly reflect the continuing northwards movement of this segment of the Eurasian plate: Svalbard has moved from the equatorial zone in the middle Devonian–early Carboniferous up to its present-day High Arctic latitudes, resulting in significant climatic changes through time (Worsley, 2008). Many tectonic processes have been imposed on the sedimentation on the shelf margins. The compressive Uralide orogeny, the proto-Atlantic rifting, the opening of the Euramerican Basin, and the final opening of the Norwegian-Greenland Sea. The sequence development has been further defined due to regional and local sea-level variations.

The late Devonian to mid-Permian was characterized first by widespread intracratonic rifting, following the late Caledonian Svalbardian compressive movements, and then by the development of an immense post-rift carbonate platform, stretching westwards to present-day Alaska (Worsley, 2008). During the Mid-Carboniferous rifting was occuring across most of Svalbard. This resulted in a number of narrow rift basins, especially in the Billefjorden area. These narrow rift basins were incised into the broader basins formed in the Early Carboniferous. The contrasting geometry of the Early and Mid-Carboniferous basins, as well as the en echelon distribution of the latter, has led to the suggestion that the latter may have resulted from oblique-slip tectonic movements (Steel & Worsley 1984). The Billefjorden Trough developed along the eastern side of the Billefjorden Fault zone between the footwall of the Nordfjorden and the hanging wall of the Ny Friesland Block during this time (Johannessen & Steel, 1992). During the mid-Permian the evaporitic deposition ceased, and shifted to cool-water carbonates, and after that to clastic deposition. This was accompanied by a general decrease of tectonic activity. The Barents Shelf was then affected by highly increased rates in subsidence, as a response to the Uralide orogeny. These subsidence rates became less and less throughout the Triassic, and the area stablilised in the late Triassic to the mid-Jurassic. Consequently, the sedimentation rates in the area rapidly decreased, and extensional tectonism established the basins and platforms that we see today in the mid-late Jurassic. The regional development during the Jurassic-Cretaceous period was dominated by fine clastic deposition, but also included the evolution of the polar Euramerican Basin. On the Northern shelf, northerly uplift was occurring, accompanied by widespread

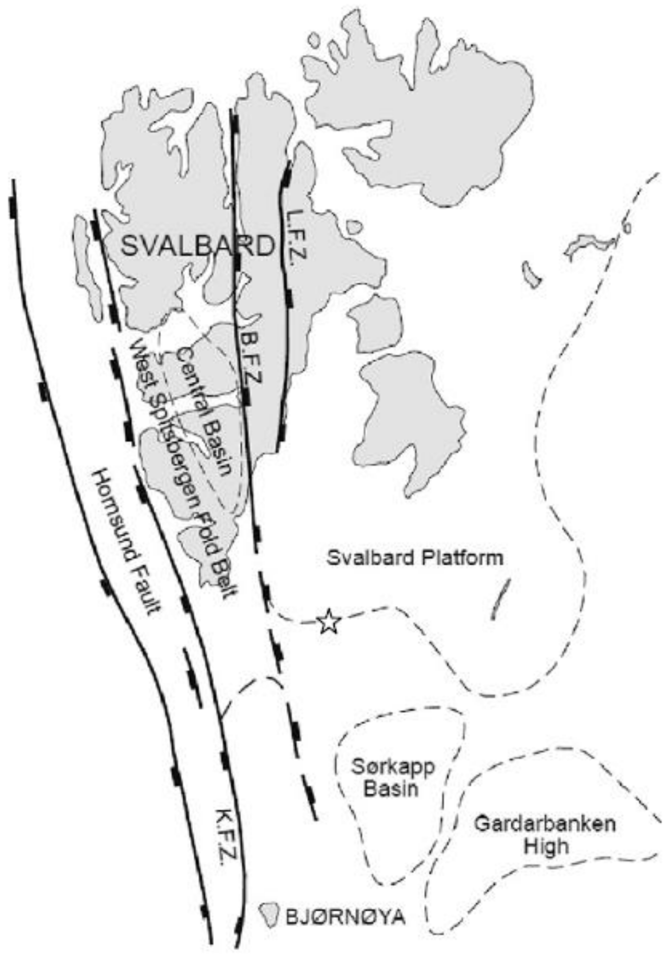

Figure 2.2: Tectonic lineaments over the Svalbard archipelago (Figure from Baelum et al., 2012)

magmatism. Throughout these time periods, Svalbard had steadily moved to the North. It moved through temperate latitudes during the Mesozoic, and was approaching 60°N during the early Cretaceous. During the early Cretaceous many deposits were intruded by the Diabasodden Suite dolerites. The latest Cretaceous and Paleogene were dominated by changing transpressive and transtensional regimes along the western plate suture, before the Eocene/Oligocene break-up and opening of the Norwegian–Greenland Sea (Worsley, 2008). After that, during the Neogene, deposition of clastic wedges from the newly formed western shelf margins occurred, caused by a large-scale depression and uplift which were a result from the repeated stages of glaciation and deglaciation of the shelf from the Miocene onwards.

2.1 Lithostratigraphy

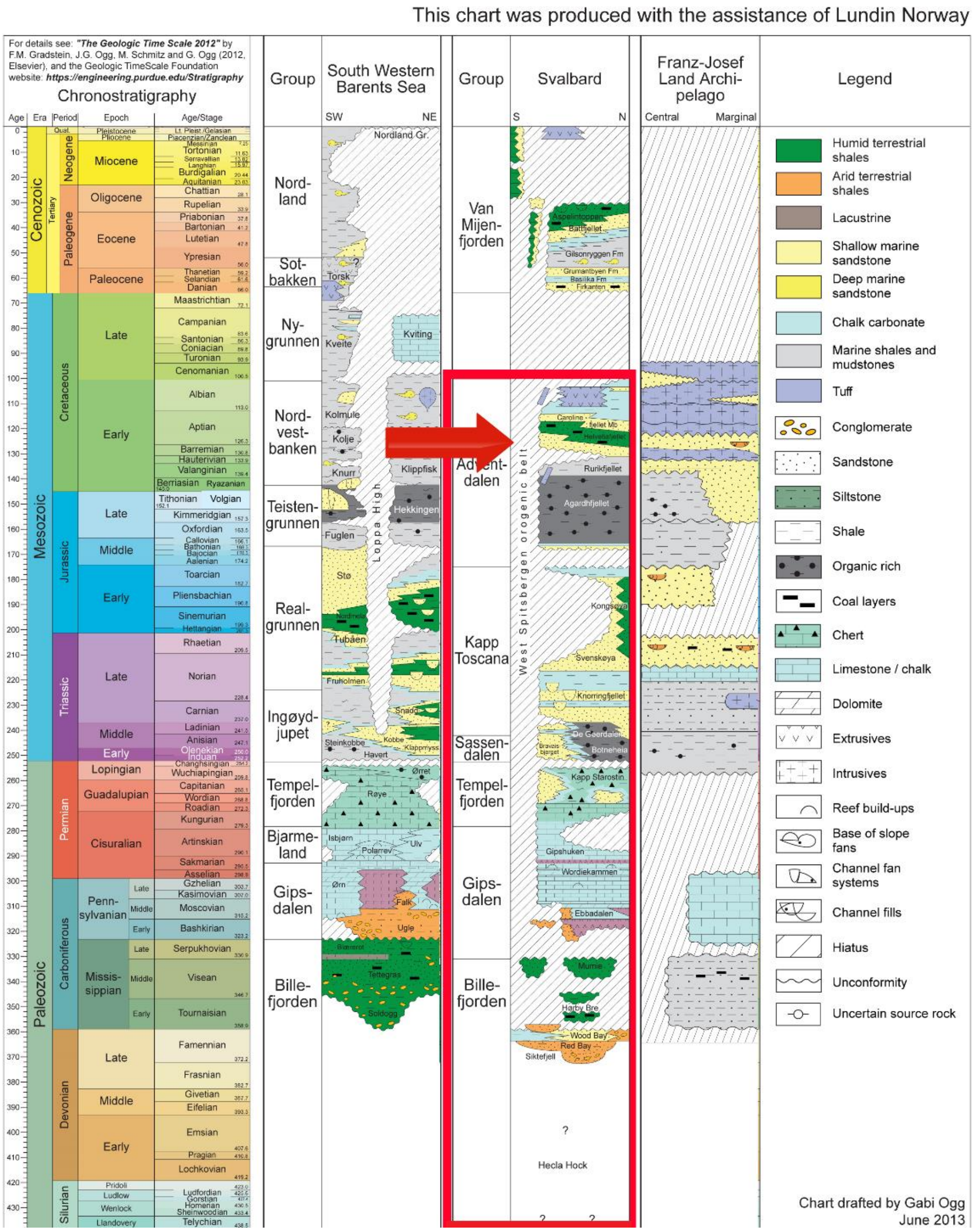

Figure 2.3: Lithostratigraphical map of Svalbard and the Barents Sea. The area marked in red signifies the host rocks in which the diabasodden suite might have intruded. While intrusions can be found in all of these groups, they are less common in the Billefjorden and Adventdalen group. The arrow indicates the timing of the intrusion event. (modified from http://nhm2.uio.no/norlex/, Naturhistorisk museum, Universitet i Oslo)

2.2 Diabasodden Suite dolerites

The dolerites that intruded Svalbard in the late Mesozoic are generally referred to as the Diabasodden Suite. It is named after the locality in northern Nordenskiöld Land. Their black, craggy cliff-like appearance is very distinctive, and they have even been described as the most distinctive Mesozoic rocks (Harland, 1973). The Mesozoic intrusions are distinguishable from other magmatic intrusions on Svalbard geochemically. The composition of the dolerites is fine- to medium-grained, consisting primarily of plagioclase laths with clinopyroxene aggregates (Senger et al., 2014). The intrusion appears in both dykes and sills, and the most occurring form of the intrusion in specific locations is a result of the stress regime in the local host rock (Maher, 2001). Sills are more dominant in the post-Caledonian sedimentary cover, whereas dykes occur more in the highly compressed Caledonian structure. During the development of the West Spitsbergen fold-and-thrust belt, the Mesozoic platform deposits have been tectonically transported up to 20 to 40 km to the east (Senger et al., 2014). Through this event, the exposed dolerite sills were detached from their feeder systems.

The late Mesozoic intrusives occur over a large part of the Svalbard archipelago (Figure 2.5). Two main intrusion centres have been identified: The central Spitsbergen dolerite centre in Inner Isfjorden, and the eastern Svalbard dolerite belt (Nejbert et al., 2011). A rough estimate of the surface area affected by magmatism on Svalbard and its surroundings is approximately 200,000 km2 (Maher, 2001). Technically, the name Diabasodden Suite is only used for the intrusives found on onshore Svalbard, while the intrusives that are found offshore are usually classified as part of the HALIP (High Arctic Large Igneous Province) or BLIP (Barents Sea Large Igneous Province; Polteau et al. 2016). The Diabasodden Suite intrusive complex is often associated with the 'Kong Karls Land lava flows' (Smith et al., 1976). Kong Karls Land is predominantly composed of basaltic lava flows and shallow intrusions which occurred during the Late Mesozoic.

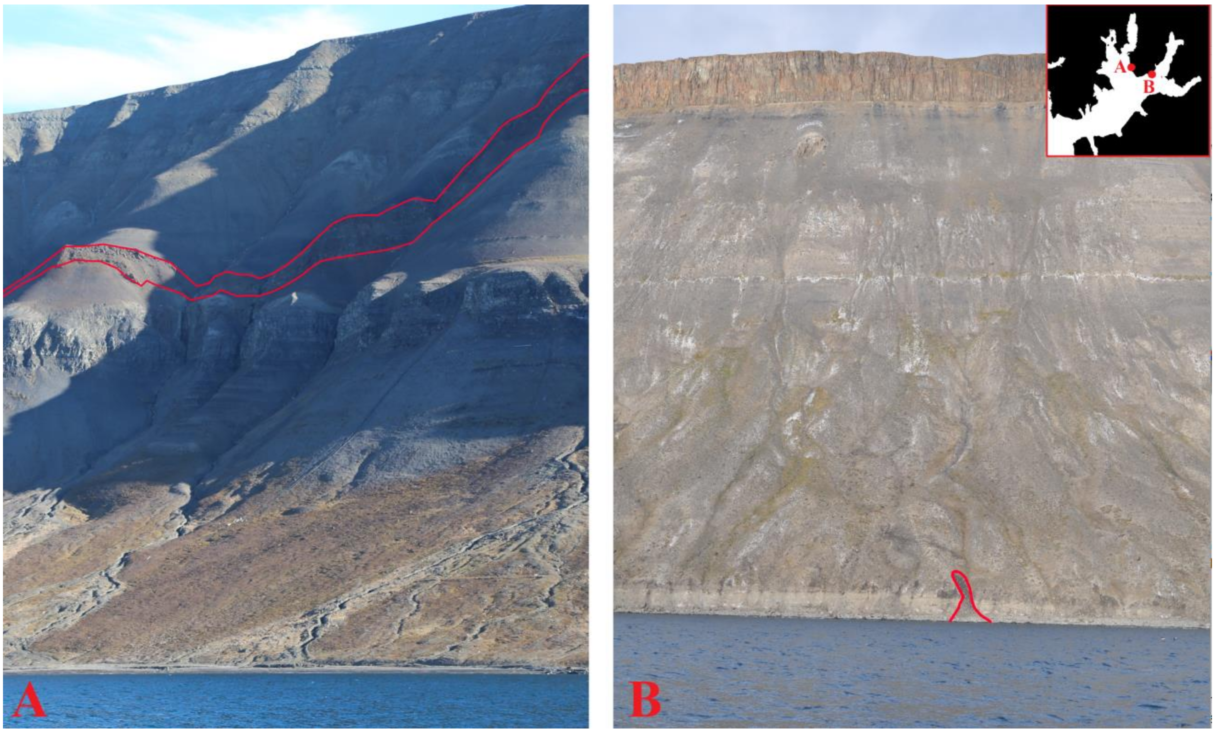

Figure 2.4: A: Two Diabasodden Suite outcrops, with a sill on the left picture (Tschermakfjellet), and an exposed dyke on the right picture (Rotundafjellet). Pictures were made by Mark Mulrooney (left) and Kim Senger (right). The mountain on picture A is approximately 400m high, and the mountain on picture B approximately 275m.

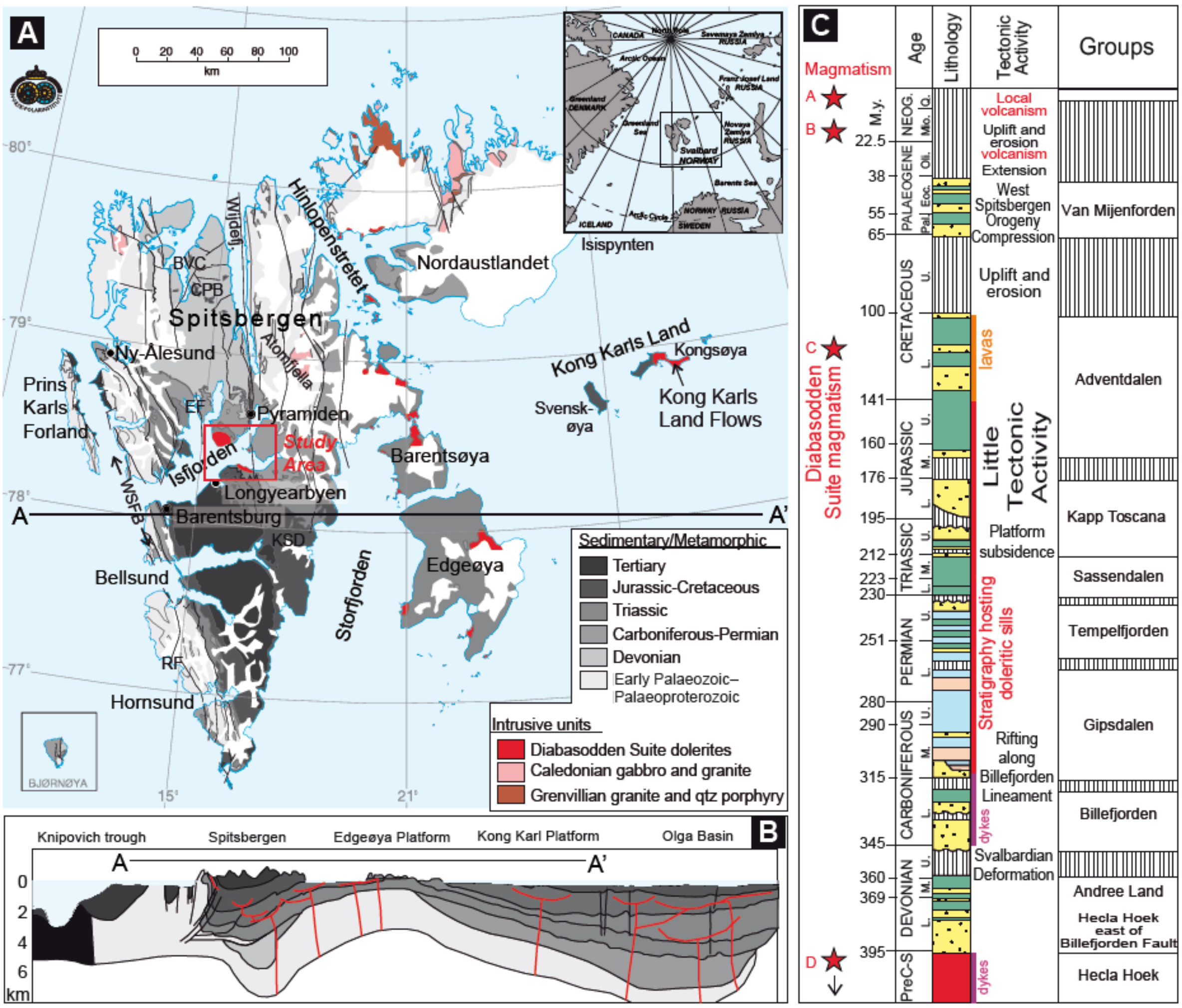

Figure 2.5: A: Geological map of Svalbard, modified from the geological map from the Norwegian Polar institute (Elvevold et al., 2007). The Diabasodden intrusives are highlighted in red. B: Geological cross-section across Svalbard, highlighting the presence of the West Spitsbergen fold-and-thrust belt (WSFB) and associated foreland basin. C: Simplified stratigraphic column of Svalbard, adapted from Nøttvedt et al. (1993), illustrating the timing of Late Mesozoic magmatism and the intruded host rock units. The red stars show separate magmatic events on the Svalbard. Figure from Senger et al. (2013).

3 Methods and data

3.1 Workflow

For the most important analysis of this research, the synthetic seismic analysis, the following workflow is used. Photos of the outcrops are taken during fieldwork. These are processed using photogrammetric software (Agisoft Photoscan Professional 64bit), creating a 3D model. Seismic interpretation of the intrusion is being made in Petrel after that, and this interpretation is the base for the 3D model that will be created of the outcrop geometry. Elastic properties are taken from Barents Sea wireline data, and are fed into the model. The 3D model and the property cubes that are created in this process are used to generate synthetic seismic models in Seisrox (Norsar), using different properties for different lithologies. The workflow is visualized in Figure 3.1.

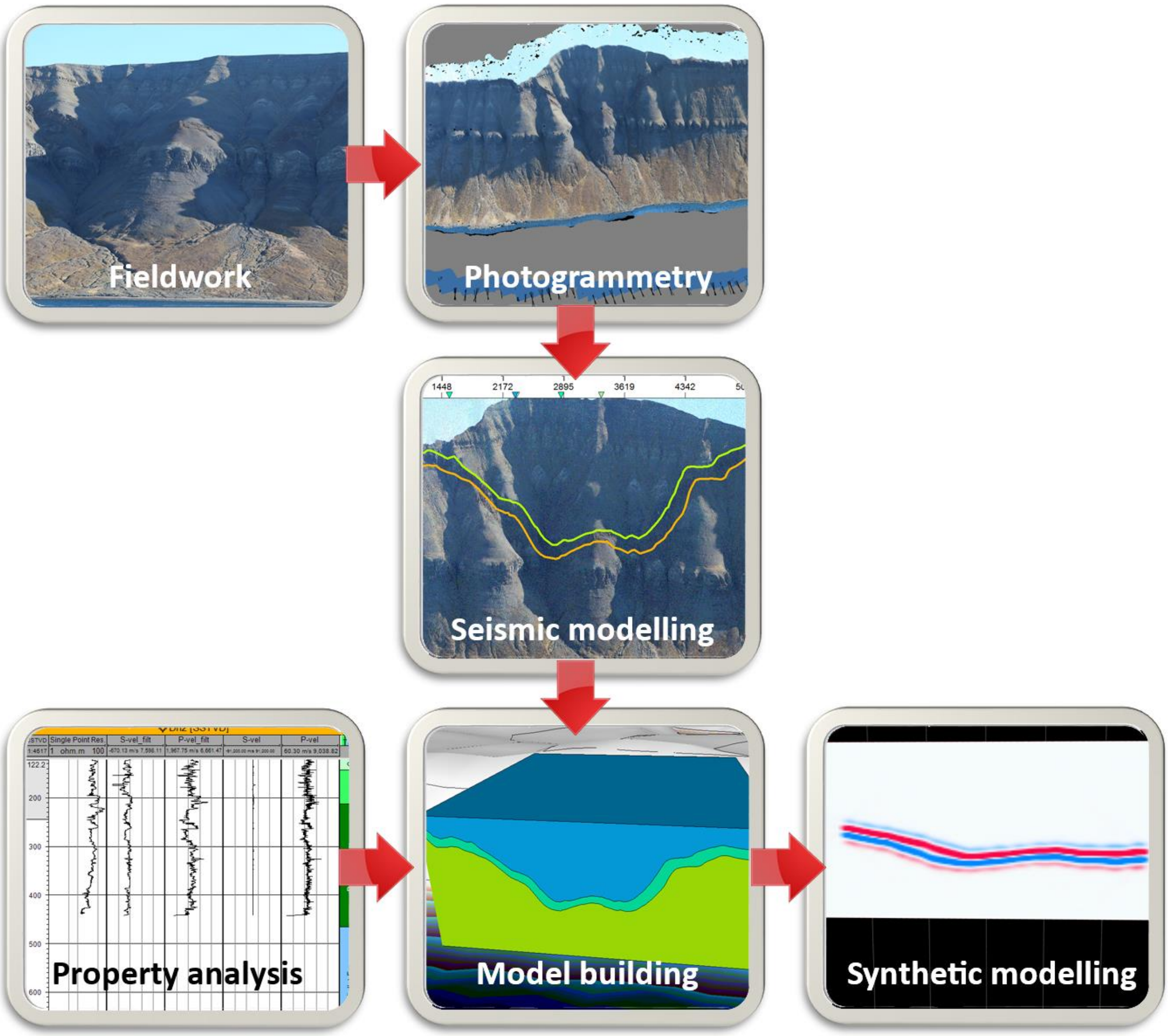

Figure 3.1: Workflow for creating synthetic seismic data.

3.2 Fieldwork

The data used for the photogrammetric analysis was collected during fieldwork by Mark Joseph Mulrooney and Kim Senger by taking photographs of the different igneous outcrops at Tschermakfjellet and Rotundafjellet during August 2016. The camera models used were NIKON D90 and Canon EOS 6D. The pictures were taken from a boat, each a few meters apart. Figure 3.2 shows in which way the pictures were taken relative to the shoreline.

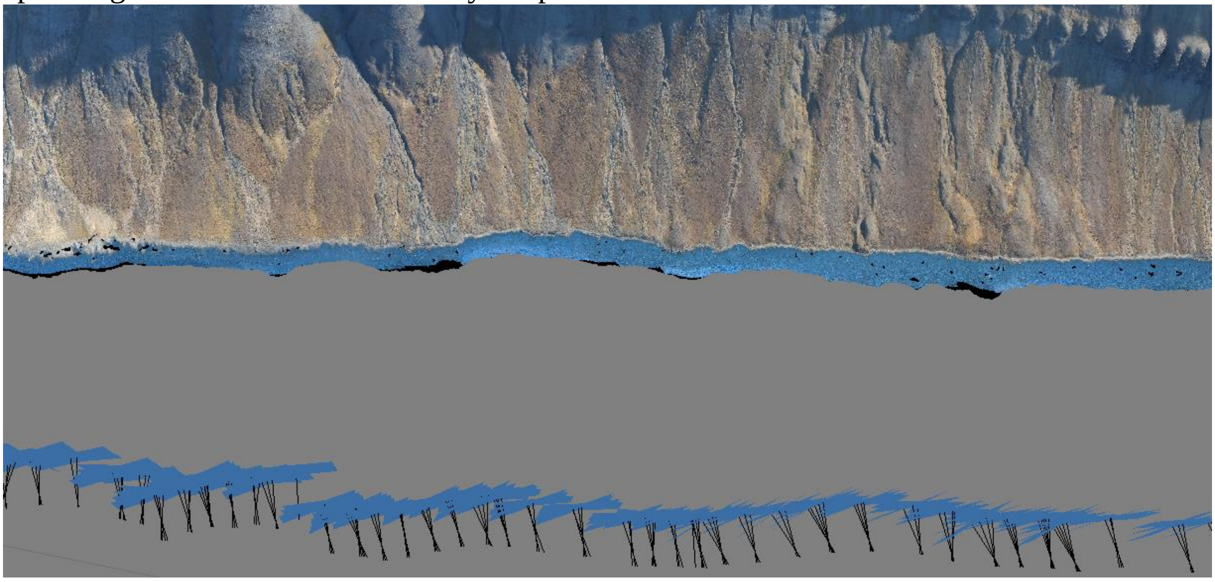

Figure 3.2: The direction and orientation of the pictures taken of the outcrops during fieldwork. The blue panels indicate the orientation of the pictures, and the black lines indicate the direction.

The data from the outcrops at Sassendalen were acquired using a LIDAR (Light Detection and Ranging) survey. The survey was conducted across the northern slope of Botneheia by Helimap Systems AG in August 2009. The acquisition system integrated a laser scanner (Riegl LMS VQ–480, average point spacing of *c.* 0.5 m) to generate a point cloud, and a high-resolution digital camera (Hasselblad H3DII–50 50 MP digital camera with a 35 mm lens, pixel size 6.0 μm) to simultaneously acquire images for texturing the laser-generated topography (Senger et al., 2013). The system was mounted obliquely on a helicopter, allowing steep outcrop topography to be captured with optimum imaging geometry (Rittersbacher et al., 2013). The model in Figure 3.3 was used in the intrusion analysis.

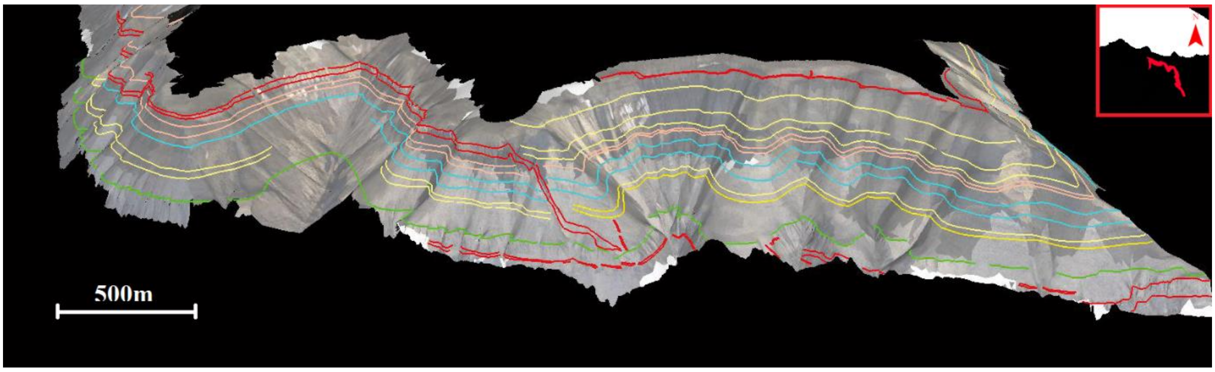

Figure 3.3: The LIDAR model of Sassendalen that was used in the outcrop analysis. Figure modified from Senger et al. (2013)

Table 3.1: The specifications of the datasets used in the research

Outcrop	Data type	Size	Number of photos	Host rock	Intrusion type	Height
1 & 2	Photogrammetry	8.0 km long	609	De Geerdalen F.	Sill	Variable
3	Photogrammetry	8.0 km long	568	Vikinghøgda	Dyke	Variable
4 & 5	LIDAR	8.3 km-long	N/A	Variable	Sill	Variable

3.3 Photogrammetric modelling

Photogrammetric modeling is a modeling solution aimed at creating 3D models from still images or photographs The acquisition principle is that of the Structure from Motion method. As the method's nameindicates, the camera is moved along or around a target, and a dense set of overlapping images is acquired. This set of images is then used to reconstruct the 3D surface ofthe target. From Saunders (2014).

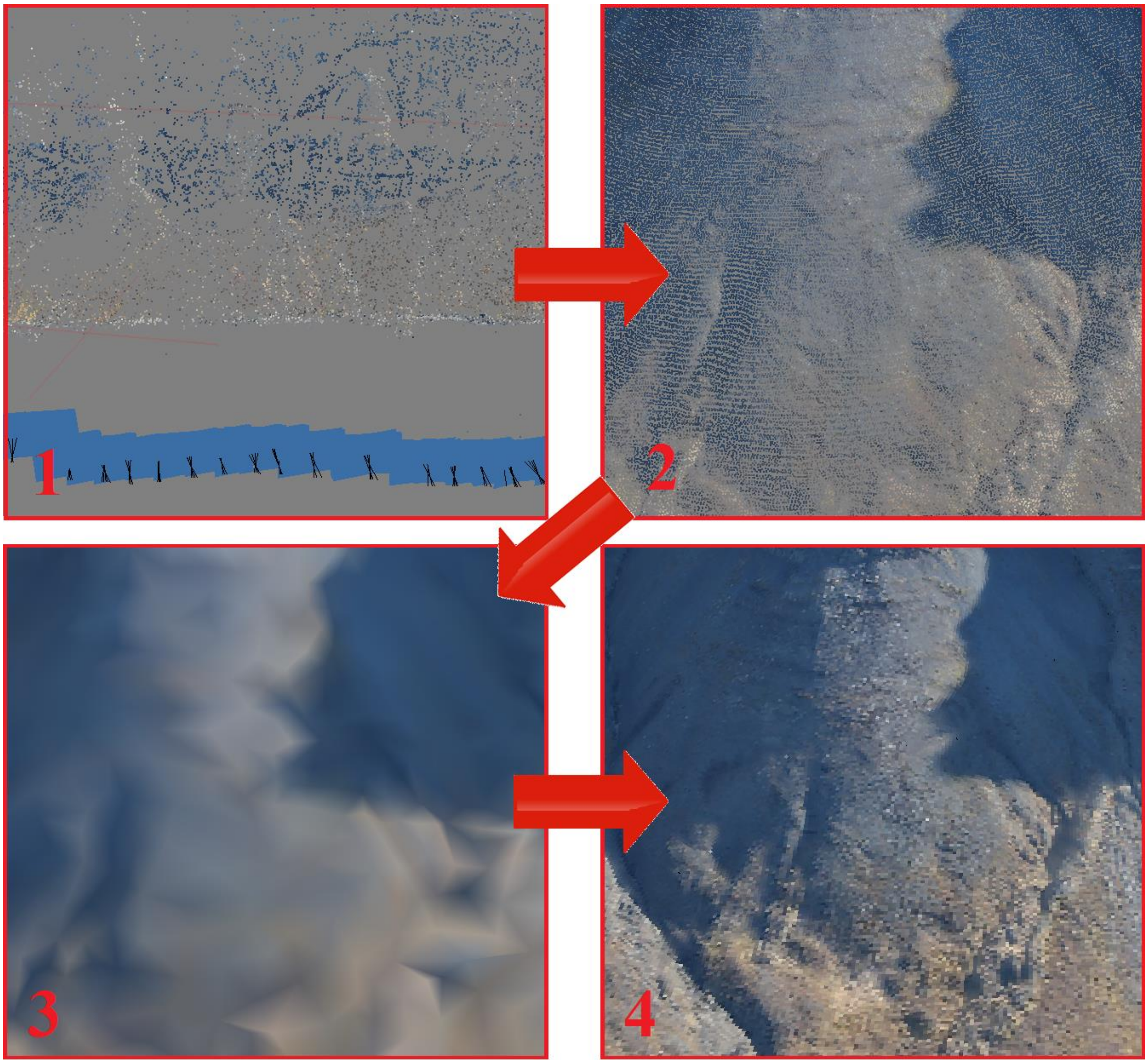

Figure 3.4: The workflow for photogrammetric modelling: Camera alignment, dense point cloud, mesh, and texture building

The output of photogrammetry is typically a map, measurement or a 3-D model. In this research it concerns a 3-D model of several mountain slopes next to Isfjorden which have visible outcrops. The workflow that is common for a photogrammetric analysis comprises of four main stages:

1: Camera alignment. The software used for the analysis searches for common points on the photographs and makes a match. It also finds the position of the camera for each picture and refines the camera calibration parameters. As a result of this, a sparse point cloud and a set of camera positions are formed.
2. Dense point cloud. A dense point cloud is built based on the sparse point cloud, the estimated camera positions and the pictures themselves.
3. Mesh building. A 3-D polygonal mesh is built, representing the surface of the object or model, based on the dense point cloud. There are several algorithmic methods available in order to generate the 3-D mesh. Which one of these is used depends on the type of object. Often after the 3-D mesh has been built, some editing is required such as closing of holes, removal of detached components, smoothing, etc.
4. Texture building. After the mesh is constructed, it can be textured and/or used for orthomosaic generation.

After these steps are completed, orthographic images of the outcrops are created for the next step of the analysis. Figure 3.4 briefly summarizes the workflow for photogrammetric modelling.

3.4 Elastic properties

The nature of this research is to test different geometries of outcrops using different parameters for the host rocks. The properties of these host rocks were derived from well logs onshore on Spitsbergen (Dh4 and Dh2), and a multitude of wells offshore in the Barents Sea. The wells that were used are shown in Table 3.1. Their location is outlined in figure 3.5. The most important parameters for the seismic modelling are P-wave velocity (Vp), S-wave velocity (Vs) and the density. The different host rock lithologies to be tested are: organic rich shales, clean sandstones, heterolithics (sandstone/shale) and Paleozoic carbonates.

Table 3.2: Wells used for property analysis. The UTM zone used is WGS 1984 UTM Zone 33N.

Well	X	Y	Depth	Location	Units
7119/12-4	890853.28	7915831.65	2910.12	Barents Sea	Hekkingen Fm., Stø Fm.
7120/12-5	926152.42	7941982.30	3630.00	Barents Sea	Hekkingen Fm., Stø Fm., Snadd Fm.
7220/6-1	898875.09	8090882.11	1539.93	Barents Sea	Snadd Fm., Ørn Fm.
7222/6-1 S	960628.05	8112469.83	2848.07	Barents Sea	Snadd Fm.
7225/3-1	1046477.79	8168900.56	4147.34	Barents Sea	Hekkingen Fm., Stø Fm., Snadd Fm., Isbjørn Fm.
7225/3-2	1048714.35	8173660.05	2208.90	Barents Sea	Hekkingen Fm., Stø Fm., Snadd Fm.
Dh4	518954.18	8681309.31	972.00	Svalbard	De Geerdalen Fm.
Dh2	512518.09	8684972.50	856.30	Svalbard	

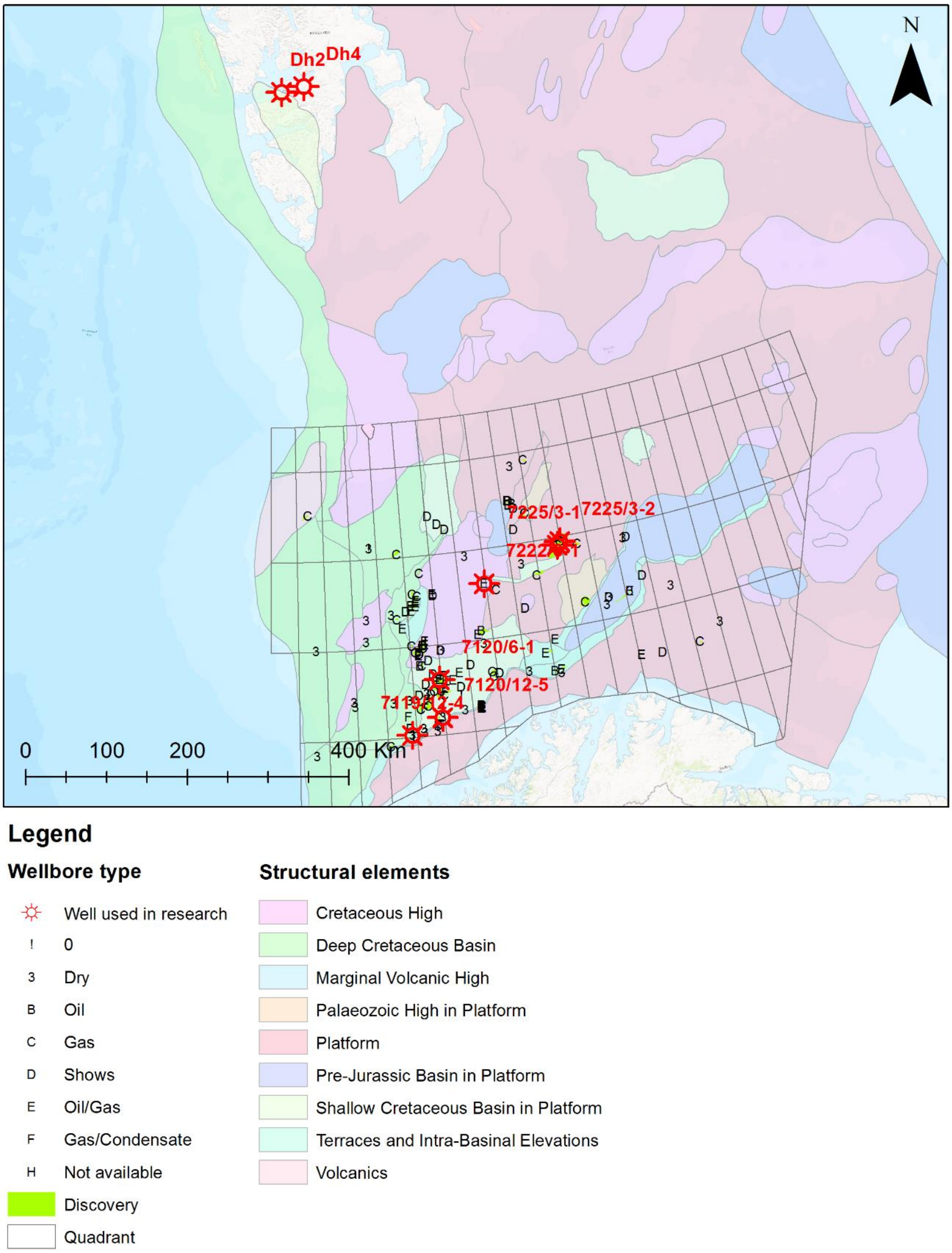

Figure 3.5: Locations of the wells used for the property analysis.

3.5 Seismic modelling

Once several different geometries have been identified, these will be converted into orthographic images using the above steps. Petrel 2015 is used for the next step. Using the seismic interpretation tool, layers are interpreted using the outcrop geometry. Where the outcrop geometry was difficult to interpret, photographs or the virtual outcrop model were used to help the identification. Based on the geometry this will result in several layers within the model. These will generally indicate the top and the base of the sill, where applicable. Once these layers have been identified, horizons are created based on these layers. Based on these horizons, a simple grid is created. The layers are used to assign zones within the model. These include the overburden zone, the intrusion zone, and the underburden zone depending on the shape of the geometry. Geometrical modelling is then used to assign properties (Vp, Vs, and density) to the different zones, and petrophysical modelling is used to assign values to these properties. The properties are converted into property cubes, which are then exported to a different software (Norsar Seisrox 2016), along with the grid used to generate these cubes. Within Seisrox, a new target model was made using the measurements of the imported grid. The target model then was assigned a Vp, Vs, and density based in the imported property cubes. The method that is used for obtaining the synthetic seismic profiles is by using a Pre-Stack Depth Migration (PDSM) simulator. The PSDM simulator creates a seismic image from the reflectivity grid of the input section, which is angle-dependent and based on the elastic properties of the model, and uses the image response of point scatterers (Anell et al., 2016), called Point-Spread Functions (PSFs) (Lecomte, 2008) to generate seimsic sections using a 3-D convolution method. The method applies 2(3)D spatial convolution operators as generated from RB (Ray based) information (Lecomte, 2008). This process is illustrated in Figure 3.6. The constant angle of incidence was set to 20 degrees. The seismic signal that was used was assumed to be a zero-phase Ricker wavelet. Frequencies of 20Hz, 30Hz and 60Hz were used to make an accurate assessment of the effect of a lower or higher frequency on seismic imaging. The average velocity was assumed to be 4000 m/s. All target models were sampled at 1m in all directions in order to avoid artefacts.

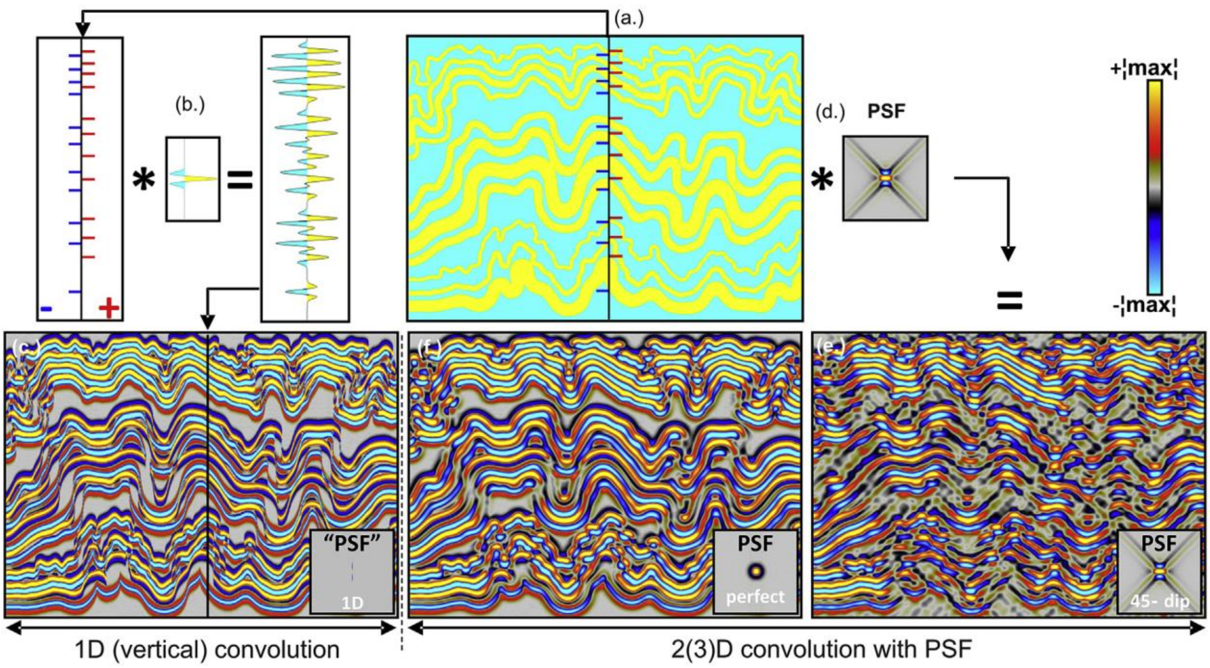

Figure 3.6: Illustration of the 3-D convolution method. (c) shows conventional 1D convolution with reflectivity logs extracted along the vertical lines. (f) shows an image obtained from using the PSF, using perfect illumination. (e) shows an image based on a more realistic PSF.

3.6 Intrusion analysis

In order to analyze the amount of intrusions of the Diabasodden suite on the Svalbard archipelago, GIS data provided by the Norwegian Polar Institute (NPI) has been used (Dallmann et al. 2015). The intrusions have been categorized based on the surrounding host rock lithology, effectively creating a database containing the most occurring host rocks for the Diabasodden suite on the Svalbard archipelago. Two databased have been used for this analysis. A geological map with a scale of 1:100 000, and a geological map with a scale of 1:250 000. The results from these maps have been combined into a single database. The analysis is based on proximity. For the purpose of this research, geological units adjacent of an intrusion lithology have been counted. Another analysis using the same dataset is to find out the length of the intrusions, thickness, and whether they are sills or dykes. In the Dyke/Sill analysis the intrusion is assumed to be a Sill if the maximum angle of the intrusion is less than 22.5 Degrees. To find out the thickness, the lowest elevation point within the intrusion has been subtracted from the highest elevation point.

4 Results

4.1 Physical properties

In order to run simulations with the provided data, it is important to know the physical properties of the most common formations in the area, and the formations you would expect in the Barents Sea. 4 Lithologies were tested, Sandstone/shale (Snadd Formation), organic rich shale (Hekkingen Formation), clean sandstone (Realgrunnen Sbgrp), and Paleozoic carbonates (Polarrev/ørn Formation). These lithologies were chosen because the data for these formations was available from Barents Sea wells, and they are equilavent to the host rock lithologies found on Svalbard. The Snadd formation relates to the De Geerdalen formation. The Hekkingen formation is roughly equilavent to the Agardfjellet formation. The Realgrunnen subgroup is to simulate the conditions of a clean sandstone lithology, and the Polarrev, ørn and Isbjørn formations are chosen to simulate the conditions for a Paleozoic carbonate host rock lithology. The elastic properties of these lithologies can be found in Table 4.1 below. Figure 4.1 and 4.2 show the raw data from the wells used in this research.

Table 4.1: Elastic properties of formations relevant to the research. The properties from the Diabasodden Suite have been taken from literature (Baelum et al., 2012)

Lithology	Formation	Vp			Vs			ρ		
		Min	Avg	Max	Min	Avg	Max	Min	Avg	Max
Sandstone/shale	Snadd	2800	**3500**	4400	1400	**1800**	2800	2.3	**2.6**	2.7
Organic rich shale	Hekkingen	2800	**3000**	3200	1500	**1600**	1700	2.2	**2.4**	2.5
Clean sandstone	Realgrunnen Sbgrp	3900	**4000**	4400	2100	**2500**	2500	2.2	**2.4**	2.7
Carbonate	Polarrev/ørn	4500	**6000**	6000	2500	**3000**	3500	2.4	**2.7**	2.8
Doleritic intrusion	Diabasodden suite	-	**6000**	-	-	**3000**	-	-	**2.9**	-

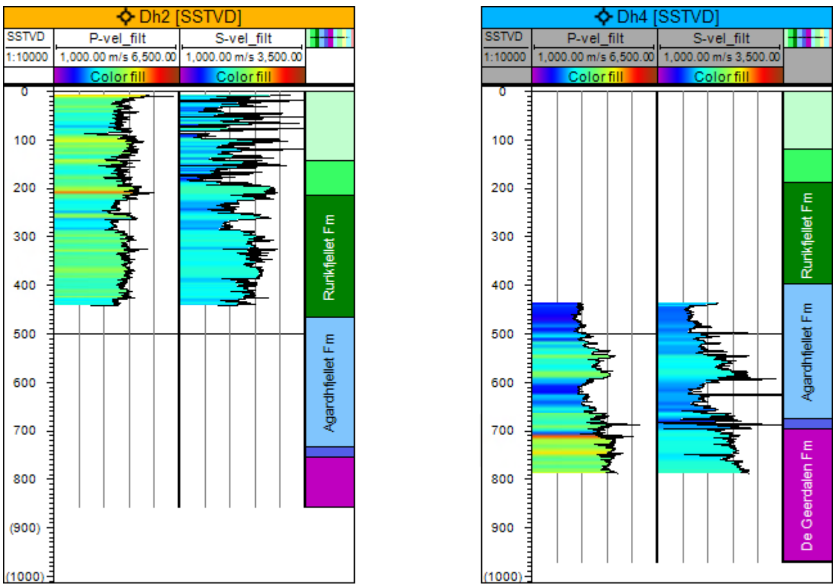

Figure 4.1 The two onshore wells on Svalbard. The main data that was used from these wells were the elastic properties for the De Geerdalen Formation

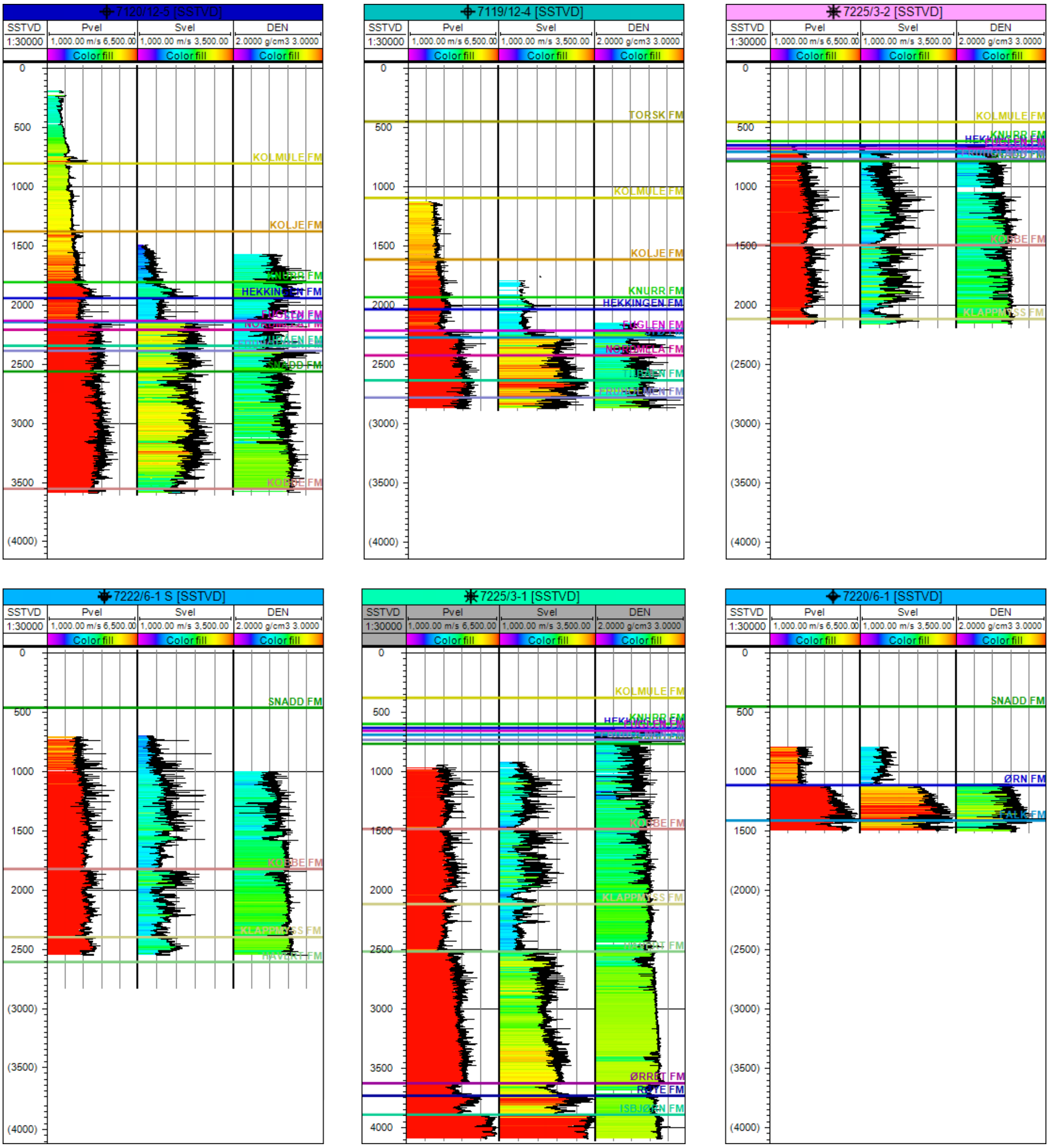

Figure 4.2: The well data from which the elastic properties were taken. In the above 3 wells, properties were taken for the Hekkingen formation, Stø formation, Snadd formation and Isbjørn formation

4.2 Intrusion analysis

There are several formations that function as a host rock for the Diabasodden suite dolerites. Table 4.2 and Figure 4.3 show the results of the host rock analysis for the Diabasodden suite intrusions. The analysis was made over the entire Svalbard archipelago using GIS data provided by the Norwegian Polar institute.

Table 4.2: the most common formations that function as a host rock for the Diabasodden suite dolerites. Intrusions with an area of less than 10m2 were filtered.

Formation	Period	Intrusions	Lithology
Agardhfjellet Formation	Mesozoic	62	Black shale, siltstone
Vikinghøgda Formation		54	Shale, siltstone
Tschermakfjellet Formation		32	Shale
De Geerdalen Formation		72	Shale, sandstone
Botneheia Formation		108	Mudstone, siltstone
Newtontoppen Granite	Paleozoic	46	Granite
Kapp Starostin Formation		169	Chert, shale, sandst.
Gipshuken Formation		68	Dolomite, limestone
Wordiekammen Formation		47	Carbonate rocks
Minkinfjellet Formation		36	Carbonates, evaporites
Other formations	Other	72	

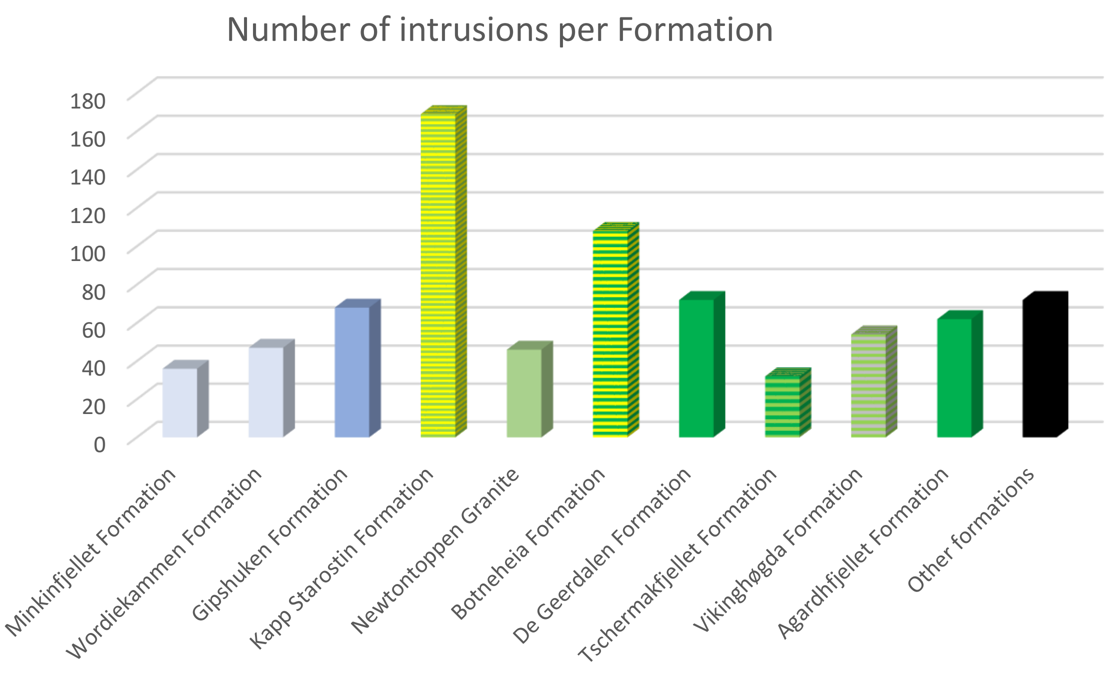

Figure 4.3: The most common host rocks for the Diabasodden suite dolerites in relation to one another. The intrusions are sorted from oldest (left) to youngest (left). (Data provided by the Norwegian Polar Institute)

Figure 4.4 shows examples of some of the doleritic intrusions in their respective host rock in different locations on Svalbard. Both dykes and sills are prevalent across Svalbard. While the results show the Minkinfjellet formation and the Newtontoppen granite as a host rock, this is not apparent in the GIS data. While there are a few cases of these units being adjacent to the Diabasodden suite intrusions, this is most likely not as a host rock. The Wordiekammen formation shows similar results, where in most cases it is simply adjacent to the doleritic intrusions. However, there are some cases where this formation functions as a host rock. This example is also shown in Figure 4.4.

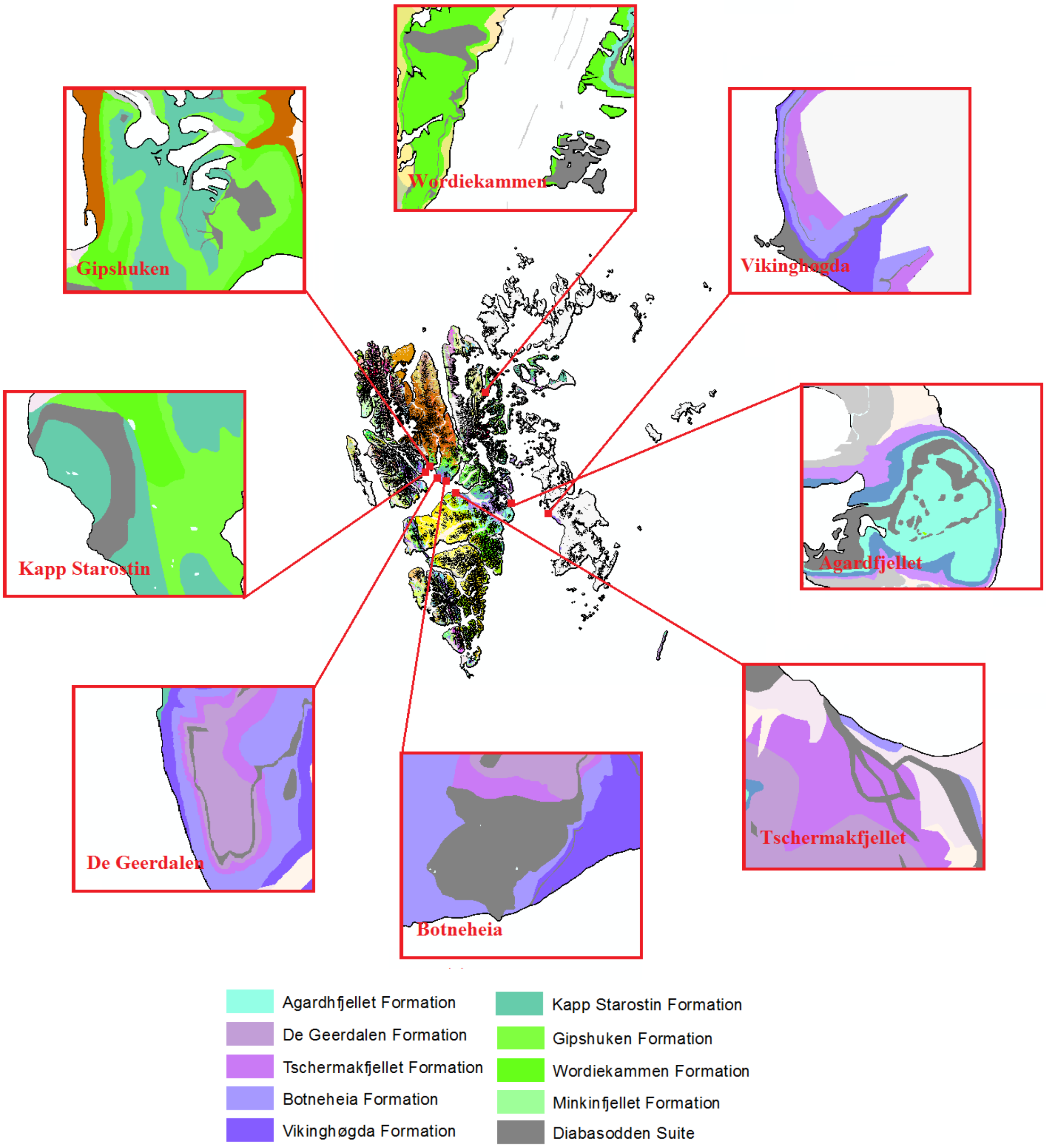

Figure 4.4: Some examples of the host rock formations in locations across Svalbard. (Data provided by the Norwegian Polar Institute)

Figure 4.5 shows the amount of intrusions per group. The results show that there is no significant difference in the amount of intrusions between the Gipsdalen group, Tempelfjorden group, Kapp Toscana group and Sassendalen group. The Billefjorden group and Adventdalen group show significantly less intrusions, with only a few intrusions in the Billefjorden group. All intrusions that belong to different groups have been counted as 'other groups'.

Table 4.3: the most common formations that function as a host rock for the Diabasodden suite dolerites. Intrusions with an area of less than 10m2 were filtered.

Group	Period	Intrusions
Adventdalen group	Mesozoic	81
Sassendalen group		224
Kapp Toscana group		202
Tempelfjorden group	Paleozoic	169
Gipsdalen group		219
Billefjorden group		26
Other groups	Other	272

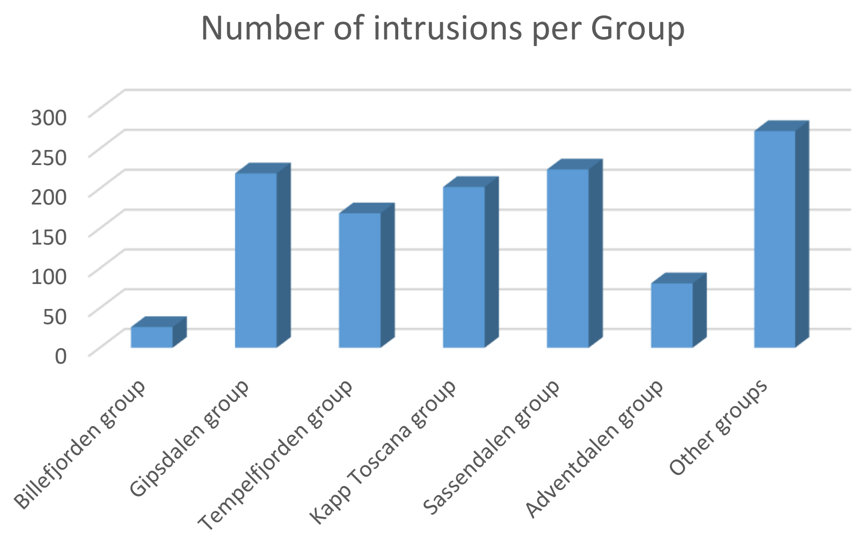

Figure 4.5: The most common groups that function as host rocks for the Diabasodden suite dolerites in relation to one another. The groups are sorted from oldest (left) to youngest (left). (Data provided by the Norwegian Polar Institute)

Another result of the intrusion analysis lists the location, area, thickness, elevation top and elevation base, and the length of the intrusion that is exposed. Also, it classifies the intrusion as a sill or a dyke. The sill to dyke ratio is shown in Figure 4.6. The percentage of sills is 91%, while the percentage of dykes is 9%, which is significantly less. The rest of these results are listed in Appendix A.

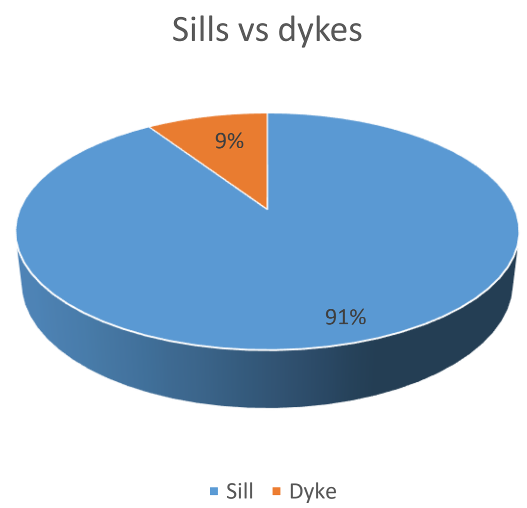

Figure 4.6: The percentage of sills compared to dykes on Svalbard. The absolute numbers are 643 sills versus 66 dykes

4.3 Geometry analysis

For the geometry analysis 5 different intrusion shapes or geometries have been tested. Geometry 1 is a bowl-shaped outcrop from Tschermakfjellet. Geometry 2 is a straight sill also at the Tschermakfjellet area. The third geometry is a dyke protruding on the beach of Rotundafjellet. Geometry 4 is a transgressive sill on the Botneheia mountain in Sassendalen. Geometry 5 consists of 2 stacked sills also in Sassendalen. Figure 4.7 shows the locations of the five test cases.

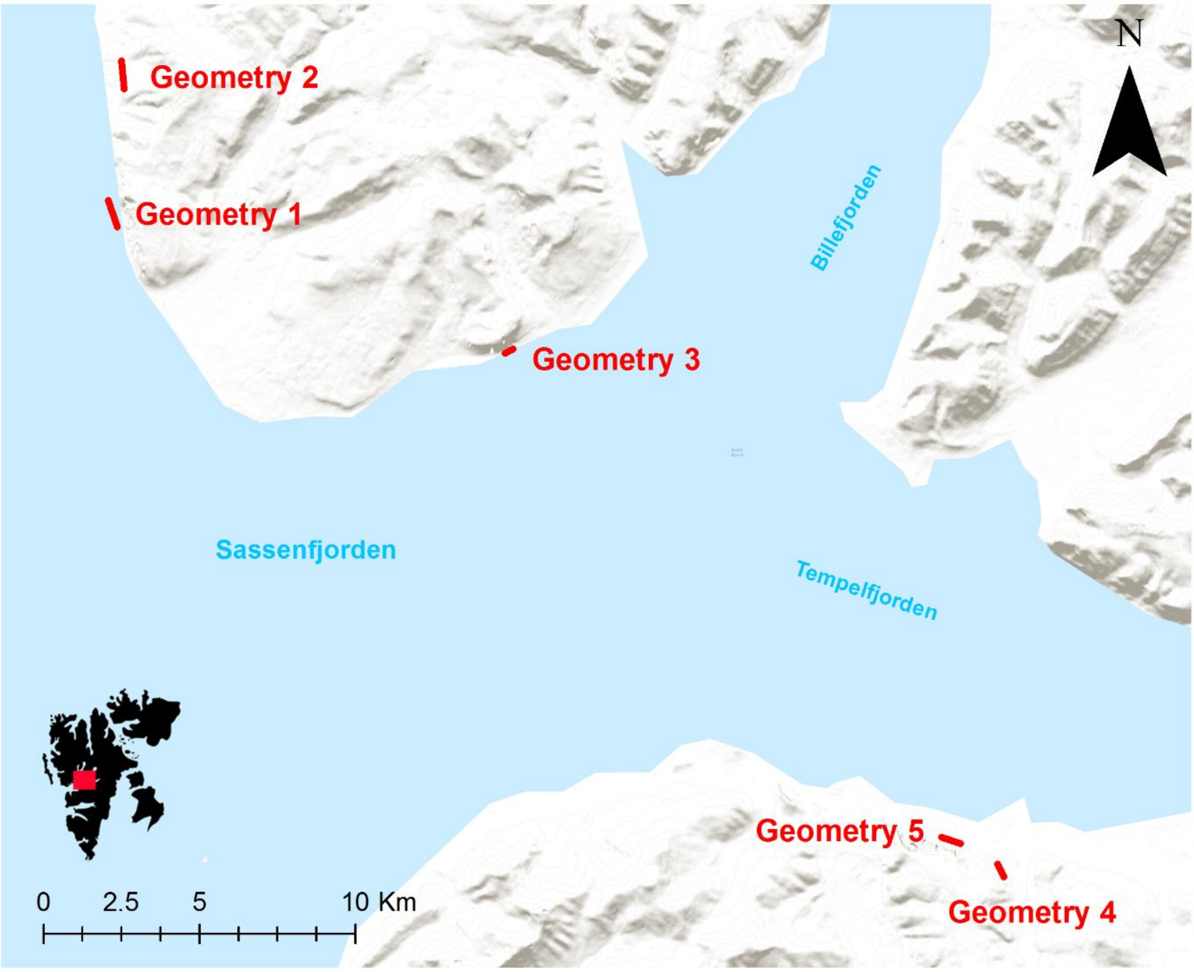

Figure 4.7: The location of the different geometries that were tested. Geometry 1 and 2 are located at Tschermakfjellet, Geometry 3 is located at Rotundafjellet, and Geometry 4 and 5 are located at Botneheia

4.3.1 Geometry 1: bowl-shaped intrusion

The first geometry is a bowl-shaped outcrop at Tschermakfjellet. The outcrop is shown together with the 3-D model that was made from the outcrop in Figure 4.8. Table 4.4 shows the properties that were used in each simulation.

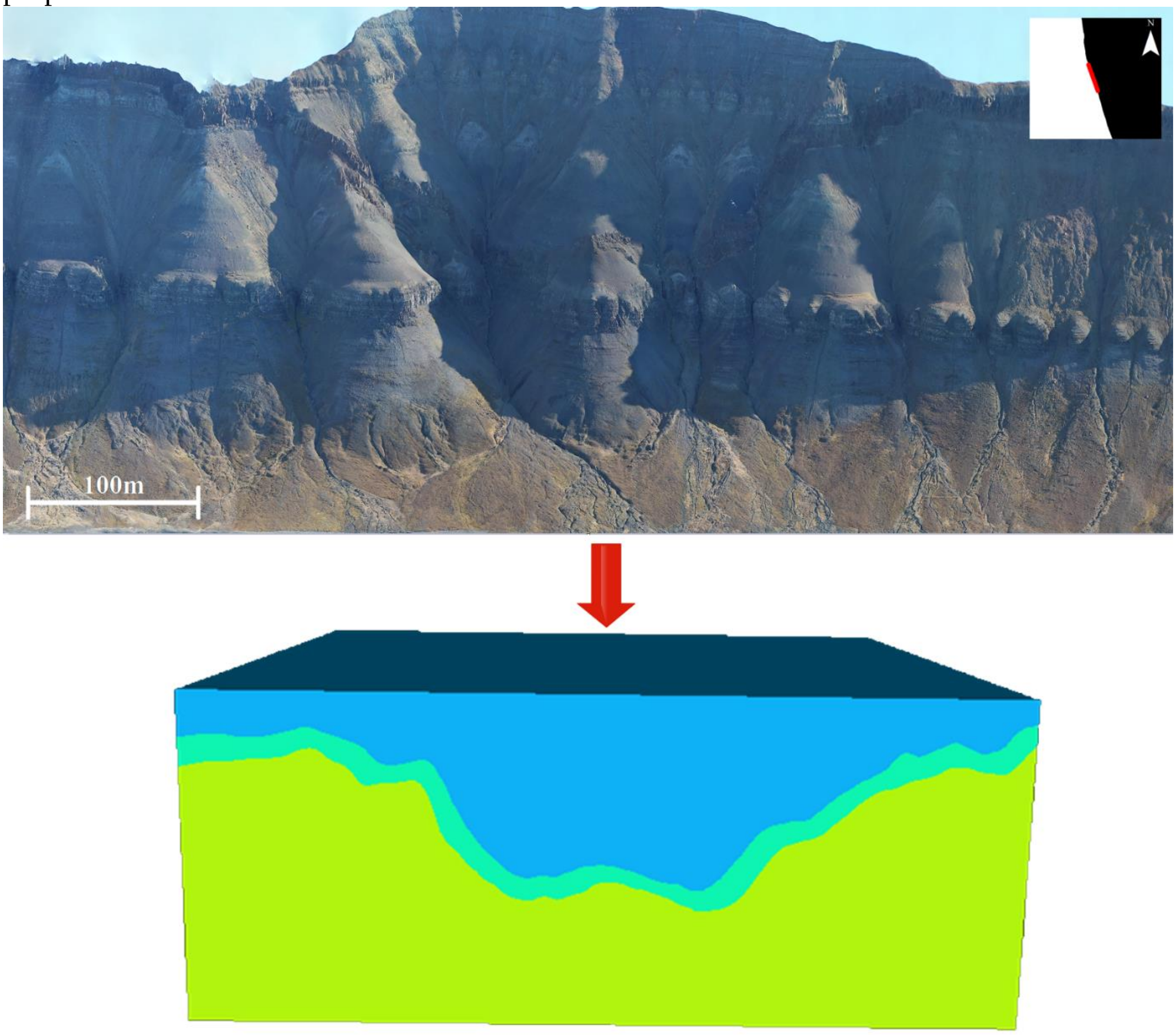

Figure 4.8: The bowl-shaped geometry at Tschermakfjellet

Table 4.4: The values used per test case for geometry 1

Test case	Formation	Vp	Vs	ρ
		Avg	Avg	Avg
Sandstone/shale	Snadd	**3500**	**1800**	**2.6**
Organic rich shale	Hekkingen	**3000**	**1600**	**2.4**
Clean sandstone	Realgrunnen Sbgrp	**4000**	**2500**	**2.4**
Carbonate	Polarrev/ørn	**6000**	**3000**	**2.7**
Doleritic intrusion	Diabasodden suite	**6000**	**3000**	**2.9**

Sandstone/shale lithology (Snadd Formation)

The sill is well visible on all frequencies, but the impedance contrast is higher for the 30Hz frequency and highest for the 60Hz frequency. The shape of the sill is also more defined on the highest frequency.

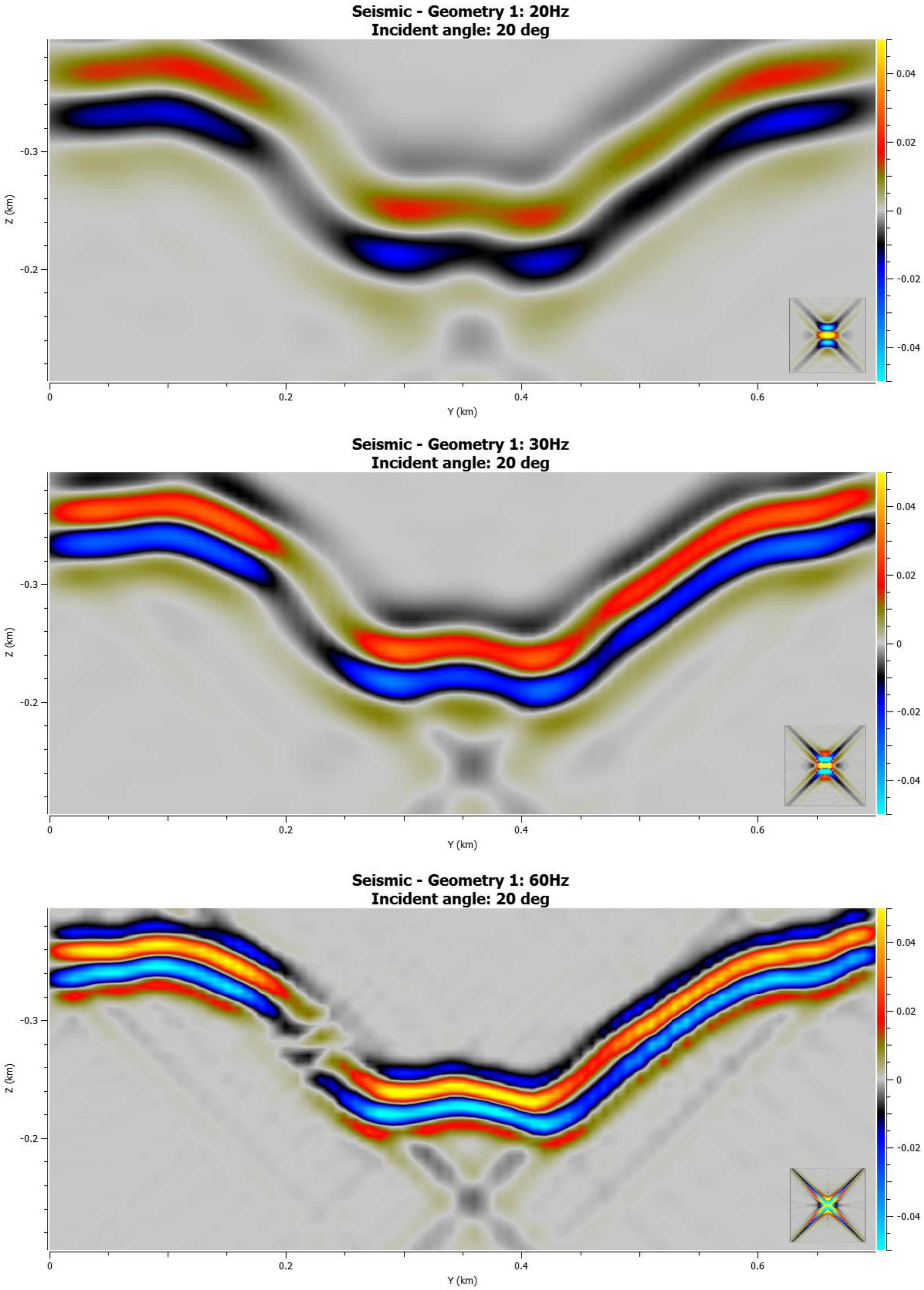

Figure 4.9: The results from the synthetic seismic simulation on the bowl-shaped outcrop using properties for a sandstone/shale lithology. The frequencies used were 20Hz (top), 30Hz (middle), and 60Hz (bottom)

Organic rich shale lithology (Hekkingen Formation)

The bowl-shape is very well visible in all frequencies, with impedance contrast being higher on higher frequencies. The shape of the sill is also more defined on the highest frequency. The impedance contrast is overall higher than on the sandstone/shale lithology due to the lower Vp and Vs.

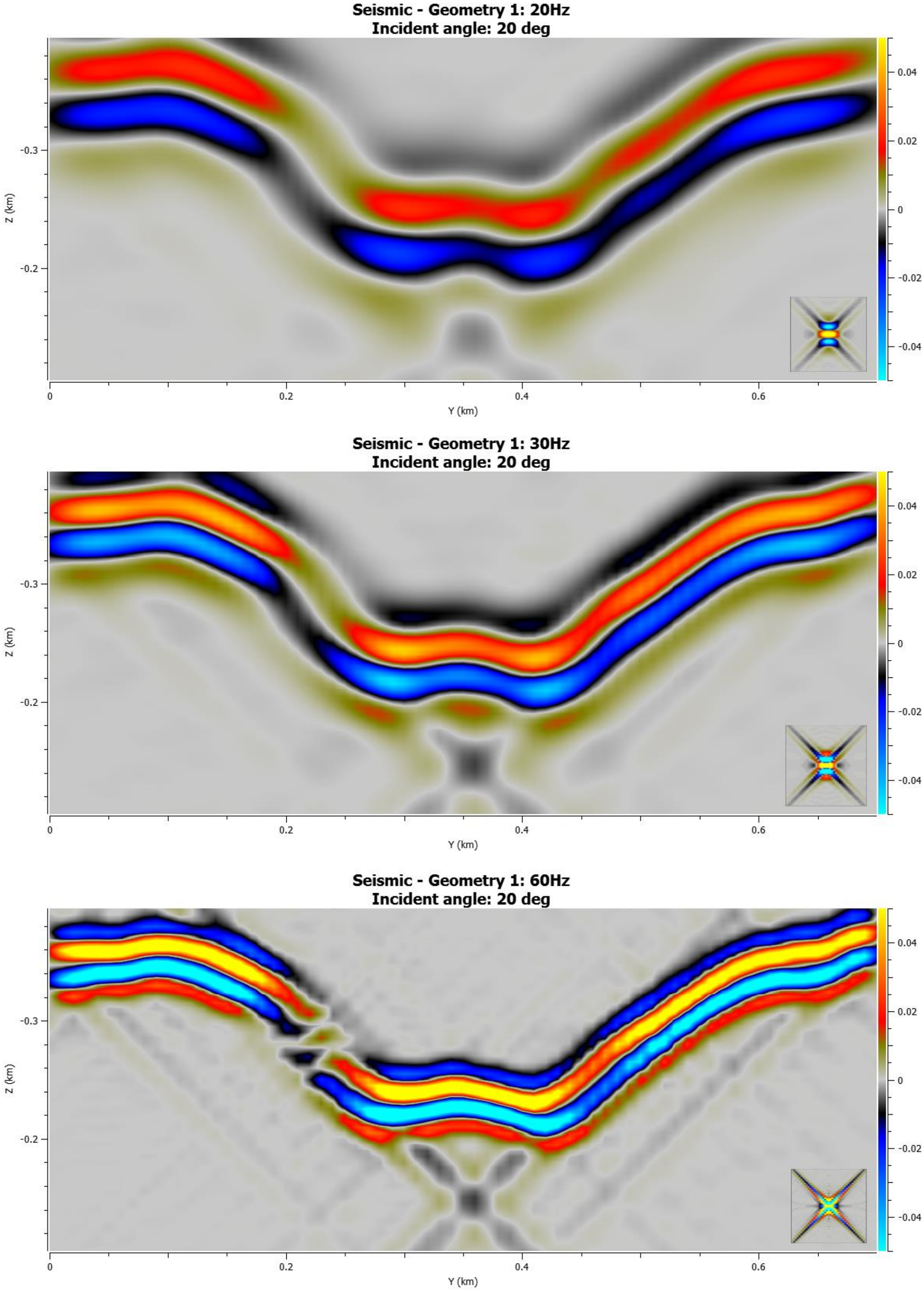

Figure 4.10: The results from the synthetic seismic simulation on the bowl-shaped outcrop using properties for an organic rich shale lithology. The frequencies used were 20Hz (top), 30Hz (middle), and 60Hz (bottom)

Clean sandstone lithology (Realgrunnen Sbgrp)

The bowl-shape is visible in all frequencies, with impedance contrast being higher on higher frequencies. The shape of the sill is also more defined on the highest frequency. The impedance contrast is overall slightly lower than on the sandstone/shale lithology due to the higher Vp and Vs.

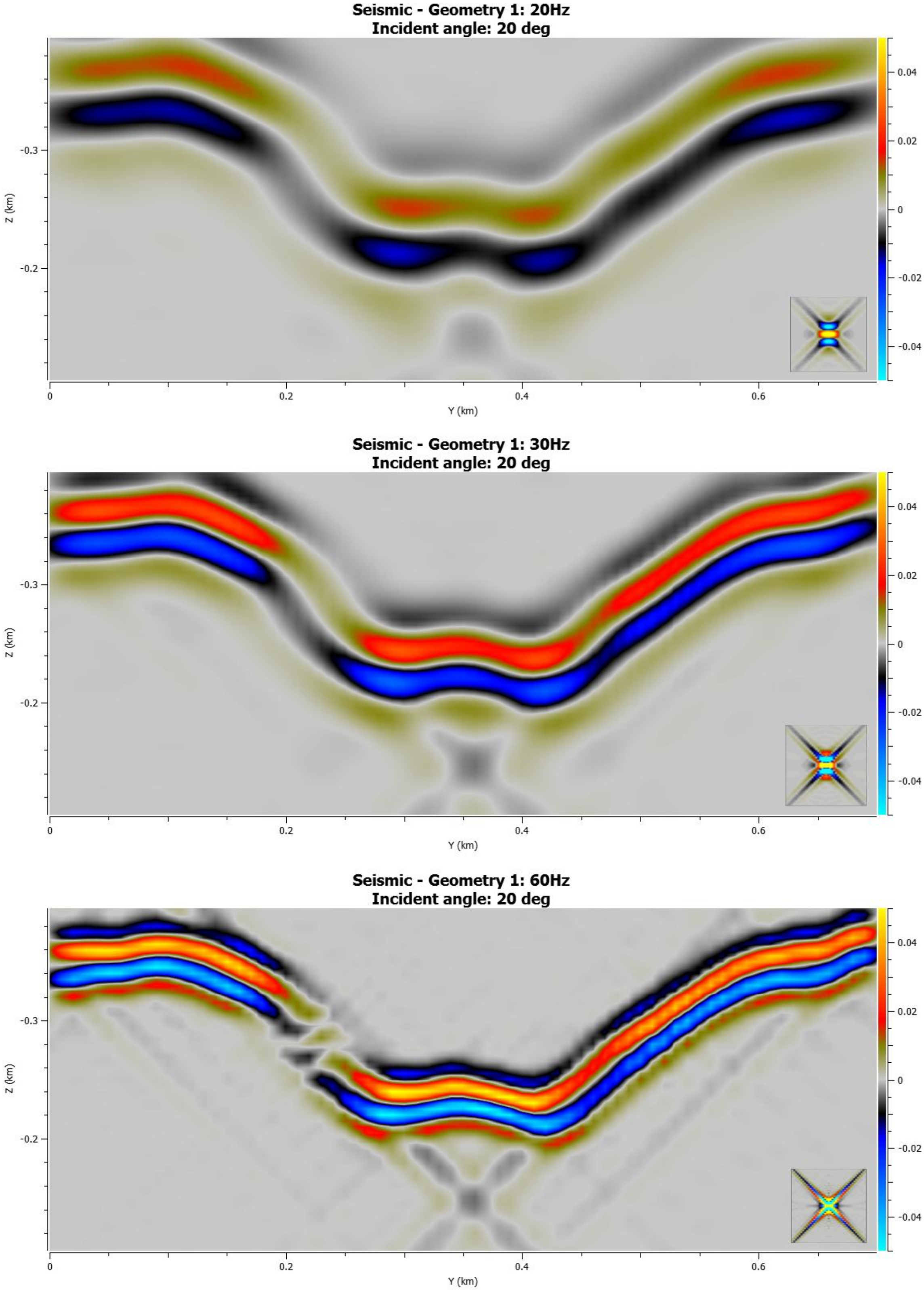

Figure 4.11: The results from the synthetic seismic simulation on the bowl-shaped outcrop using properties for a clean sandstone lithology. The frequencies used were 20Hz (top), 30Hz (middle), and 60Hz (bottom)

Paleozoic carbonates lithology (Polarrev/ørn Formation)

The bowl-shape is only barely visible in the lowest frequency. On higher frequencies the shape becomes more defined with a higher contrast, but visibility is still poor due to the high Vp and Vs which match the Vp and Vs of the intrusion.

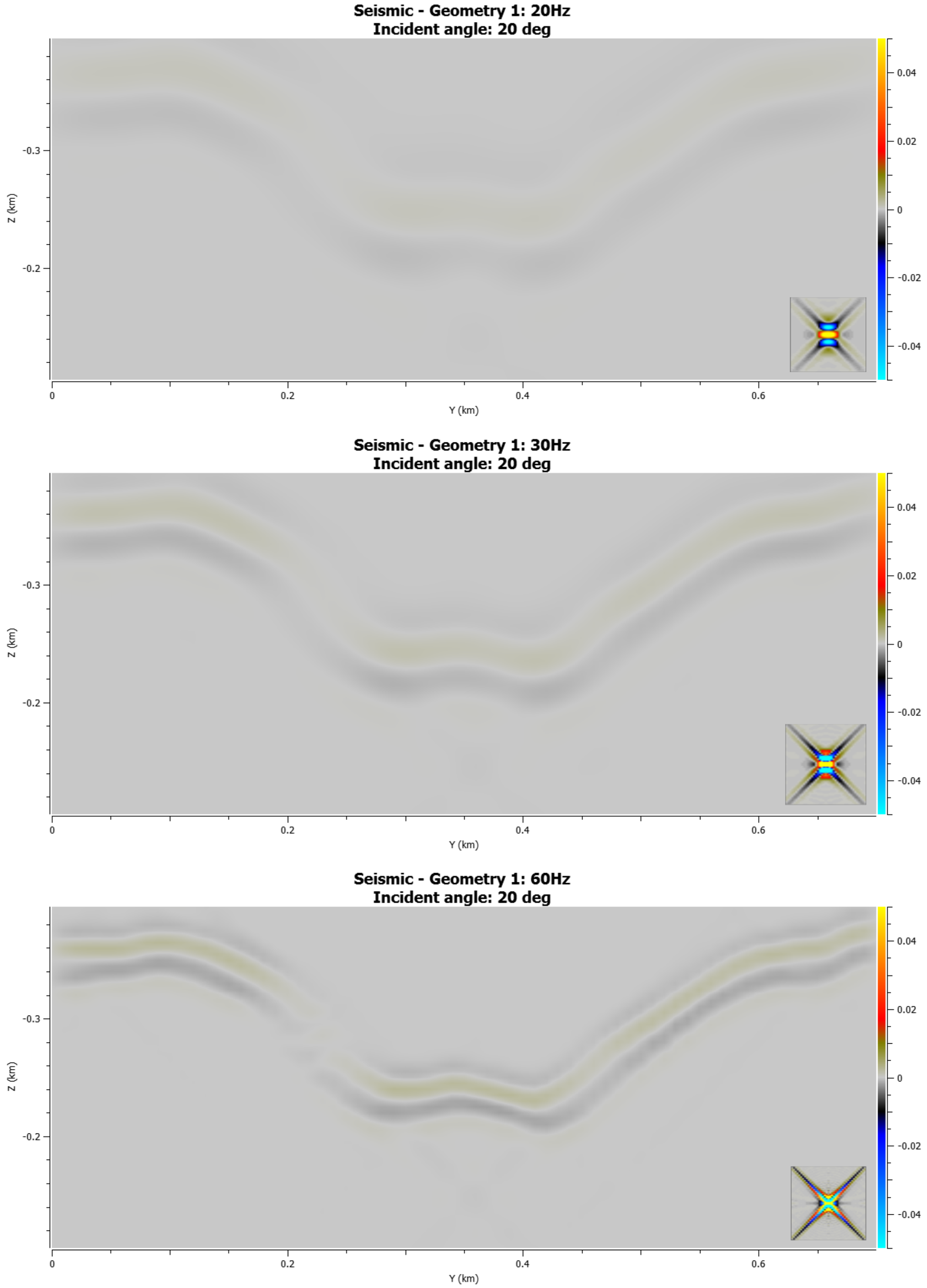

Figure 4.12: The results from the synthetic seismic simulation on the bowl-shaped outcrop using properties for a Paleozoic carbonate lithology. The frequencies used were 20Hz (top), 30Hz (middle), and 60Hz (bottom)

To sum up, the impedance contrast for the sandstone/shale lithology is visible and should be identifiable on seismic data. The contrast for the organic rich shale lithology is slighly higher and should show up even more clearly in the data. The contrast for the clean sandstone lithology is slighly lower, but still has decent visibility. The Paleozoic carbonate lithology has very poor visibility, and may only be visible in seismic data on high frequencies if there are no other reflectors near. The bowl-shape is a fairly recognizable shape, so even if the impedance contrast is low, it might still be distinguishable if there are not too many other reflectors nearby. Figure 4.13 shows the original picture of the outcrop with the synthetic seismic data draped over it.

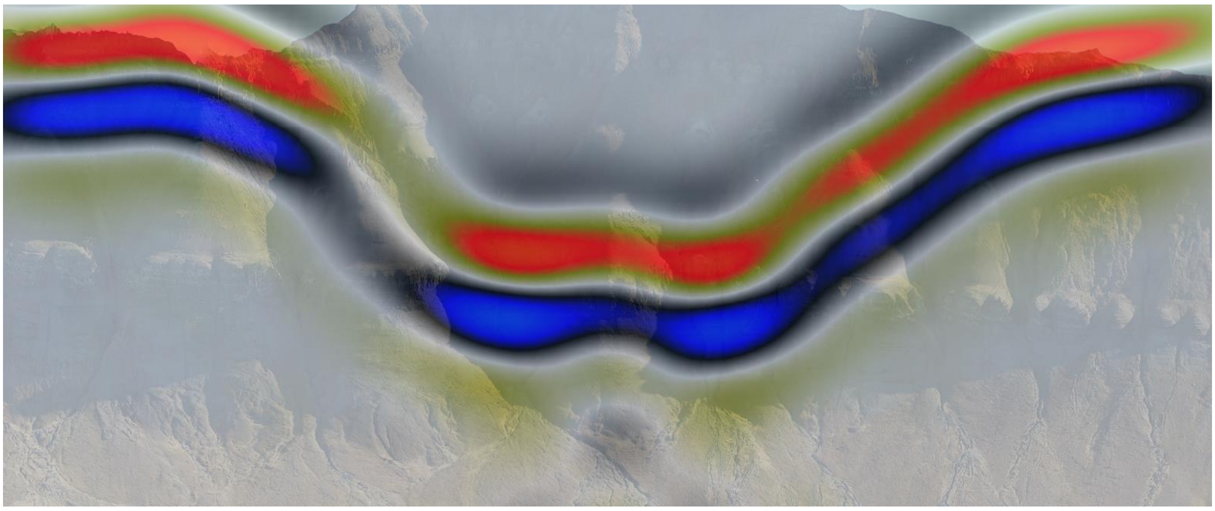

Figure 4.13: The original picture of the outcrop combined with the synthetic seismic (Sandstone/shale lithology, 20Hz)

4.3.2 Geometry 2: Straight sill

The second geometry is a straight sill at Tschermakfjellet. The outcrop is shown in Figure 4.14 along with the 3-D model that was created from this outcrop. This geometry doesn't have any complicated shapes, but can be used as a point of reference to compare the other geometries to. Table 4.5 shows the properties that were used in each simulation.

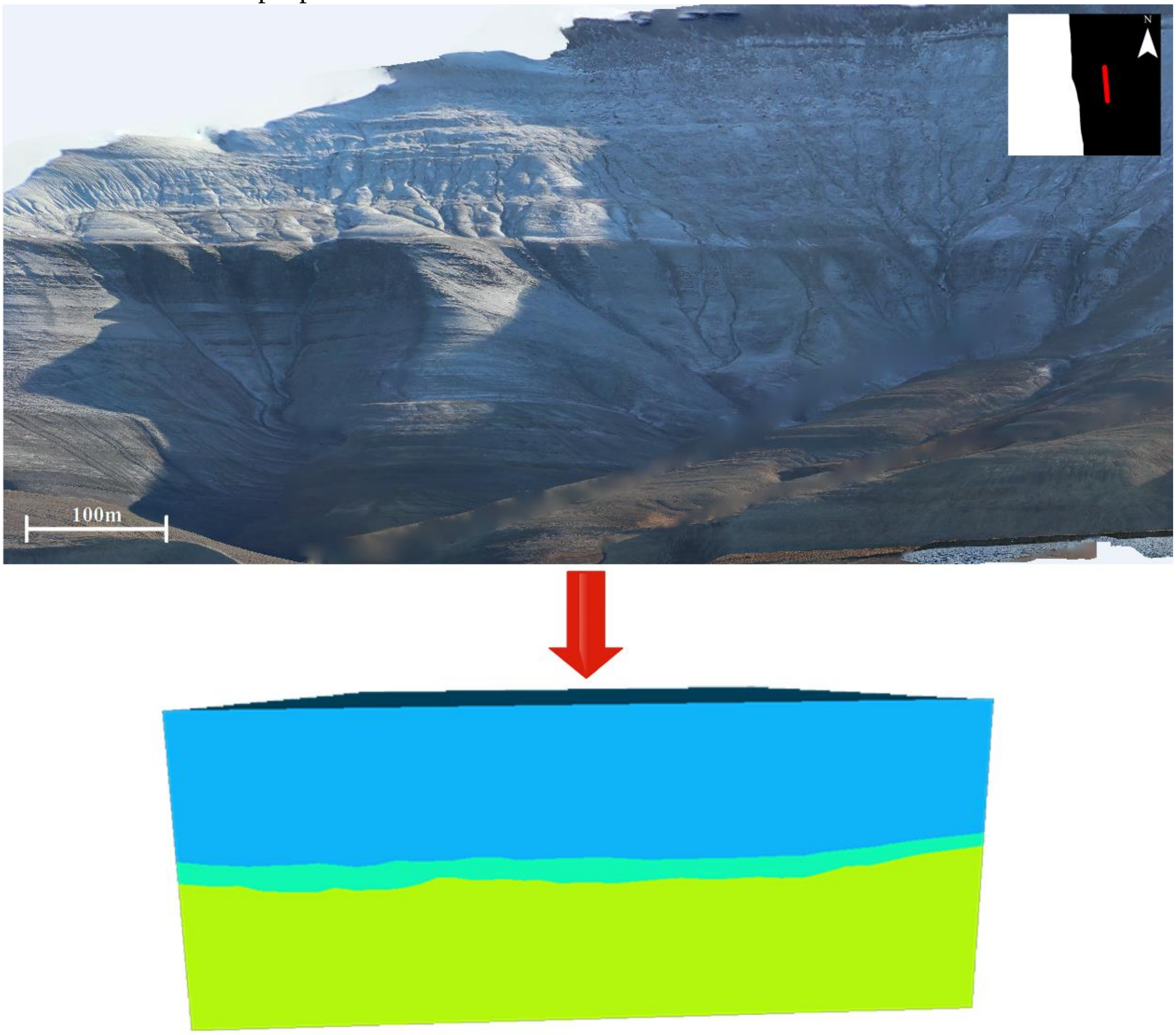

Figure 4.14: The straight sill at Tschermakfjellet

Table 4.5: The values used per test case for geometry 2

Test case	Formation	Vp	Vs	ρ
		Avg	**Avg**	**Avg**
Sandstone/shale	Snadd	**3500**	**1800**	**2.6**
Organic rich shale	Hekkingen	**3000**	**1600**	**2.4**
Clean sandstone	Realgrunnen Sbgrp	**4000**	**2500**	**2.4**
Carbonate	Polarrev/ørn	**6000**	**3000**	**2.7**
Doleritic intrusion	Diabasodden suite	**6000**	**3000**	**2.9**

Sandstone/shale lithology (Snadd Formation)

The straight sill is well visible on all frequencies, but the impedance contrast is higher for the 30Hz frequency and highest for the 60Hz frequency. Small variations within the sill appear to be more pronounced on the 60Hz frequency. Due to the straight shape the sill might be confused with a regular lithology change.

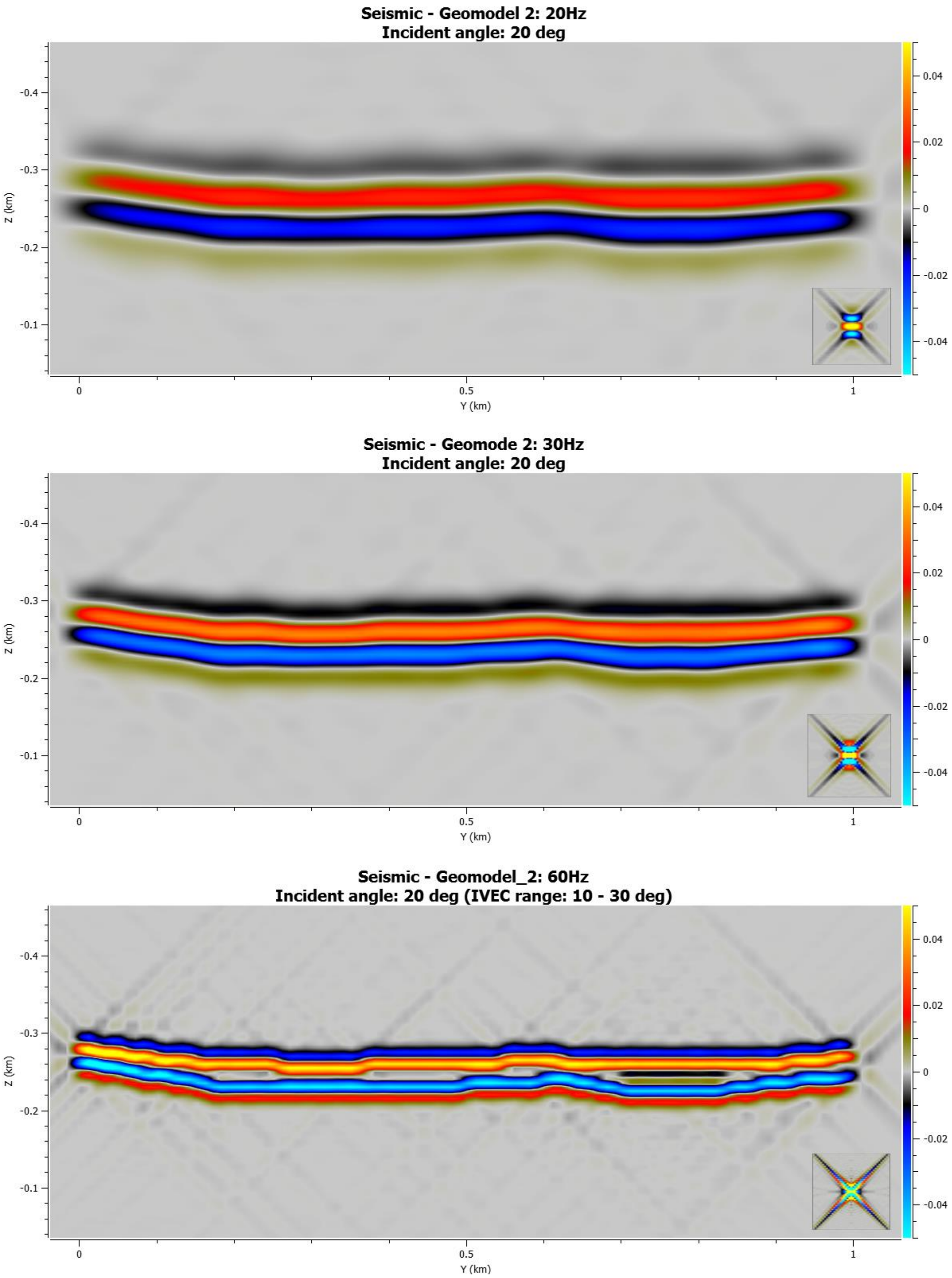

Figure 4.15: The results from the synthetic seismic simulation on the straight sill using properties for a sandstone/shale lithology. The frequencies used were 20Hz (top), 30Hz (middle), and 60Hz (bottom)

Organic rich shale lithology (Hekkingen Formation)

The straight sill is very well visible on all frequencies, but the impedance contrast is higher for the 30Hz frequency and highest for the 60Hz frequency. The overall impedance contrast is higher than the sandstone/shale lithology due to the lower Vp and Vs.

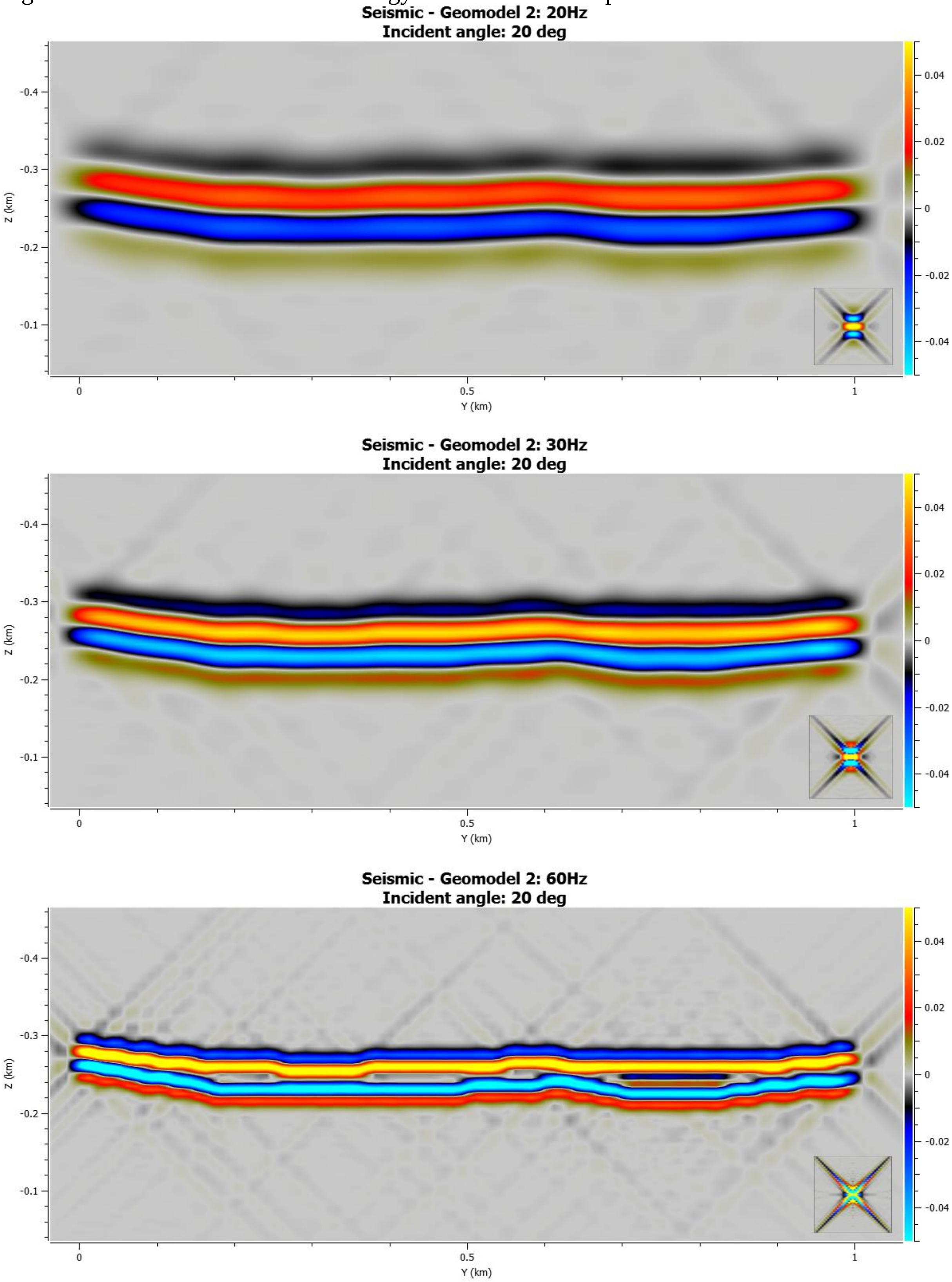

Figure 4.16: The results from the synthetic seismic simulation on the straight sill using properties for an organic rich shale lithology. The frequencies used were 20Hz (top), 30Hz (middle), and 60Hz (bottom)

Clean sandstone lithology (Realgrunnen Sbgrp)

The straight sill is visible on all frequencies, but the impedance contrast is higher for the 30Hz frequency and highest for the 60Hz frequency. The overall impedance contrast is slightly lower than the sandstone/shale lithology due to the higher Vp and Vs.

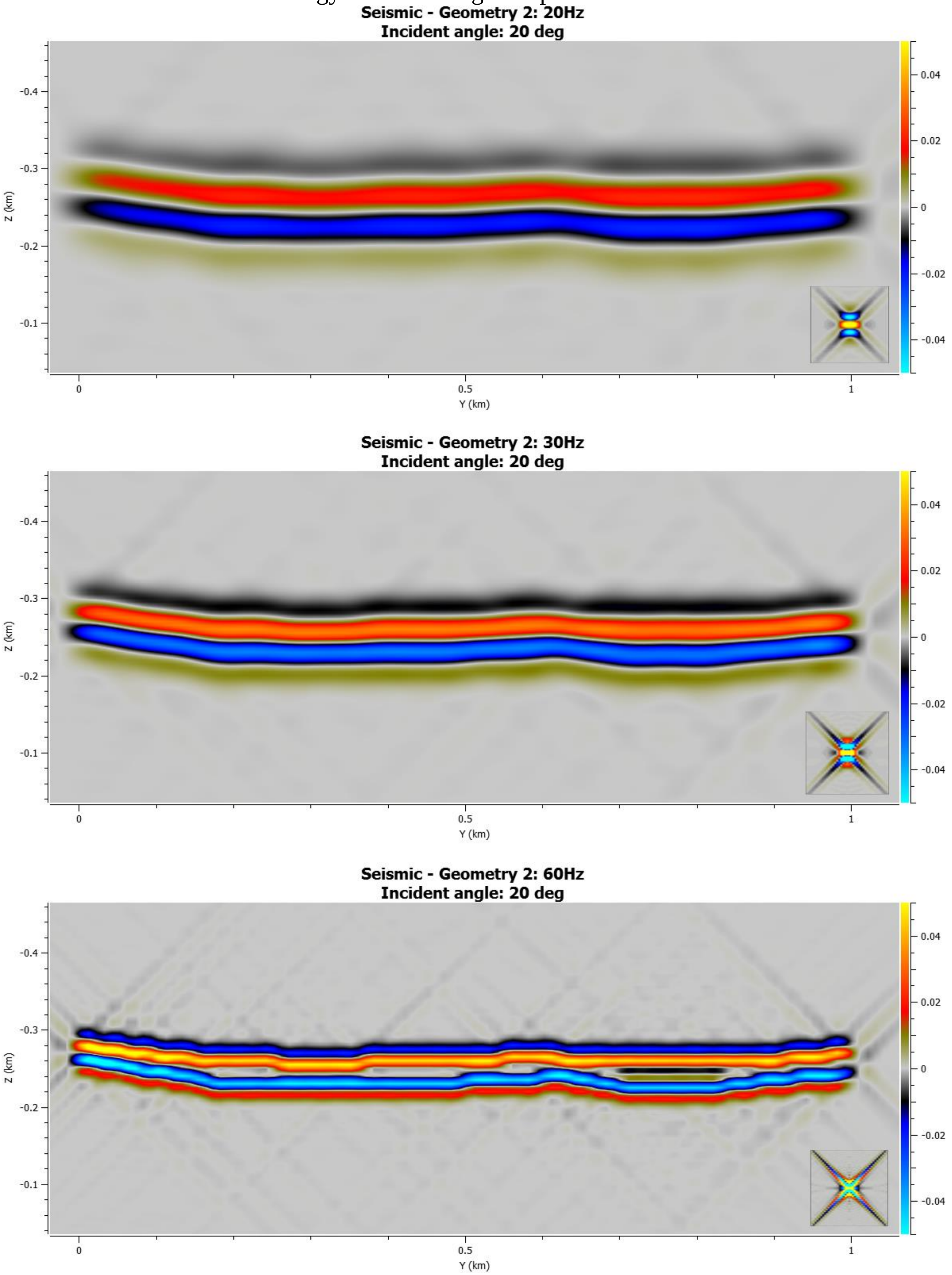

Figure 4.17: The results from the synthetic seismic simulation on the straight sill using properties for a clean sandstone lithology. The frequencies used were 20Hz (top), 30Hz (middle), and 60Hz (bottom)

Paleozoic carbonates lithology (Polarrev/ørn Formation)

The straight sill is only barely visible on the 20Hz frequency, and only slightly better on the 30Hz and 60Hz frequencies. This is due to the host rock and the intrusion having the same Vp and Vs, with only a small difference in the density.

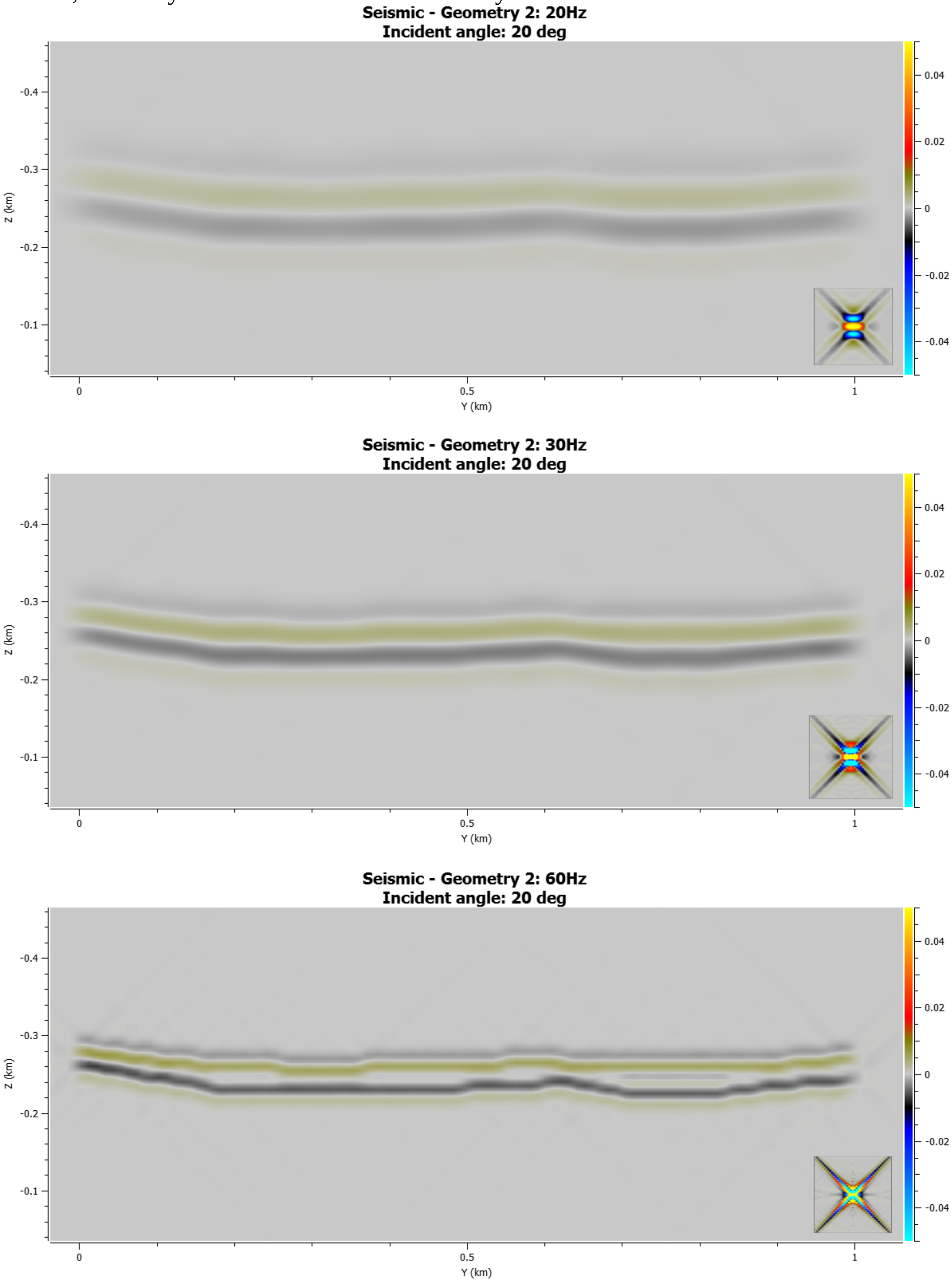

Figure 4.18: The results from the synthetic seismic simulation on the straight sill using properties for a Paleozoic carbonate lithology. The frequencies used were 20Hz (top), 30Hz (middle), and 60Hz (bottom)

To sum up, the impedance contrast for the sandstone/shale lithology is visible and should be identifiable on seismic data. The contrast for the organic rich shale lithology is slighly higher and should show up even more clearly in the data. The contrast for the clean sandstone lithology is slighly lower. The Paleozoic carbonate lithology has very poor visibility, and would make it very difficult to recognize the intrusion in seismic data. Due to the straight shape of the sill, it might be hard to distinquish from other reflectors unless the impedance contrast is very high. In shale and sandstone/shale the outcrop might be distinguishable, but in clean sandstone it might be more difficult, and very unlikely in carbonates. Figure 4.19 shows the original picture of the outcrop with the synthetic seismic data draped over it.

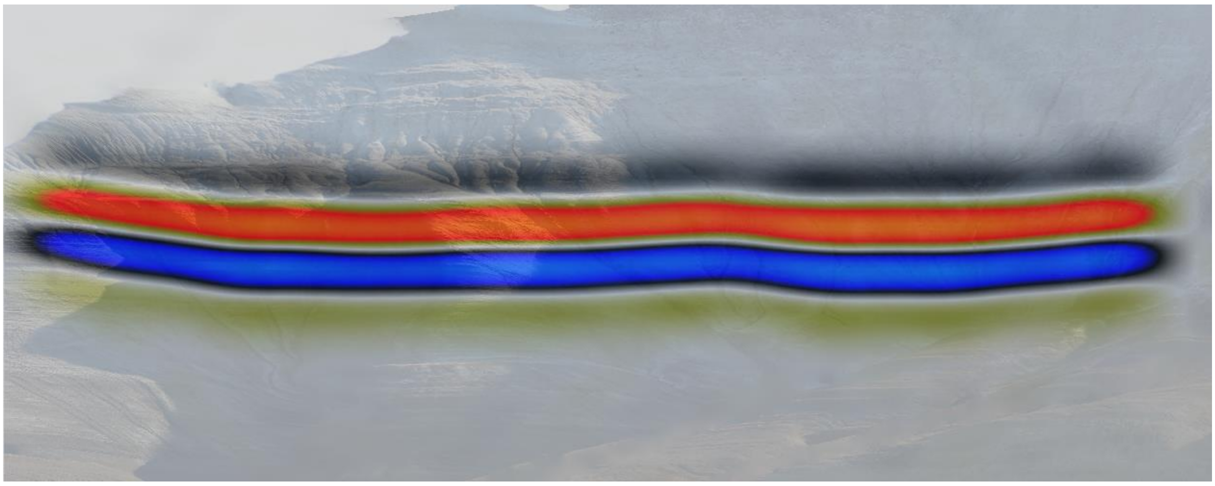

Figure 4.19: The original picture of the outcrop combined with the synthetic seismic (Sandstone/shale lithology, 20Hz)

4.3.3 Geometry 3: Rotundafjellet Dyke

The third geometry is a feeder dyke on the beach of Rotundafjellet. While only a small part of the dyke is exposed on the beach, it can be assumed that it goes all the way up to the sill at the top of the mountain and feeds into the sill. The shape of the sill is mostly assumed for the purpose of this simulation. Figure 4.20 shows both the original outcrop image and the 3-D cumbe that was generated from this outcrop. Table 4.6 shows the properties that were used in the simulation.

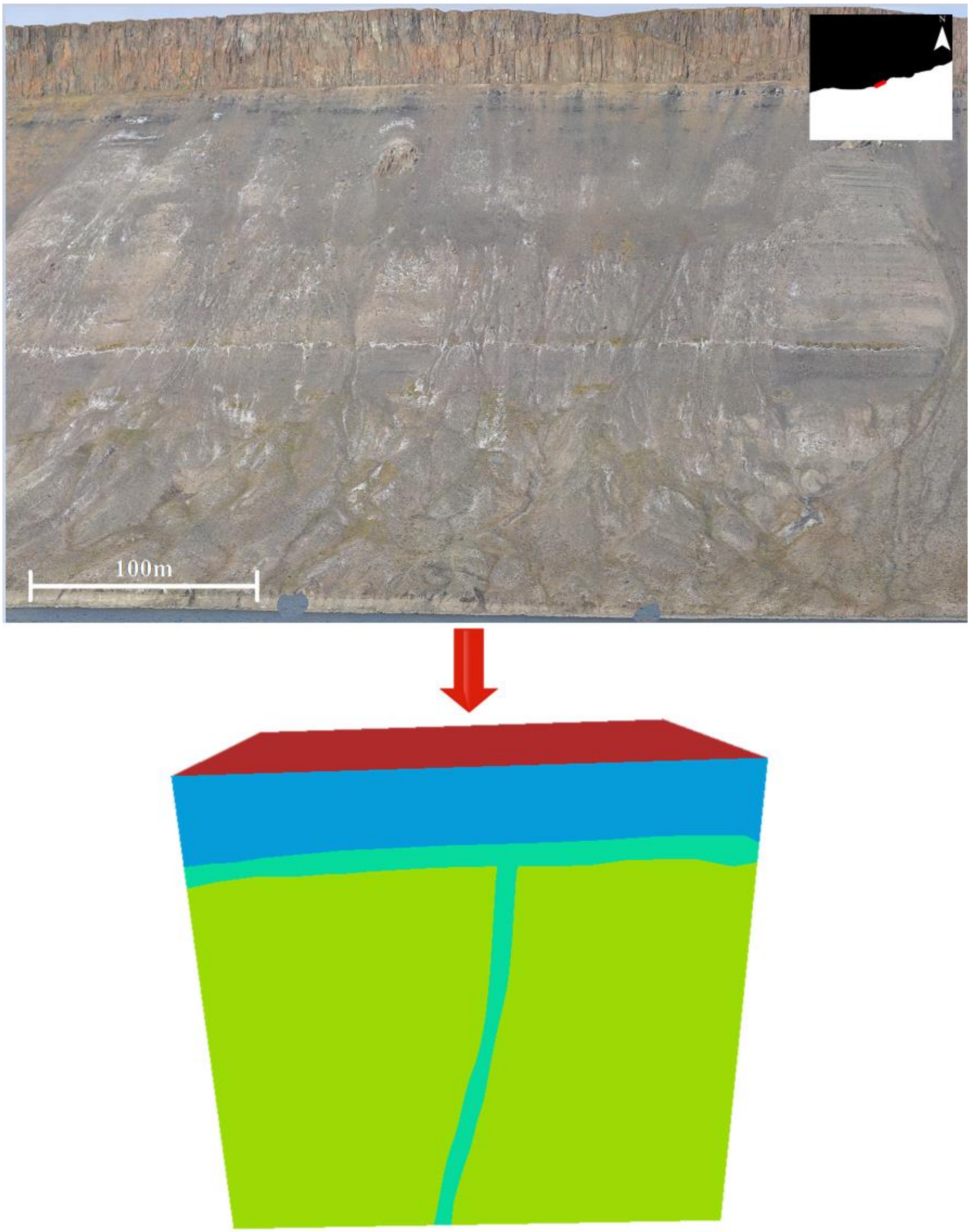

Figure 4.20: The dyke at Rotundafjellet beach

Table 4.6: The values used per test case for geometry 3

Test case	Formation	Vp	Vs	ρ
		Avg	**Avg**	**Avg**
Sandstone/shale	Snadd	**3500**	**1800**	**2.6**
Organic rich shale	Hekkingen	**3000**	**1600**	**2.4**
Clean sandstone	Realgrunnen Sbgrp	**4000**	**2500**	**2.4**
Carbonate	Polarrev/ørn	**6000**	**3000**	**2.7**
Doleritic intrusion	Diabasodden suite	**6000**	**3000**	**2.9**

Sandstone/shale lithology (Snadd Formation)

The sill is well visible on all frequencies, but the dyke is only slightly visible on 30Hz and a little more visible on 60Hz.

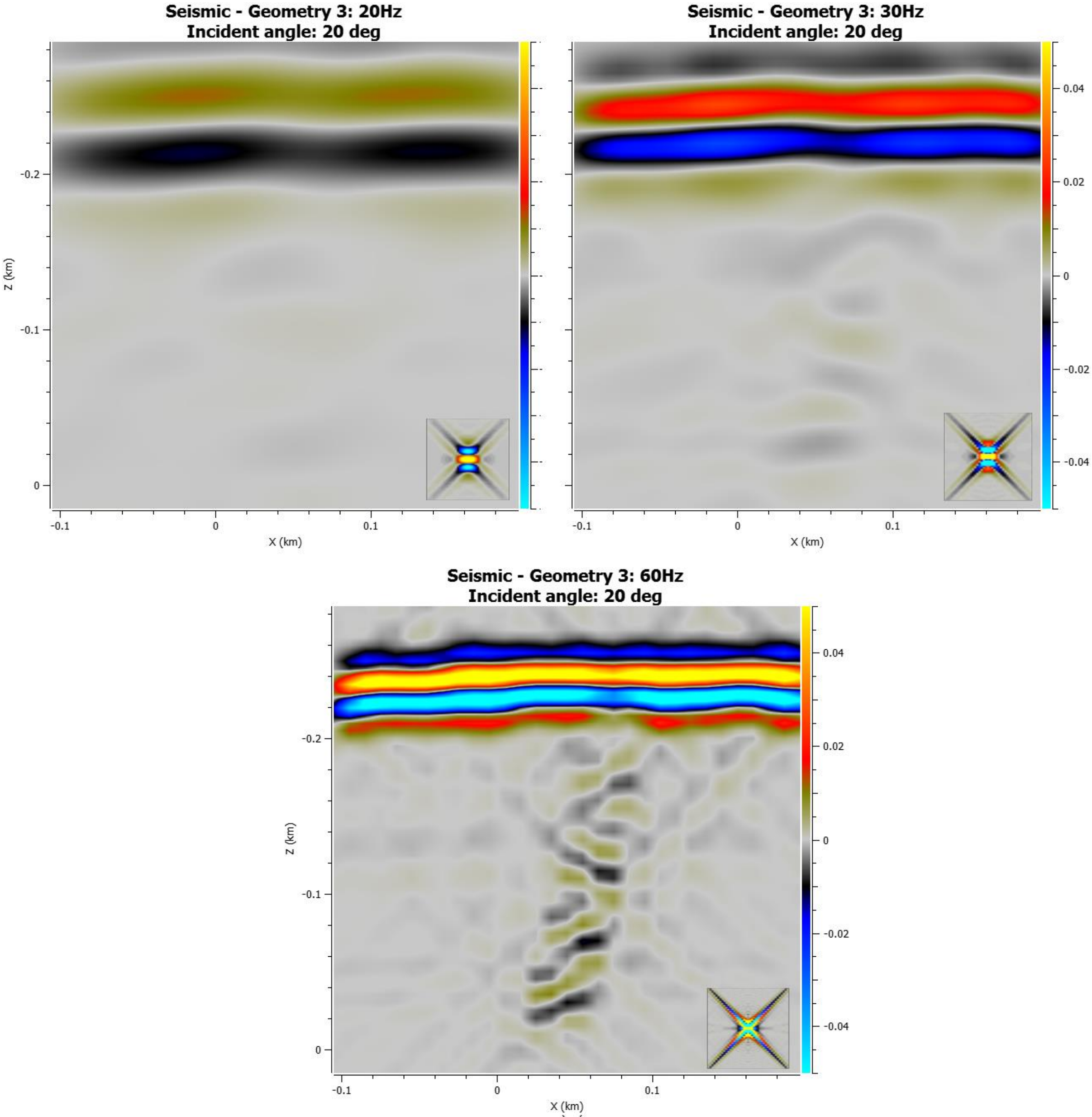

Figure 4.21: The results from the synthetic seismic simulation on the feeder dyke using properties for a sandstone/shale lithology. The frequencies used were 20Hz (top), 30Hz (middle), and 60Hz (bottom)

Organic rich shale lithology (Hekkingen Formation)

The sill is very well visible on all frequencies, but the dyke is only slightly visible on 30Hz and a little more visible on 60Hz. The overall impedance contrast is slightly higher than the sandstone/shale lithology due to the low Vp and Vs.

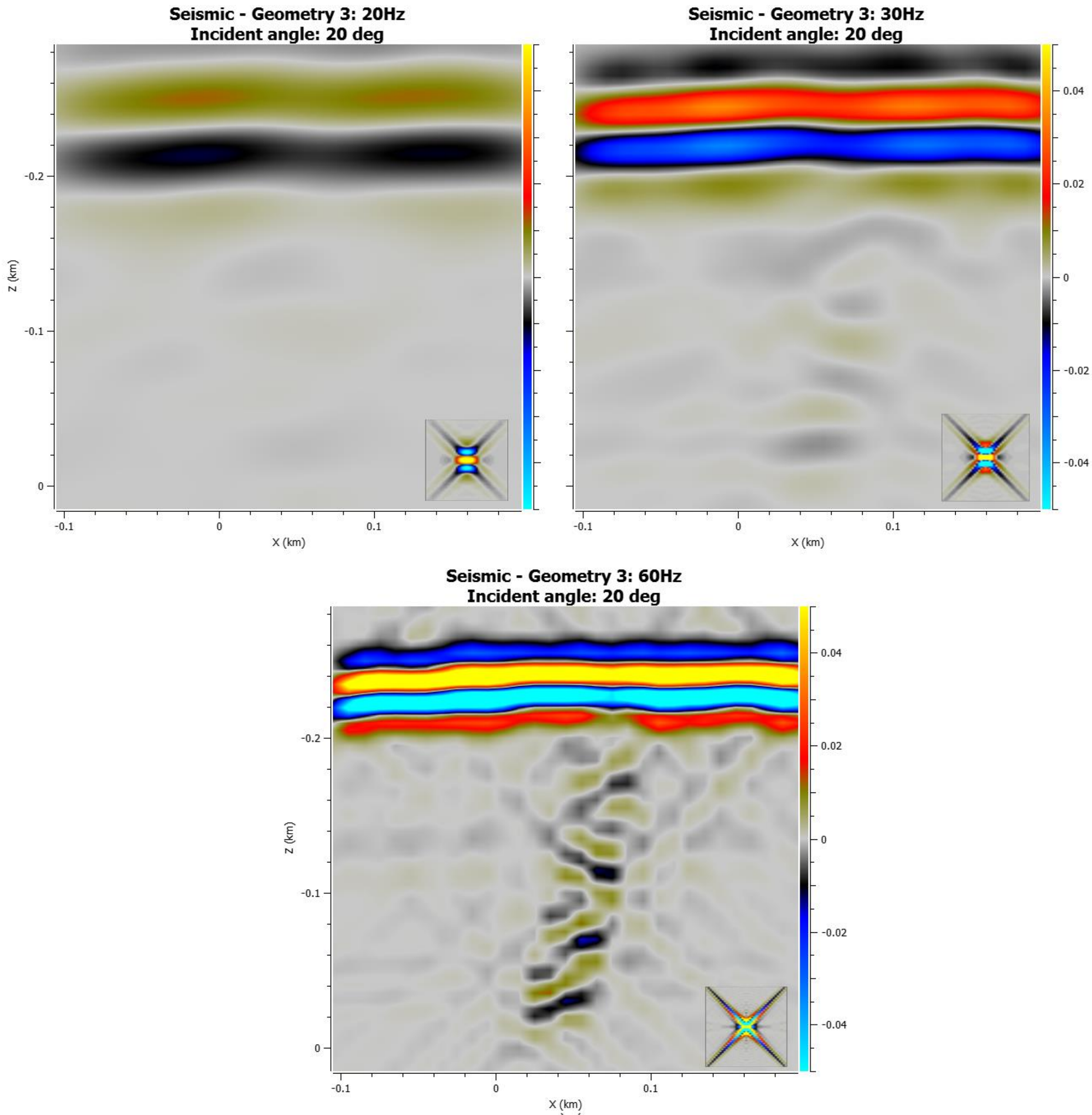

Figure 4.22: The results from the synthetic seismic simulation on the feeder dyke using properties for an organic rich shale lithology. The frequencies used were 20Hz (top), 30Hz (middle), and 60Hz (bottom)

Clean sandstone lithology (Realgrunnen Sbgrp)

The sill is visible on all frequencies, but the dyke is only slightly visible on 30Hz and a little more visible on 60Hz. The overall impedance contrast is slightly lower than the sandstone/shale lithology due to the high Vp and Vs.

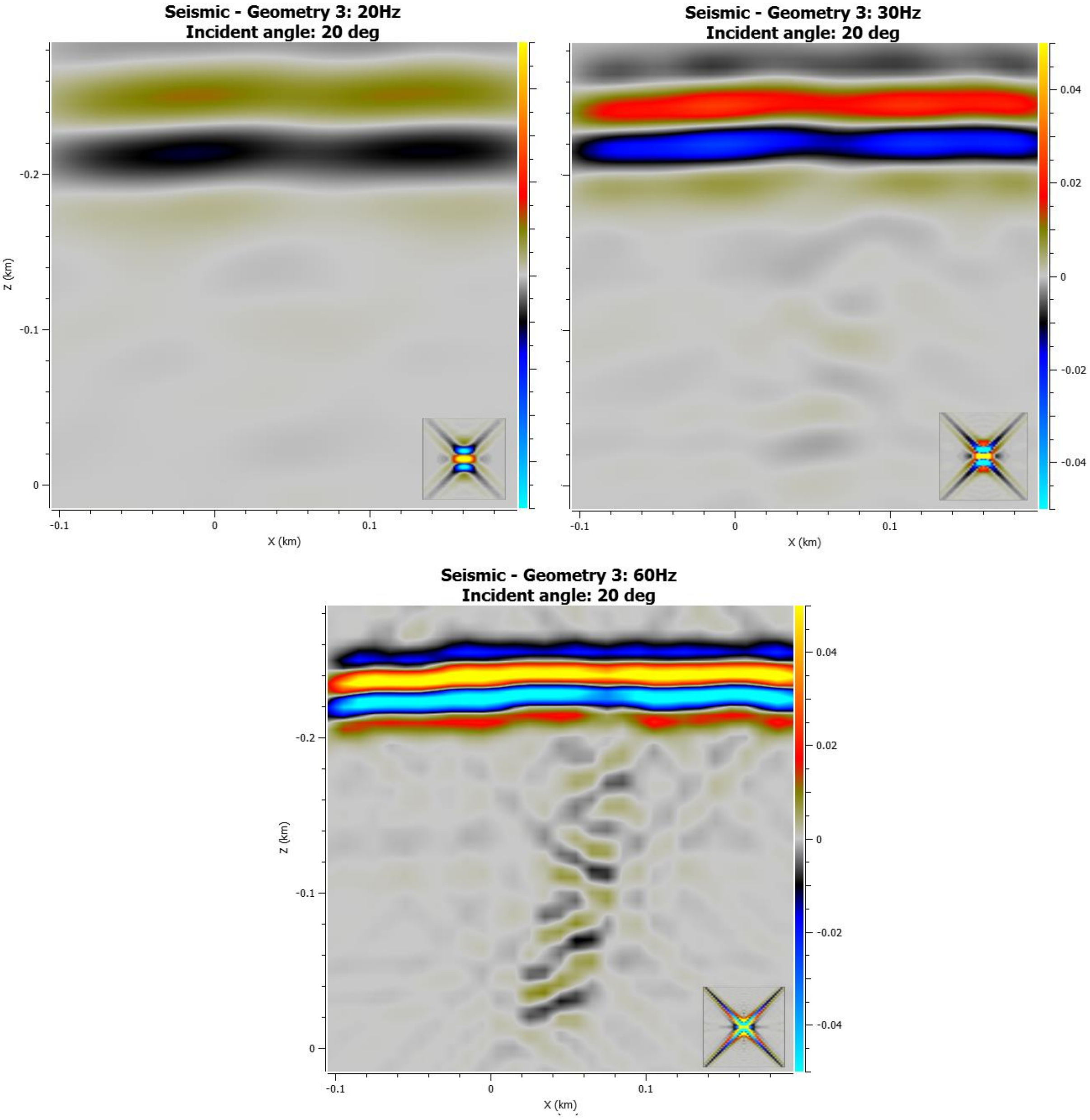

Figure 4.23: The results from the synthetic seismic simulation on the feeder dyke using properties for a clean sandstone lithology. The frequencies used were 20Hz (top), 30Hz (middle), and 60Hz (bottom)

Paleozoic carbonates lithology (Polarrev/ørn Formation)

The sill is slightly on all frequencies, but the dyke is only completely invisible on the 20Hz and 30Hz frequencies. It is slightly visible on 60Hz, but not enough to identify it as a separate feature. The reason for this is that the Vp and Vs of the host rock are similar the Vp and Vs of the intrusion, with only a slight difference in the density.

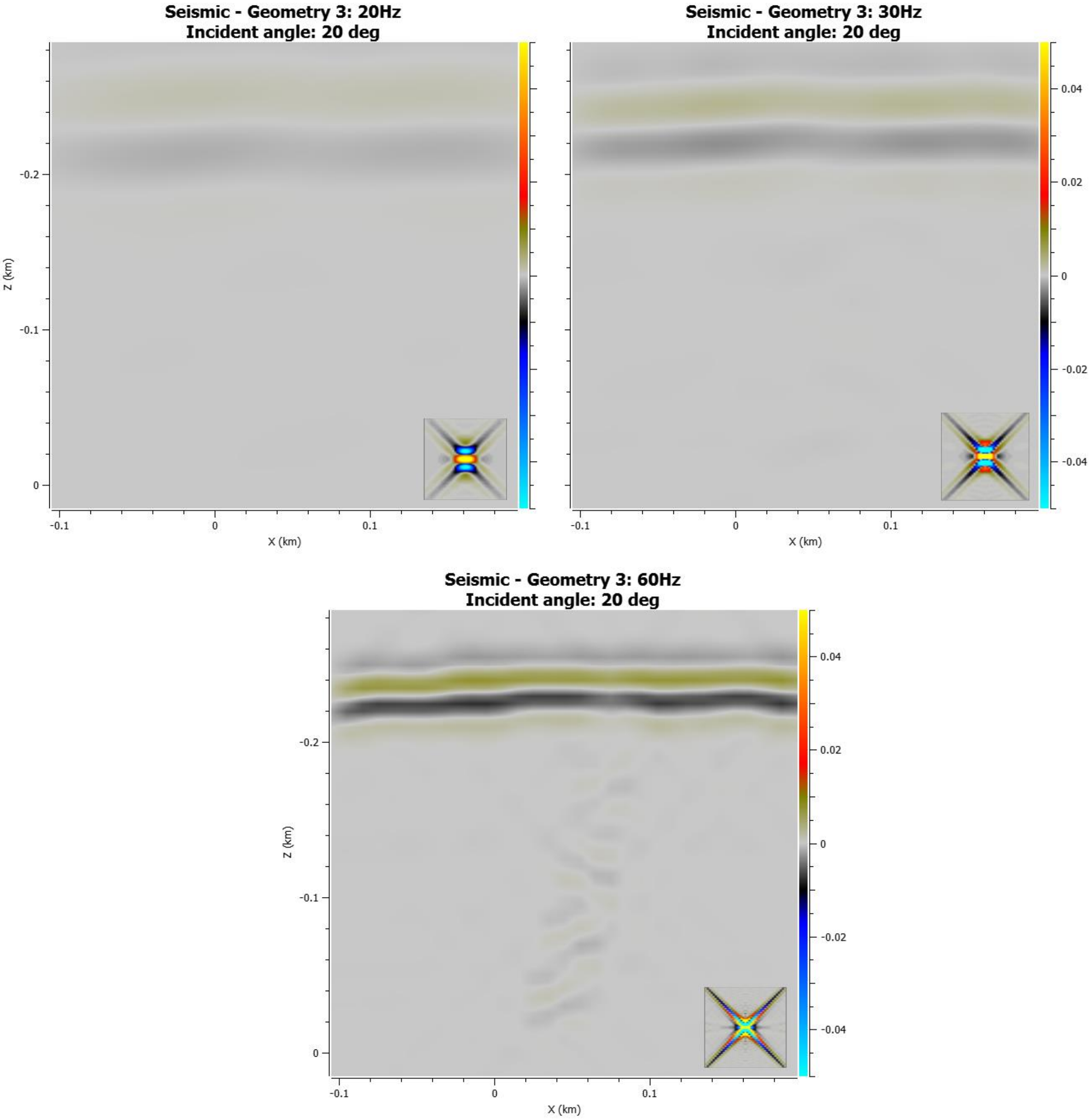

Figure 4.24: The results from the synthetic seismic simulation on the feeder dyke using properties for a Paleozoic carbonate lithology. The frequencies used were 20Hz (top), 30Hz (middle), and 60Hz (bottom)

To sum up, the impedance contrast for the straight sill should be sufficient in any lithology to view in seismic data, except for the carbonates. For the dyke however, the contrast is only high enough in a sandstone/shale or shale lithology (and maybe sandstone) with a high frequency (60Hz). Due to the orientation of the dyke, different angles of incidence are required to fully image the geometry. Figure 4.25 shows the original picture of the outcrop with the synthetic seismic data draped over it.

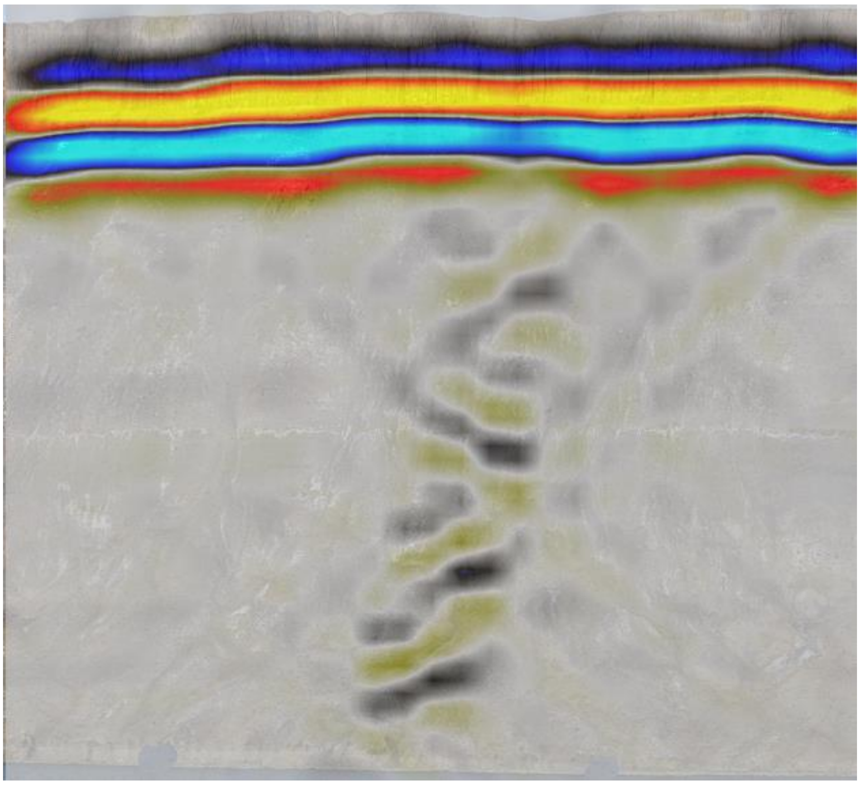

Figure 4.25: The original picture of the outcrop combined with the synthetic seismic (organic rich shale lithology, 60Hz). The dyke is only exposed on the beach

4.3.4 Geometry 4: Transgressive sill

The fourth geometry is sill with a transgressive section in the middle on Botneheia. The original picture of the outcrop is shown in figure 4.26 along with the 3-D model that was generated from the geometry of the outcrop. The properties that were used in each simulation are shown in table 4.7.

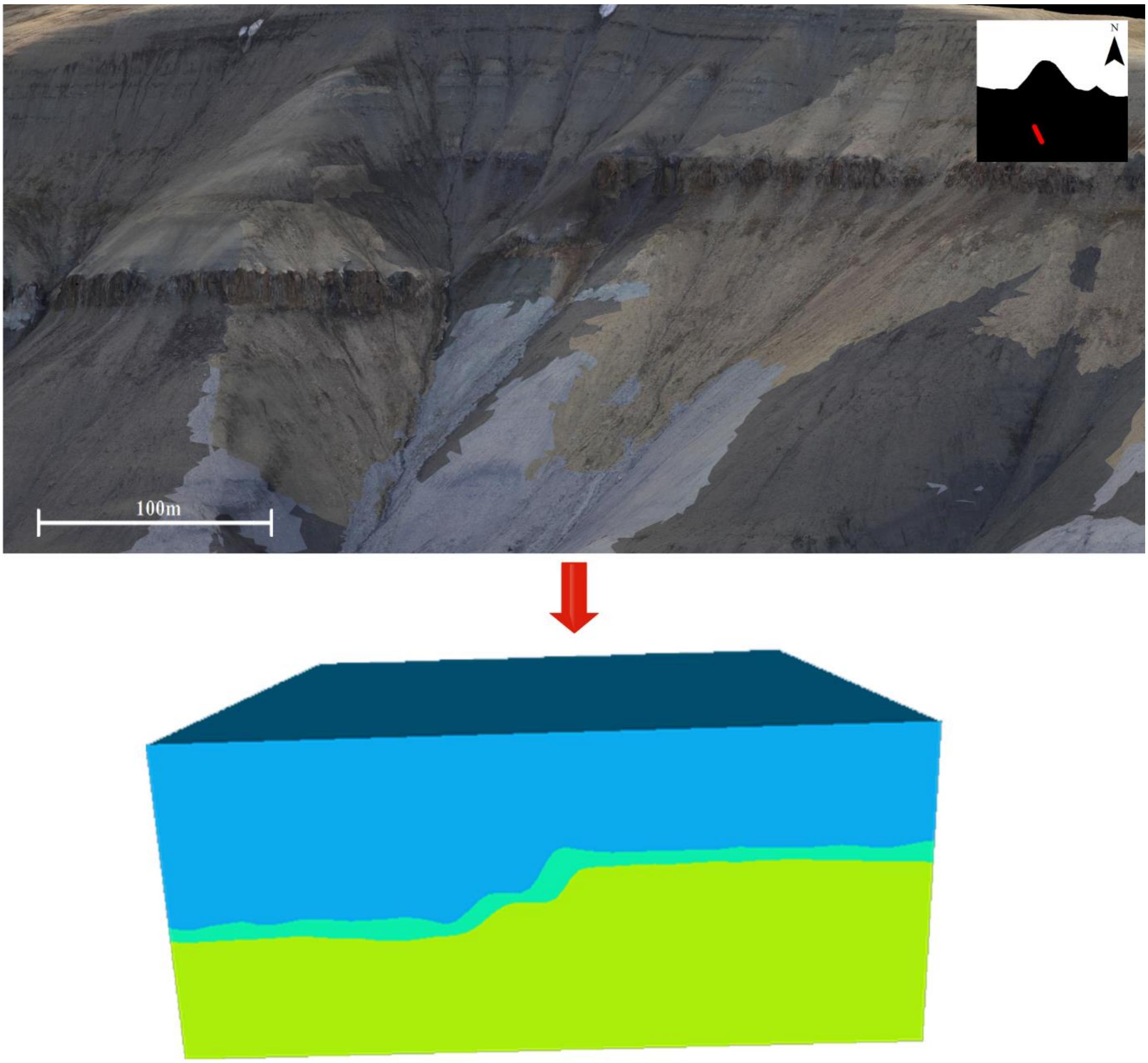

Figure 4.26: The transgressive sill at Botneheia

Table 4.7: The values used per test case for geometry 4

Test case	Formation	Vp	Vs	ρ
		Avg	**Avg**	**Avg**
Sandstone/shale	Snadd	**3500**	**1800**	**2.6**
Organic rich shale	Hekkingen	**3000**	**1600**	**2.4**
Clean sandstone	Realgrunnen Sbgrp	**4000**	**2500**	**2.4**
Carbonate	Polarrev/ørn	**6000**	**3000**	**2.7**
Doleritic intrusion	Diabasodden suite	**6000**	**3000**	**2.9**

Sandstone/shale lithology (Snadd Formation)

The sill is well visible on all frequencies, but it hardly retains the transgressive shape on 20Hz. The transgressive nature of the sill is more apparent on 30Hz and 60Hz.

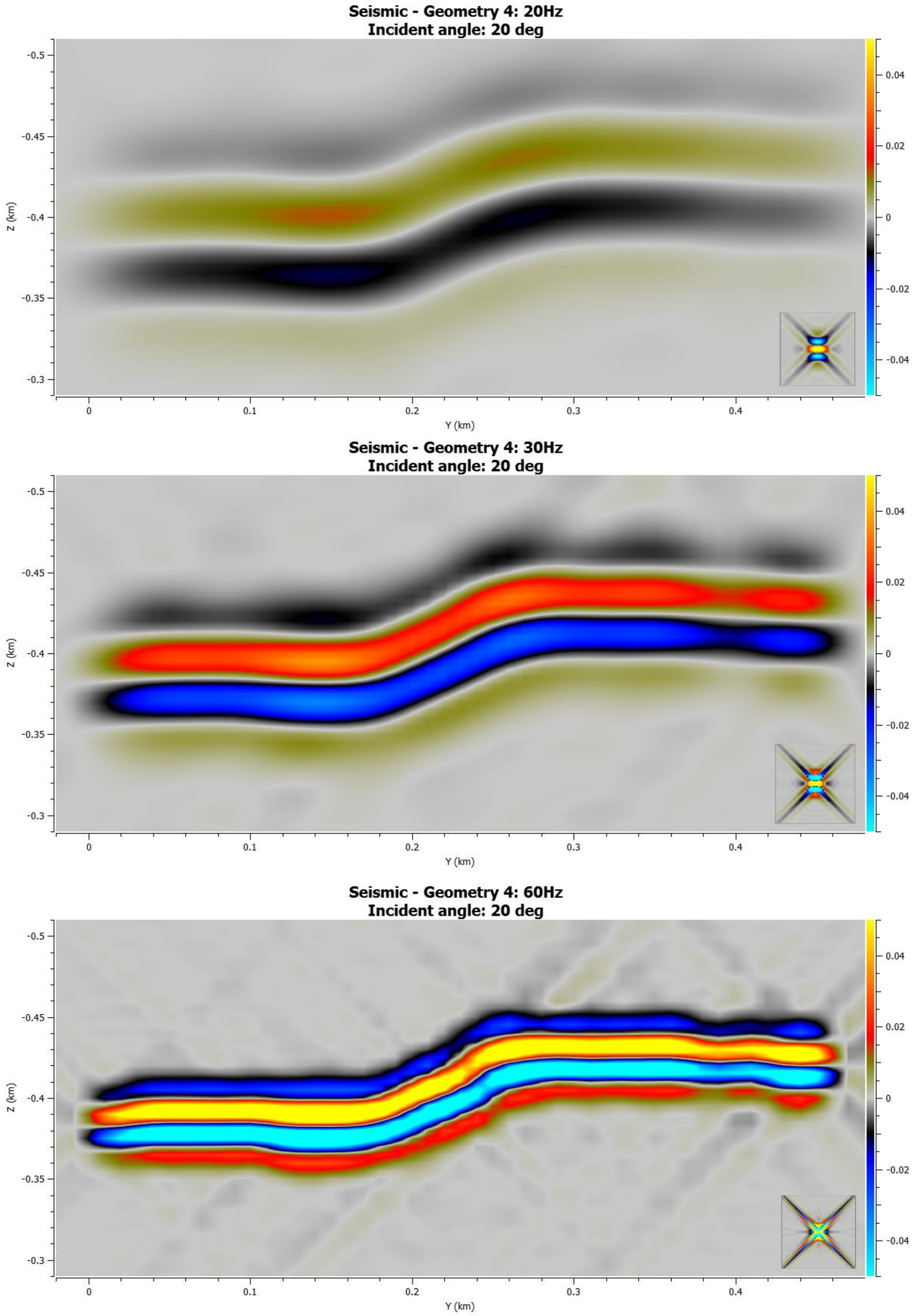

Figure 4.27: The results from the synthetic seismic simulation on the transgressive sill section using properties for a sandstone/shale lithology. The frequencies used were 20Hz (top), 30Hz (middle), and 60Hz (bottom)

Organic rich shale lithology (Hekkingen Formation)

The sill is very well visible on all frequencies, but the transgressive shape is hard to distinguish at a frequency of 20hz. The transgressive nature of the sill is more apparent on 30Hz and 60Hz. The overall impedance contrast is slightly higher than the sandstone/shale lithology due to the low Vp and Vs.

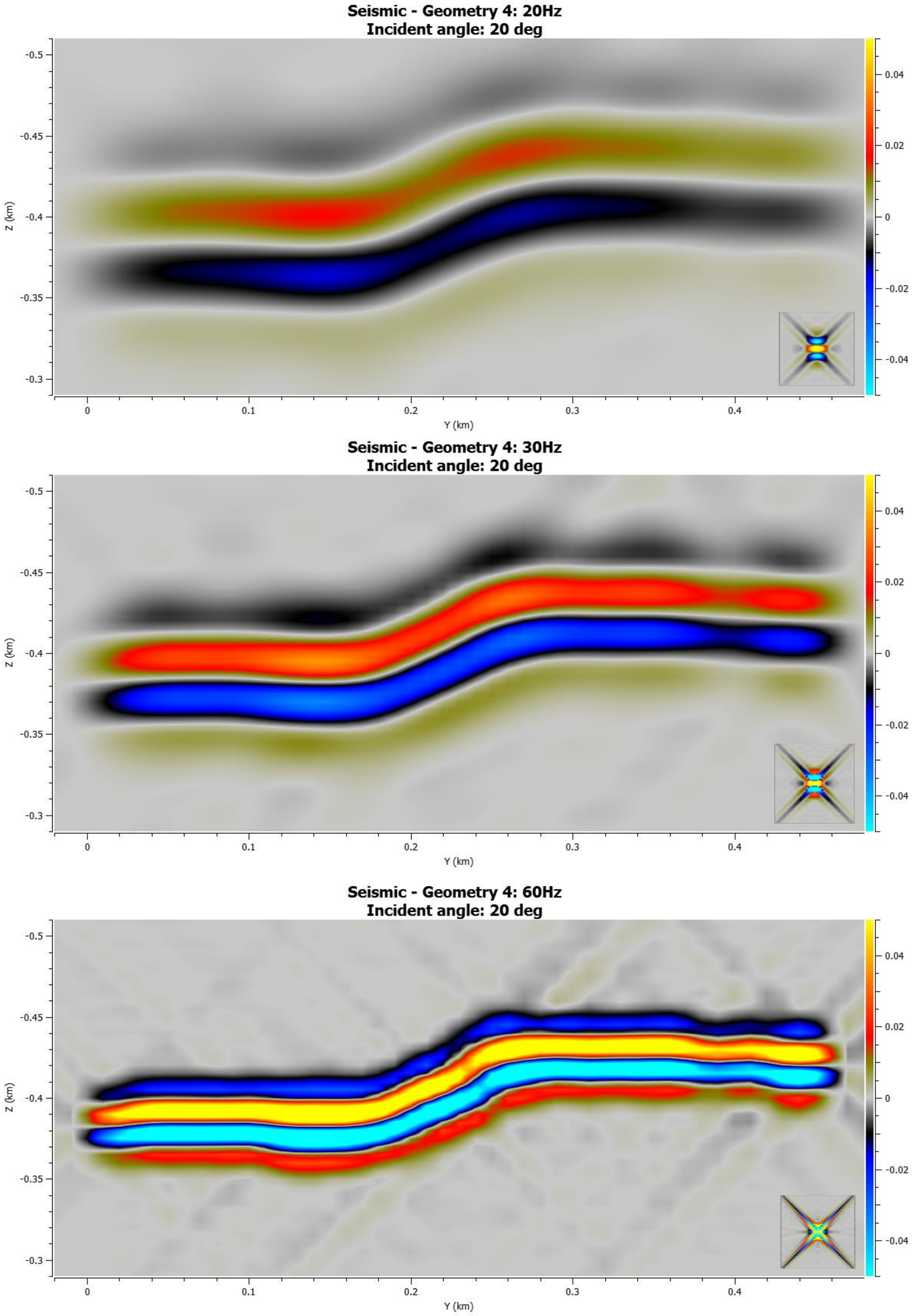

Figure 4.28: The results from the synthetic seismic simulation on the transgressive sill section using properties for an organic rich shale lithology. The frequencies used were 20Hz (top), 30Hz (middle), and 60Hz (bottom)

Clean sandstone lithology (Realgrunnen Sbgrp)

The sill is visible on all frequencies, but the transgressive shape is hard to distinguish at a frequency of 20hz. The transgressive nature of the sill is more apparent on 30Hz and 60Hz. The overall impedance contrast is slightly lower than the sandstone/shale lithology due to the high Vp and Vs.

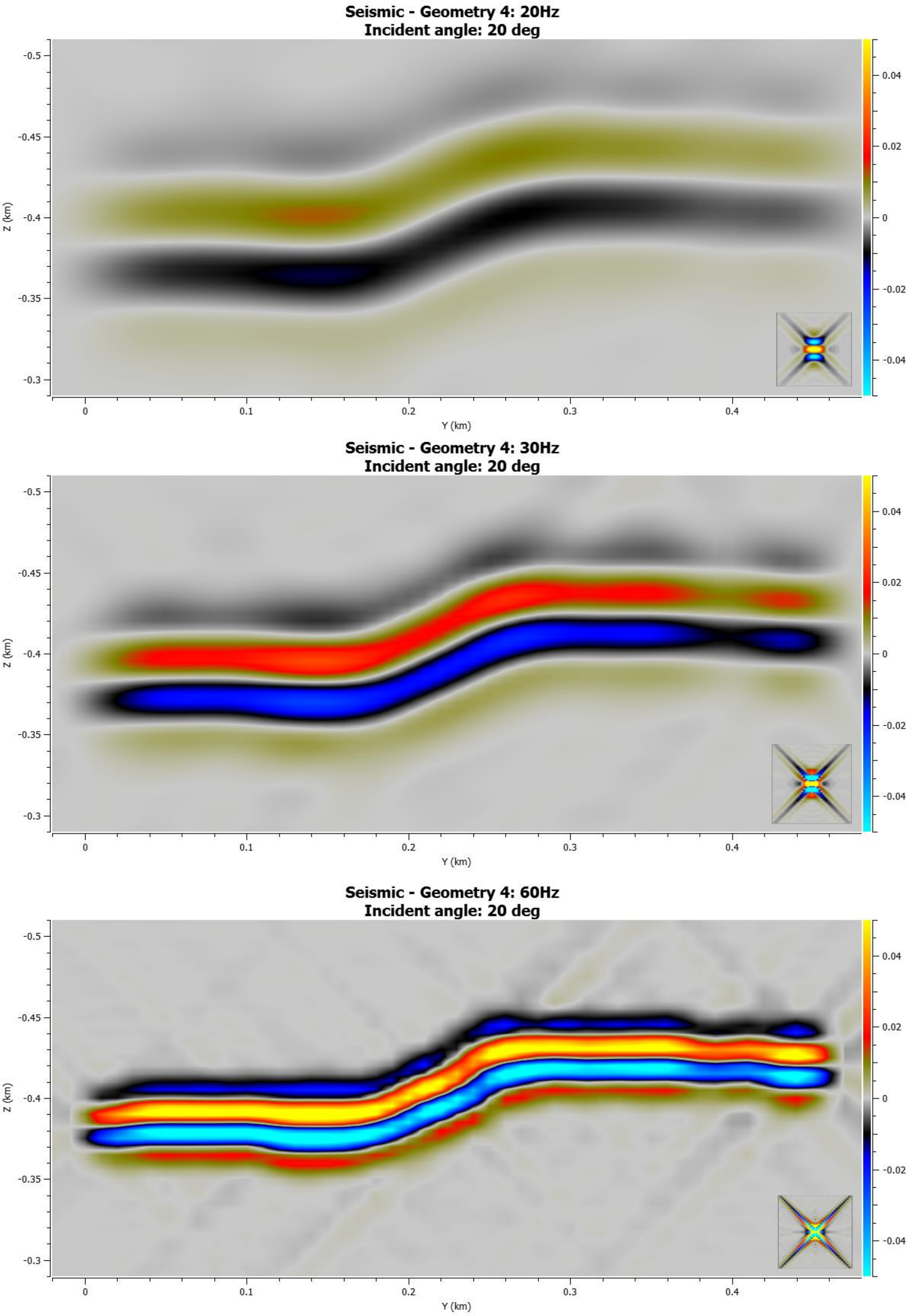

Figure 4.29: The results from the synthetic seismic simulation on the transgressive sill section using properties for a clean sandstone lithology. The frequencies used were 20Hz (top), 30Hz (middle), and 60Hz (bottom)

Paleozoic carbonates lithology (Polarrev/ørn Formation)

The sill is poorly visible on 20 and 30Hz, but has a higher visibility on 60Hz. Due to there being no difference between the Vp and Vs of the sill and the host rock, it would be almost impossible to distinguish this layer from other layers in real seismic data.

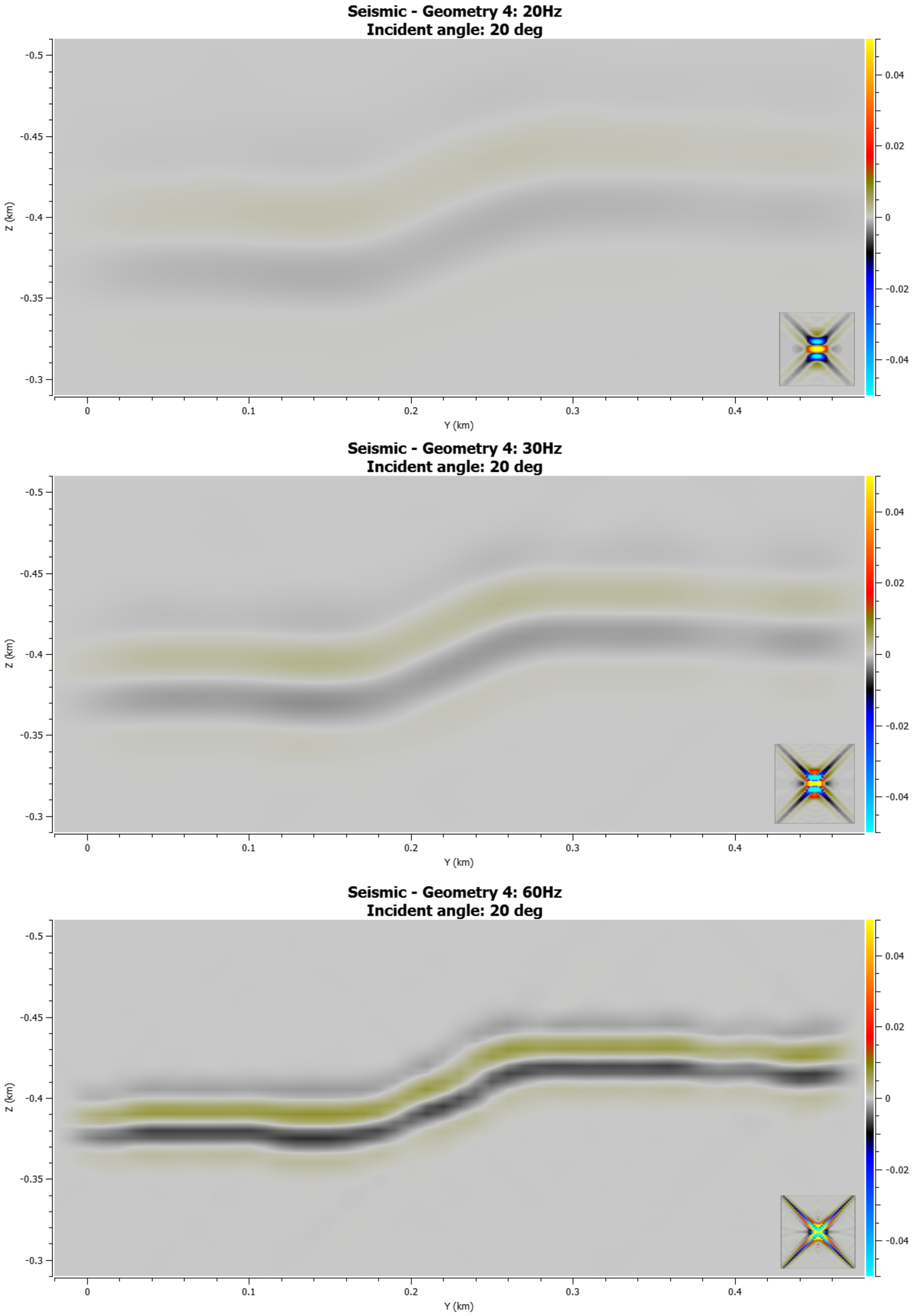

Figure 4.30: The results from the synthetic seismic simulation on the transgressive sill section using properties for Paleozoic carbonate lithology. The frequencies used were 20Hz (top), 30Hz (middle), and 60Hz (bottom)

To sum up, the impedance contrast for the sandstone/shale lithology is visible and should be identifiable on seismic data. The contrast for the organic rich shale lithology is slighly higher and should show up even more clearly in the data. The contrast for the clean sandstone lithology is slighly lower. The Paleozoic carbonate lithology has very poor visibility, and would make it very difficult to recognize the intrusion in seismic data. The transgressive section is difficult to retain on lower frequencies, as smoothing makes the transgressive effect less pronounced. Therefore it can be assumed that on lower frequencies the geometry would be difficult to identify in seismic data, unless the impedance contrast is very high. Figure 4.31 shows the original picture of the outcrop with the synthetic seismic data draped over it.

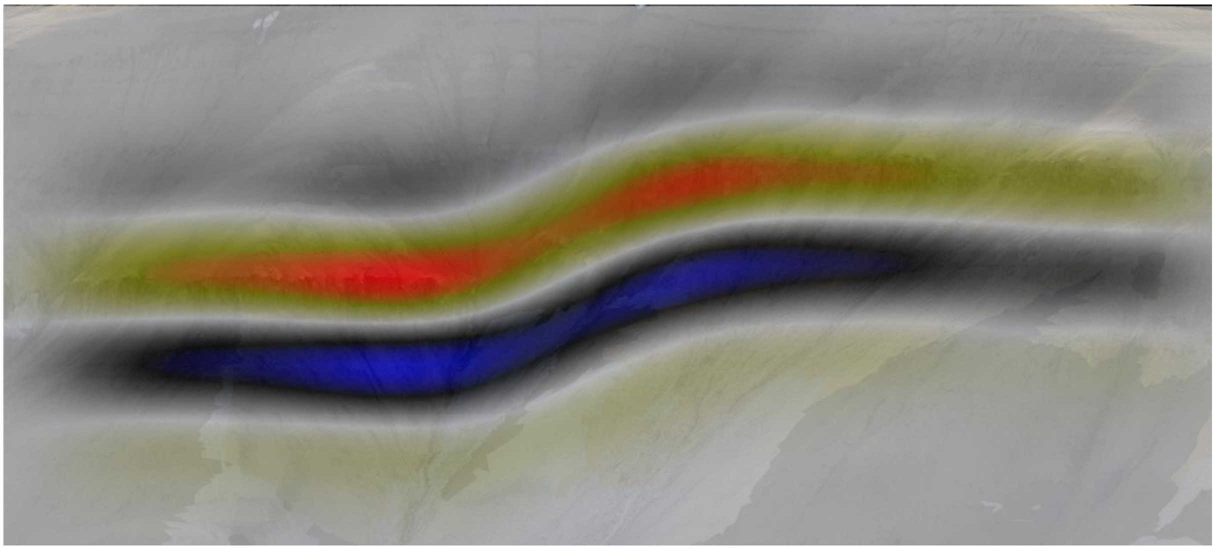

Figure 4.31: The original picture of the outcrop combined with the synthetic seismic (Sandstone/shale lithology, 20Hz)

4.3.5 Geometry 5: Stacked sills

The fifth geometry shows 2 outcrops which are stacked above each other. The top sill has a dipping transgressive section and the lower sill is straight. The original figure of the outcrop and the 3-D cube that was modelled after this outcrop are both shown in figure 4.32. The properties that were used in each simulation are shown in table 4.8.

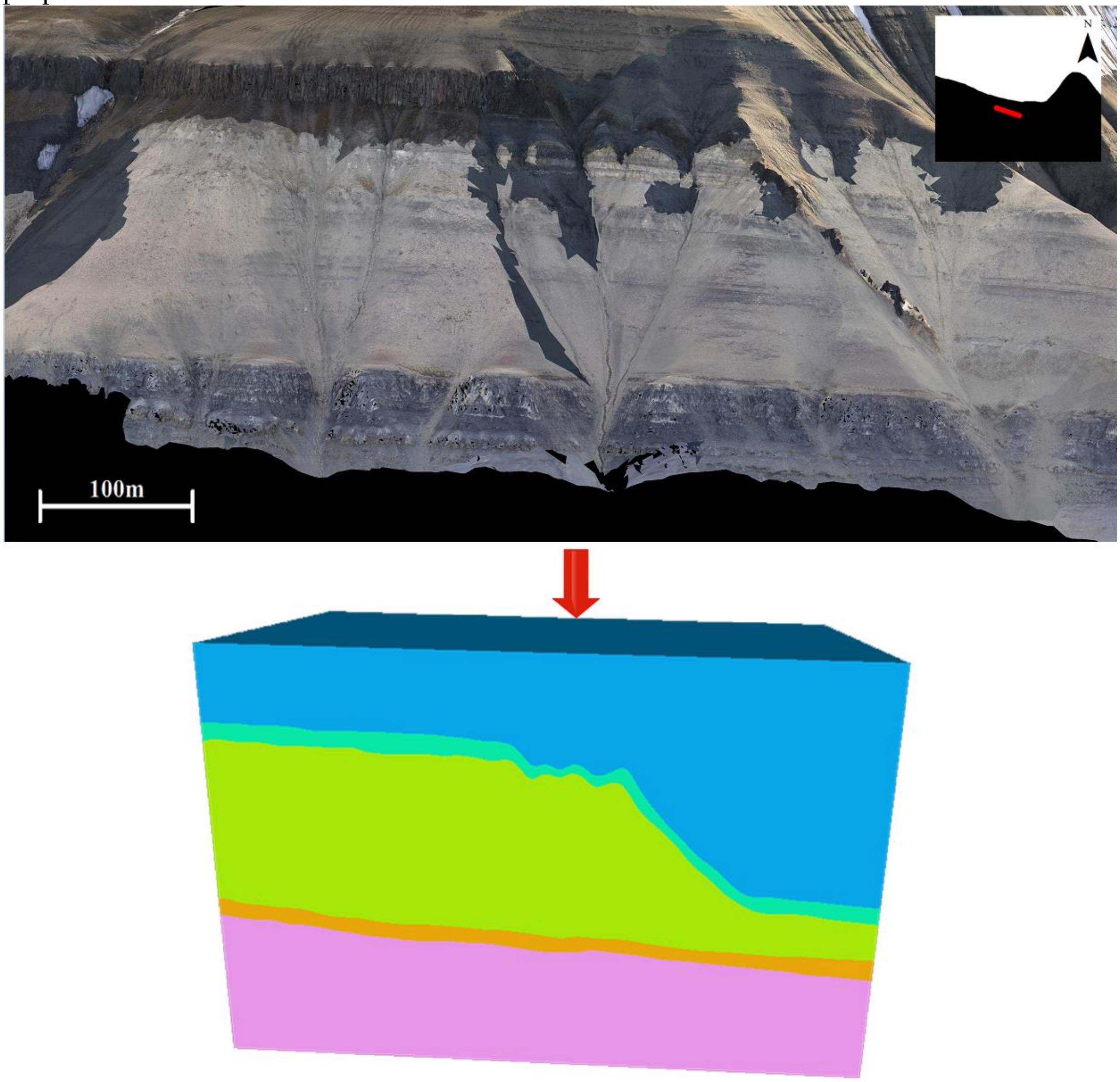

Figure 4.32: The stacked sills at Botneheia

Table 4.8: The values used per test case for geometry 5

Test case	Formation	Vp	Vs	ρ
		Avg	**Avg**	**Avg**
Sandstone/shale	Snadd	**3500**	**1800**	**2.6**
Organic rich shale	Hekkingen	**3000**	**1600**	**2.4**
Clean sandstone	Realgrunnen Sbgrp	**4000**	**2500**	**2.4**
Carbonate	Polarrev/ørn	**6000**	**3000**	**2.7**
Doleritic intrusion	Diabasodden suite	**6000**	**3000**	**2.9**

Sandstone/shale lithology (Snadd Formation)

Both sills are well visible on all frequencies, but on lower frequencies the signals can blend into each other right of the transgressive section of the top sill due to their close proximity to each other. On higher frequencies it is easier to distinguish the intrusions.

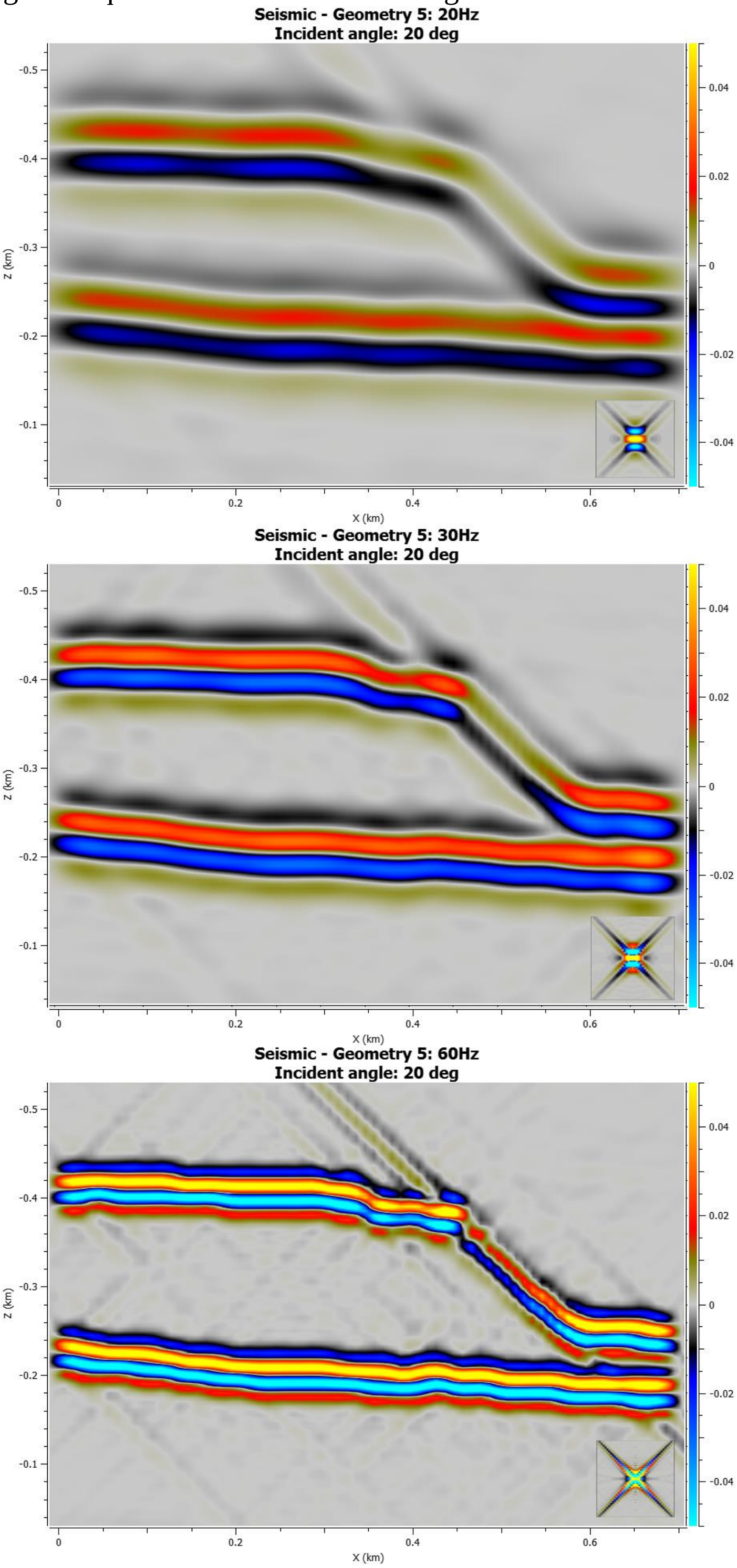

Figure 4.33: The results from the synthetic seismic simulation on the stacked sills using properties for a sandstone/shale lithology. The frequencies used were 20Hz (top), 30Hz (middle), and 60Hz (bottom)

Organic rich shale lithology (Hekkingen Formation)

Both sills are well visible on all frequencies, but on lower frequencies the signals can blend into each other right of the transgressive section of the top sill due to their close proximity to each other. The impedance contrast is slightly higher than the sandstone/shale lithology.

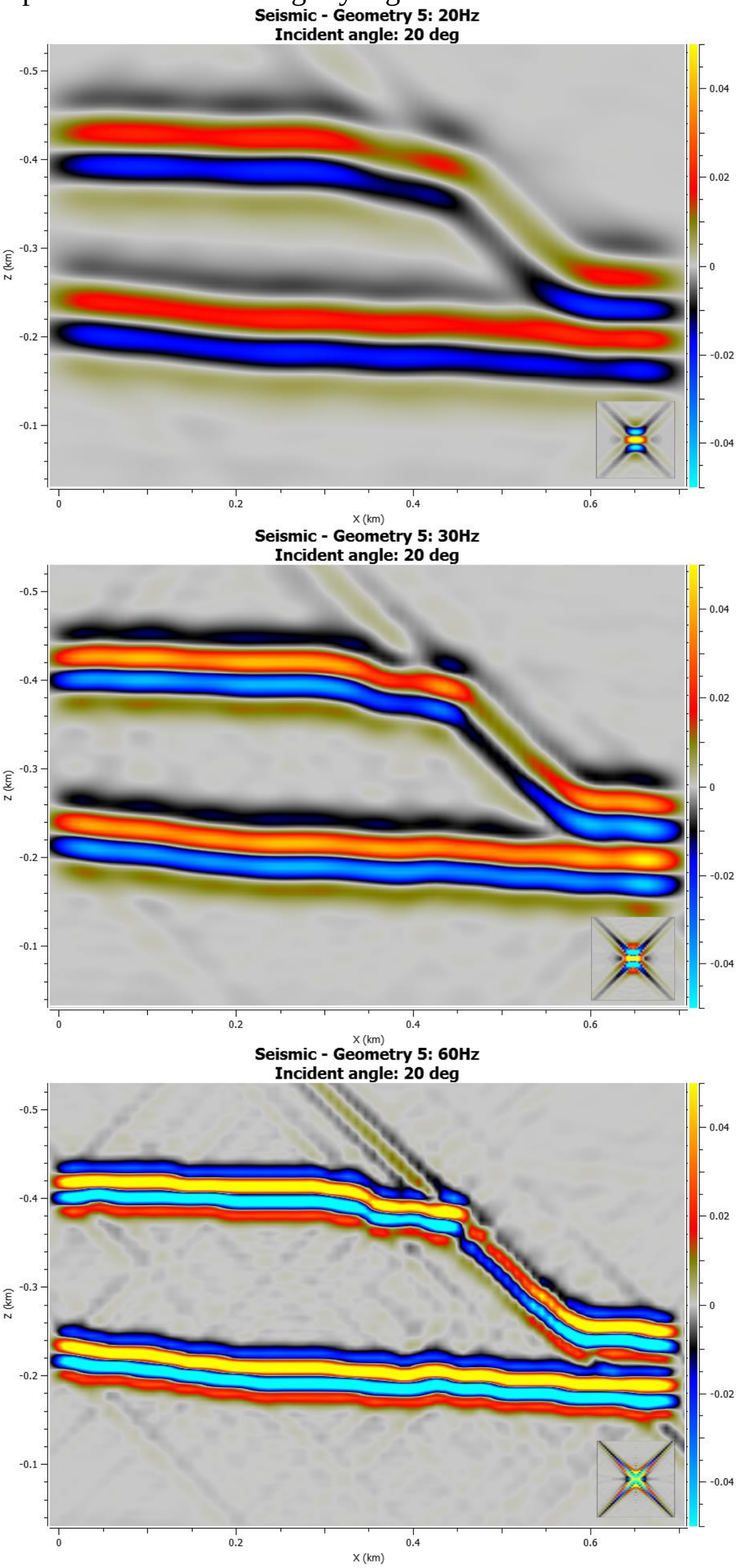

Figure 4.34: The results from the synthetic seismic simulation on the stacked sills using properties for an organic rich shale lithology. The frequencies used were 20Hz (top), 30Hz (middle), and 60Hz (bottom)

Clean sandstone lithology (Realgrunnen Sbgrp)

Both sills are visible on all frequencies, but on lower frequencies the signals can blend into each other right of the transgressive section of the top sill due to their close proximity to each other. The impedance contrast is slightly lower than the sandstone/shale lithology.

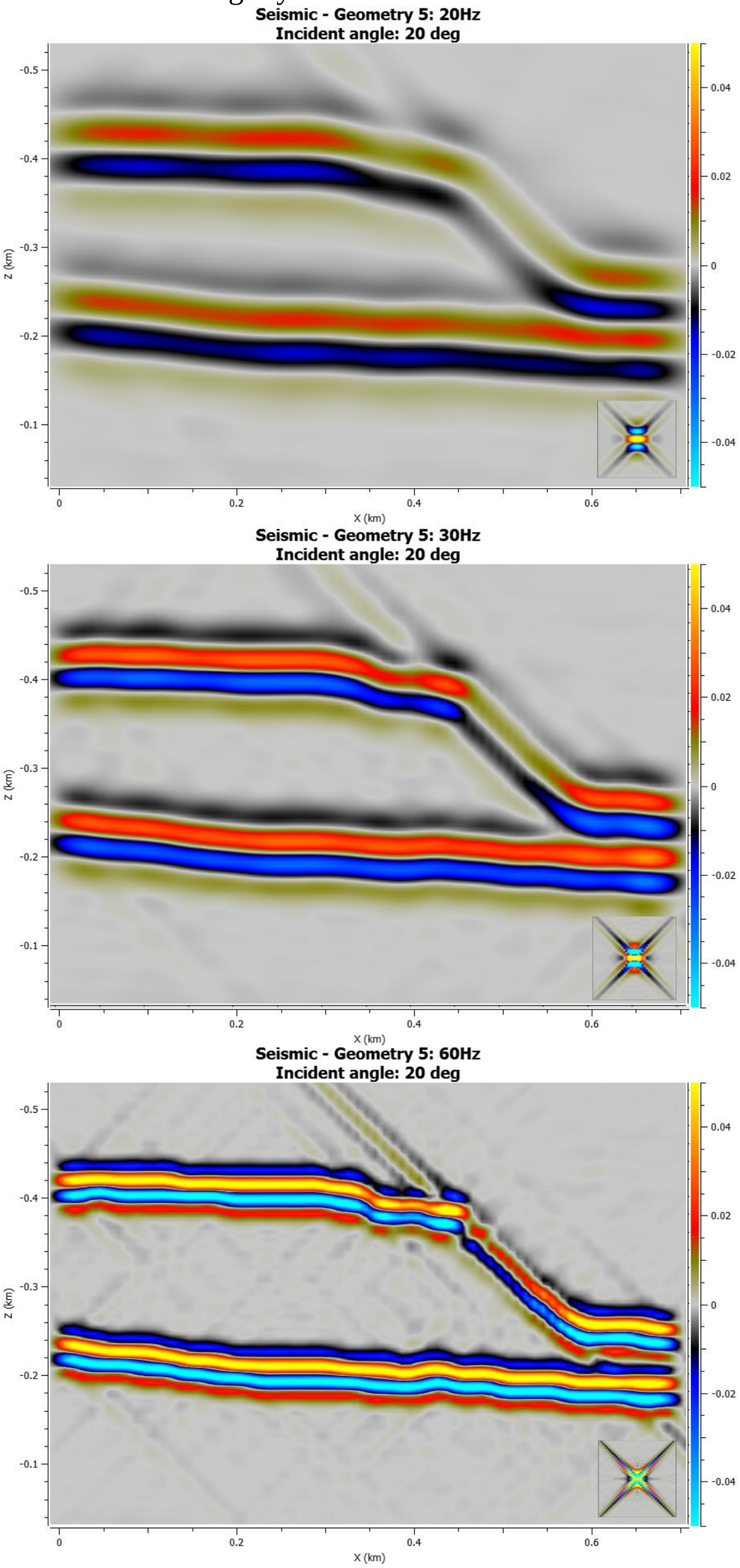

Figure 4.35: The results from the synthetic seismic simulation on the stacked sills using properties for a clean sandstone lithology. The frequencies used were 20Hz (top), 30Hz (middle), and 60Hz (bottom)

Paleozoic carbonates lithology (Polarrev/ørn Formation)

Both sills are almost invisible on lower frequencies and the signals can blend into each other right of the transgressive section of the top sill due to their close proximity to each other. On higher frequencies the contrast would likely still be too low to identify the sills.

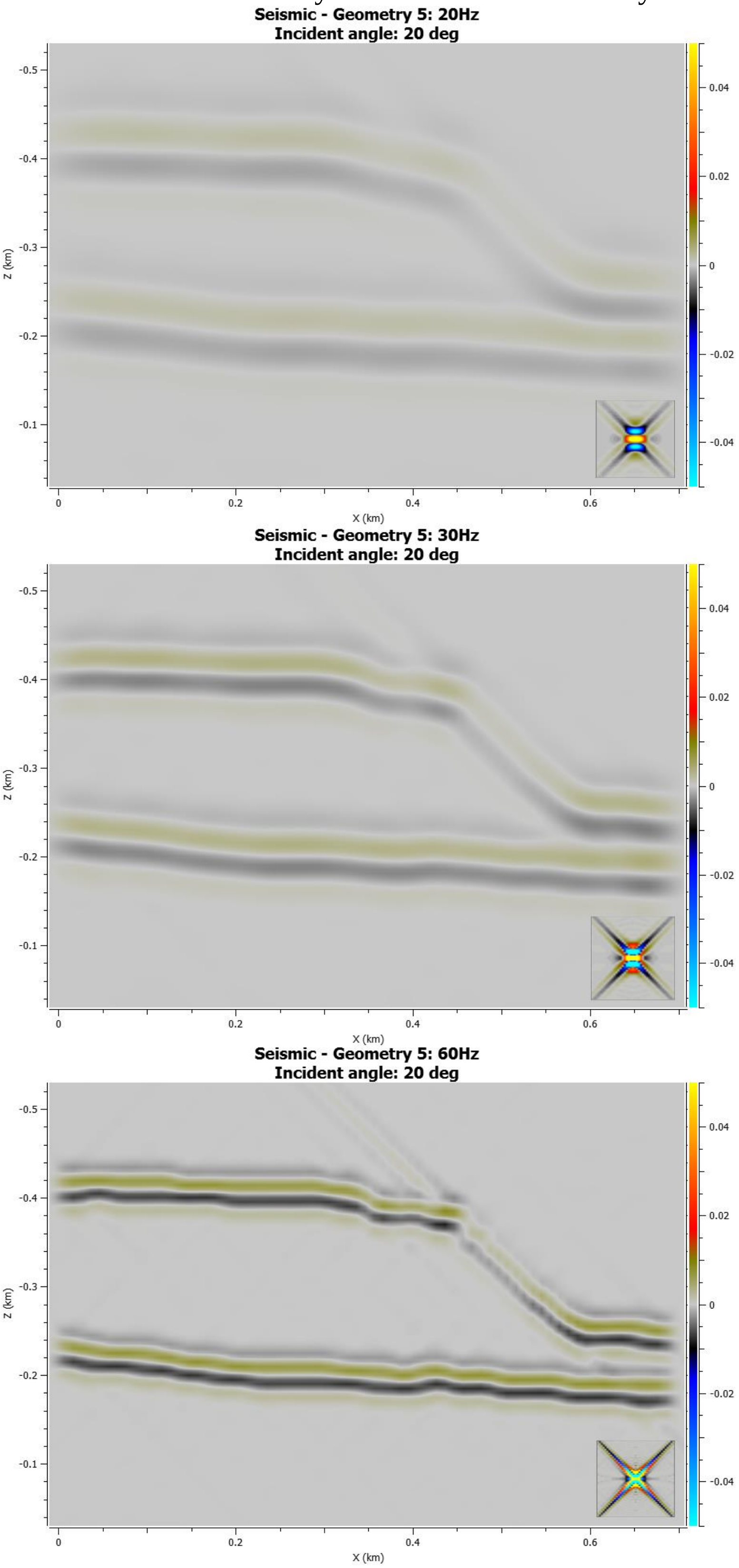

Figure 4.36: The results from the synthetic seismic simulation on the stacked sills using properties for a Paleozoic carbonate lithology. The frequencies used were 20Hz (top), 30Hz (middle), and 60Hz (bottom)

To sum up, the impedance contrast for the sandstone/shale lithology is visible and should be identifiable on seismic data. The contrast for the organic rich shale lithology is slighly higher and should show up even more clearly in the data. The contrast for the clean sandstone lithology is slighly lower. The Paleozoic carbonate lithology has very poor visibility, and would make it very difficult to recognize the intrusions in seismic data. Due to the close proximity of the two sills after the transgressive section of the top sill, it would be difficult to tell whether there are two intrusions, or one thicker intrusion on lower frequency settings. On higher frequencies the shapes are easier to tell apart. Figure 4.37 shows the original picture of the outcrop with the synthetic seismic data draped over it.

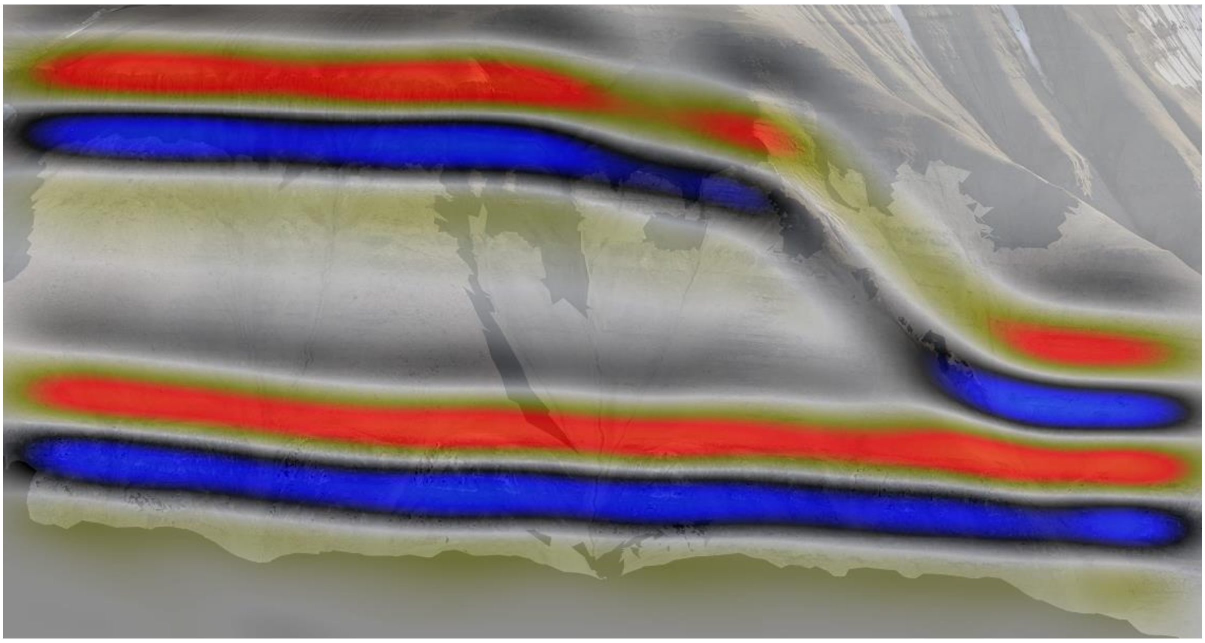

Figure 4.37: The original picture of the outcrop combined with the synthetic seismic (Sandstone/shale lithology, 20Hz)

5 Discussion

In this section the results from the last section will be evaluated and discussed. First, the results from the intrusion analysis in ArcGIS will be discussed. This will include the combined results and the different formations individually. After that, the synthetic seismic results will be discussed. The discussion will be divided into separate parts, discussing a different outcrop in each part. After this, a general summary regarding evaluation of the different geometries will follow.

5.1 Intrusion analysis

The intrusion analysis shows which formations are most likely to function as a host rock for the Diabasodden suite dolerites. The results show that the Kapp Starostin formation is the most prevalent host rock. The Kapp Starostin formation generally consists of siltstone and sandstone. Therefore this formation (or a Barents Sea equilavent) would have slightly less contrast than the sandstone/shale test case, and slightly more than the clean sandstone test case, although these already look fairly similar to each other. Regarding the groups, it is shown that the Gipsdalen, Tempelfjorden, Kapp Toscana and Tempelfjorden groups all have similar amounts of intrusions. The Adventdalen group and Billefjorden group have less, with the Billefjorden group having the least amount of intrusions. These are also the youngest and oldest groups in which the Diabasodden suite dolerites have intruded. Therefore, it could be a matter of depth of the formation during the time of intrusion. It should be noted that the analysis was based on the proximity of host rock units; units that were adjacent to an intrusion unit was classed as a host rock. Not all units that are adjacent are host rocks though, and in order to get a completely accurate overview of the amount of host rocks for the Diabasodden suite, one would have to go through the data manually.

The results for the dyke vs sill analysis show that sills on Svalbard amount to 91% of the intrusions, and dykes to 9% of the intrusions. Eide et al., (2016) came to a similar conclusion:'From the 22 km section presented in this paper, 90 – 95% of the intrusive material visible in the section is in the form of sills, with only 5 – 10% represented by dykes'. This suggests that within a sedimentary basin at depth, a strong bias will exist towards horizontal or bedding-parallel fluid barriers, rather than vertical fluid barriers (Eide et al., 2016). The exceptions to this would be within dyke swarms, which are more commonly associated with igneous centres (Jerram & Bryan 2015).

5.2 Synthetic seismic analysis

The first geometry shows a bowl-shaped sill. While the shape of the sill is clearly visible at lower incidence angles, it becomes harder to distinguish the shape at higher incidence angles. Due to the scale of the sill, incidence angles over 30 will likely result in loss of small details due to lateral smoothing. It is also worthy to mention that while at higher frequencies (60Hz) the sill shows a very high impedance contrast, certain features might be lost at lower frequencies (20Hz) due to the smoothing effect. The exception to this might be on dipping features, where on higher frequencies the dipping section might lose some visibility. The different host rock lithologies tested also offer different results. Whereas organic rich shales show a large impedance contrast, the Paleozoic carbonates offer very little contrast. In the test case, the only difference between the intrusion and the surrounding host rock is the density of the lithologies, which explains the low visibility of the intrusion in this case.

The second geometry shows a straight sill as you can encounter in many places on Svalbard. This geometry is tested as an offset to the other geometries to see how a straight sill compares to sills and dykes with more complicated geometries. While in general the results are similar to the first geometry, it should be noted that changing the incidence angle has less effect on the imaging of the sill. Due to the lack of a dip in the geometry, a loss of detail due to lateral smoothing is less likely. However, due to the lack of a complicated shape, the intrusion would be difficult to identify on actual seismic data, because it would be undistinguishable from a normal lithology change.

The third geometry shows a dyke intrusion on the beach of Rotundafjellet. However, due to the sub-vertical geometry and it being a non-horizontal reflector, it is almost impossible to identify in the synthetic seismic image at lower frequencies. At higher frequency ranges the dyke is still only barely visible and pushing the limits of both horizontal and vertical resolution. It shows up in the data, but it is hardly distinguishable as a separate feature. It can be assumed that vertical intrusions on this scale will be hard to identify in regular seismic data. In most studies of offshore, subsurface intrusive complexes that utilize seismic reflection data, it is not possible to constrain the role of un-imaged vertical, dyke-like sources in transporting magma through the sedimentary fill of a basin (Schofield et al. 2015; Lecomte et al. 2016) This does not offer any explanation the geometry of the dyke however. In order to test the geometry further, a thicker dyke has been used using the same shape as the original intrusion (Figure 5.1). With low frequency, the thicker dyke appears to have a pull up effect on the straight sill, but is still invisible. Only on 60Hz it appears more visible. While it would still be difficult to identify it on this scale in offshore seismic data, it can be possible using the right frequency and incidence angle. For this geometry it shows that using a larger incidence angle (>30) actually benefits the visibility of the intrusion due to its vertical orientation. The straight sill at the top of the simulation yields the same results as the second geometry as they have similar shapes.

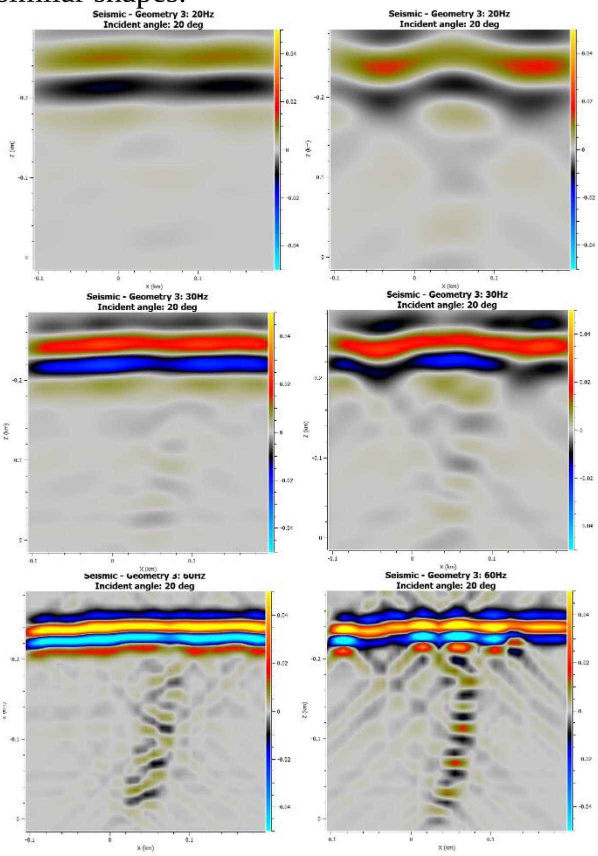

Figure 5.1: The original seismic model on the left, and the thicker seismic model on the right.

The fourth geometry shows a transgressive sill near Botneheia. The results for this geometry are fairly similar to the results of the first geometry. It should be noted however that the incidence angle is more important on this geometry than on the first one. Due to its transgressive nature, the parts of the intrusion on either side of the dip can be mislabeled as separate layers. If the incidence angle is >30, the dip would be hardly visible, which would make it difficult to identify it as part of the same layer. This pitfall should also be considered while identifying sills in a large sill complex, where there are several sills and it might be even more difficult to see where one intrusion ends and another begins.

Geometry 5 shows 2 stacked sills on the Botneheia mountain. The different lithologies show the same results as the other geometries; Low/no impedance contrast between the intrusion and the Paleozoic carbonates, high impedance contrast between the organic rich shales and the intrusion, with the contrasts for the clean sand and the sand/shale lithologies being somewhere in between. However, due to the stacking of the sills and their close proximity, they are hard to separate from each other on low frequencies (<20Hz), especially with a high impedance contrast. Therefore, the assumption can be that higher frequencies (>30Hz) are more suited to display stacked sills which are in close proximity to each other in seismic data. Changing the incidence angle to >30 might result in the dip of the top intrusion becoming invisible, which can result in the lower half of the top intrusion being identified as part of the second intrusion. It should be considered that this is simulated data however, and some aspects of seismic imaging which occur in real seismic data might not show up on the synthetic seismic. Seismic attenuation is one of those effects, which would mean that a high amplitude layer can result in a loss of seismic energy, causing the layers below to show a lower contrast. In this case that would mean that even though the properties for both sills are the same, the lower sill should have a lower seismic impedance contrast than the top layer.

It should be considered for all geometries that were tested that the elastic properties (P-wave velocity, S-wave velocity and density) of both the host rock and intrusion can vary significantly. While in these test cases the elastic properties have been set to a static number, there often is a high variation in these numbers. Intrusion and host rock properties are never completely uniform throughout the lithology, so in a way this research only tests the seismic imaging of these geometries in an ideal situation. This is also discussed in Anell et al., (2016) where a similar case is done for growth faults on edgeøya. The modelled impedance contrast might be the result of the synthetic models being simplified as they are based solely on observations of onshore lithologies, and hence lacking information about higher velocity/density contrasts generated by erosion and/or condensation (Anell et al., 2016). Considering the ranges in which these properties occur, it should also be considered that variations between the intrusion and the host rock are not large by definition. Even in these test cases there are lithologies that offer no difference between the host rock properties and the intrusion properties. A good example of this is that of the Paleozoic carbonates, which have been tested with a Vp estimated to be 6000 m/s, identical to the Vp used for the intrusion. This creates the possibility of not only small differences in properties, but also overlapping property ranges. This would make it almost impossible to identify some igneous intrusions in seismic data, regardless of the shape. For this reason, variations in seismic impedance that must be considered for the modelling of seismic data range from large contrasts to no contrast. Therefore it can be stated that not all intrusions can be identified just on the assumption of a high impedance contrast. Host rocks and intrusions can have a high impedance contrast, but don’t necessarily have to.

Another aspect of these intrusions to consider is the scale on which they occur. Due to the possibility of losing details at higher angles of incidence at this scale, it might be beneficial to

compare images obtained at different angles. This might make it possible to differentiate between smoothing effects and actual seismic geometries. If images with a small angle of incidence show different seismic patterns than the images with a higher angle, the small-angle images are probably more trustworthy.
Seismic attenuation is also an issue. While in the simulation the depth of the intrusions was classed as being above sea level, it should be noted that igneous outcrops on seismic scale are generally found far below sea level. This would make the data sensitive to seismic attenuation, or a loss of seismic energy in the propagating wave, which would result in a lower resolution of the seismic data.

Anell et al. (2016) came to the following conclusion: 'Modelling of various features on the scale identified in the outcrops at Kvalpynten - sandstone lenses and channels, igneous intrusions, IHS - suggests that most generate relatively weak seismic signatures at high velocities. Non-fractured subhorizontal igneous intrusions are likely to create a strong impedance contrast, although complex vertical connections will probably not be distinguishable, and a lower velocity contrast would make them relatively indistinct from massive sandstones. The scale of many incised sand-filled channel bodies is sufficient to be detected in seismic data, assuming a sufficient velocity contrast, but many are likely to be lost in the poor quality of the available data at present'. The results from this research appear to be agreeing with this conclusion. The igneous intrusions tested in this research all offer high impedance contrast using shale or shale/sandstone lithologies as host rocks, where it would be hard to map intrusions in host rocks where they would have a low impedance contrast. Geometry 3, with the sub-vertical feeder dyke also seems a similar result to what this conclusion suggests, that vertical connection will most likely not be distinguishable.

The scale of these outcrops should also be considered, regardless of their orientation. The thickness of the outcrops tested in this research range from 10m to 30m, where in seismic reflection datasets, apart from at very shallow depths, vertical seismic resolution is typically in the region of 15 – 60 m (Magee et al., 2015). Therefore, the cases presented in this research may in some cases be too thin to be resolvable. This would certainly be the case in many offshore basins along the NE Atlantic Margin, where sill complexes are present at relatively deep levels in the contemporaneous basin fill (>3 km) (Eide et al., 2016). This is often also the case within the Barents Sea.

A general point that can be taken from these results is that using simulations such as this teaches us how certain intrusion geometries may behave in seismic data, despite the fact that in most cases these intrusions would be subseismic in scale. Other authors have found that up to 88% of the intrusions found in wells within sill complexes might be below the vertical seismic resolution limit (Schofield et al., 2015), which emphasizes how important it is to understand the effect of geometries on seismic visualization. A caveat of testing these geometries using synthetic seismic data however, is that they are still only simulations. Several factors that would occur in real seismic data are not taken account in this simulation, such as seismic attenuation, a greater variety in lithologies within a basin, a greater variety in elastic properties, and the presence of other geological features. It may however, help bridge the data integration gap between onshore igneous outcrops, and seismic scale outcrops. It affords understanding of the scale and level of detail possible to discern and link between onshore and offshore data, leading to better interpretation, understanding limitations and potential pitfalls. It is clear that the modelling creates a higher level of confidence in interpreting many features (Anell et al., 2016). Although the simulations are not perfect, the 2(3)D convolution method used in this research is the most reliable method available to researchers right now, especially compared to the 1D convolution method. The 1D convolution should be disregarded in favour of existing 2(3)D convolution approaches (RB and FW), not only for modelling with applications to interpretation issues, well ties and similar, but also for seismic inversion which relies much on the 1D model. 2(3)D convolution approaches open up for PSDM-image modelling and can account for realistic overburden effects and detailed target structures such as those provided by digital outcrop mapping (Lecomte et al., 2016).

5.3 Implications for the petroleum system

Igneous intrusions may affect any one of the 5 main elements of a petroleum system. They can affect these elements directly or indirectly. When an intrusion forms a seal or a reservoir they form a direct part of the petroleum system. Indirectly it can affect the charge, migration, reservoir, trap and seal within a petroleum system in several ways. In a volcanic basin where significant intrusions are present, maturation is further influenced both by the local presence of hot igneous bodies and an enhanced regional heat flow (Senger et al., 2017) Igneous intrusions have the ability to act either as conduits or barriers to fluid flow. They are also linked to the origin of the natural fracture network (Senger et al., 2015). The intrusion geometry influences the fracturing by affecting the cooling joints. Additional fractures due to the presence of the intrusion will affect the fractures in the host rock above and below the intrusion. Structurally complex zones, such as dyke-sill junctions like the third geometry that was tested in this research, are typically associated with enhanced fracturing and represent the most permeable zones (Chevallier et al., 2001). Migration routes may also be affected by the geometry of igneous intrusion, where in certain cases dykes may function as a way for hydrocarbons to bypass the seal, creating a migration shadow. Igneous intrusions may also affect the reservoir. Igneous bodies may intrude organic rich shales, which increases the local maturation of the organic matter contained within and storing the generated hydrocarbons. This would be visible as a high impedance contrast within seismic data. Igneous intrusions may also form hydrocarbon traps. Similarly to sealing faults, impermeable intrusions such as dykes or stocks cross-cutting stratigraphy, may generate numerous traps for migrating hydrocarbons (Senger et al., 2017). The potential of a trap is often directly related to the geometry of the intrusion. Dipping features and cross-cutting intrusions may form a trap in the presence of other geological features, such as sealing faults or salt diapirs. Igneous intrusions may also destroy existing traps. The seal may also be influenced by igneous intrusions. Depending on the geometry, the often impermeable nature of intrusions make it a valid candidate for a seal rock. Seal rock may also be compromised by an intrusion, providing a bypass for hydrocarbons. All in all, igneous intrusions have various effects on the petroleum system, but the effects on the elements that are most dependent on the geometry of the intrusion are the migration, trap, and seal.

6 Conclusions and future research

6.1 Conclusions

This research presents a study in seismic modelling of five igneous outcrops on Svalbard. The data from fieldwork, wells, GIS, and 3-D LIDAR surveys are combined to achieve the following goals: 1. Assessing the imaging of different igneous geometries on seismic data. 2. Assessing the detection thresholds regarding the scale and elastic property contrast for sills and dykes. 3. Assessing the effect host rock elastic properties have on seismic imaging of igneous intrusions. 4. Assessing how the shape of different intrusions affect the petroleum system. The conclusions are listed below.

- There are far more sills exposed on Svalbard than dykes, with sills being 91% of the intrusions and dykes being 9% of the intrusions.
- The detection thresholds of igneous intrusions depend on the dominant frequency, angle of incidence, size of the intrusion, overburden effects and elastic properties. What can be seen within seismic data varies greatly between datasets and basins.
- The elastic properties have a significant effect on the seismic imaging of igneous intrusions. If the difference between elastic properties of the host rock and intrusion is large, the impedance contrast will be high. Consequently, if the difference between the properties is low, the impedance contrast will be small and features will not be distinguishable in seismic data.
- Igneous intrusions affect the petroleum system in different ways, but the elements that are most affected by the shape of an intrusion are the migration, trap, and seal. Igneous intrusions may function as a way to bypass a seal, may form or destroy traps, and can function as a seal due to its often impermeable nature.
- While 3-D synthetic seismic modelling may provide insights on regular seismic imaging, there are many factors which are not taken into account, such as seismic attenuation, variety of properties within a lithological unit, and the presence of other geological units.

6.2 Future research and knowledge gaps

The results of this research can be used as a starting point for future research to improve our collective understanding of the way igneous intrusions are imaged in seismic data.
There are certainly knowledge gaps left regarding seismic modelling of intrusion geometries. For one, there are more geometries that may be tested, such as laccoliths or vertical shapes. Also, while this research may provide a bridge between comparing offshore seismic data and onshore observations, the knowledge gap is still there, albeit smaller. 2(3)D convolution methods are not perfect yet, but they may offer researchers assistance on accurately identifying features in offshore seismic data. As for future research, it is recommended that more shapes will be tested. Software development regarding 2(3)D convolution should also continue, and in the future it may be possible to simulate synthetic seismic images more accurately. Seismic effect such as seismic attenuation, the presence of other geological features, and the variation of properties within a geological unit are not taken into account in current simulations, but

perhaps as the software continues to develop these aspects may be implemented. Another survey that might be tried is to collect seismic data from the 5 outcrops that were modelled in this research. Comparing the actual seismic data to the modelled synthetic data may provide new insights regarding the onshore-offshore link between seismic datasets.

References

Anell. I., Lecomte, I., Braathen, A. and Buckley, S. (2016). Synthetic seismic illumination of small-scale growth faults, paralic deposits and low angle clinoforms: A case study of the Triassic successions on Edgeøya, NW Barents Shelf. Submitted to Marine and Petroleum Geology.

Chevallier, L., Goedhart, M. and Woodford, A.C. (2001). The influences of dolerite sill and ring complexes on the occurrence of groundwater in Karoo fractured aquifers: a morpho-tectonic approach. Water Resource Commission Reports, WRC Report No. 937/1/01, 165.

Dallmann, W.K. (ed.) (2015). Geoscience Atlas of Svalbard. Norwegian Polar Institute Report Series 148. Tromsø, Norway: Norwegian Polar Institute.

Eide, C.H., Schofield, N., Jerram, D.A. and Howell, J.A. (2017). Basinscale architecture of deeply emplaced sill complexes: Jameson Land, East Greenland. Journal of the Geological Society, 174 (1), 23-40.

Elvevold, S., Dallmann, W., Blomeier, D., (2007). Geology of Svalbard. Norwegian Polar Institute, Tromsø, p. 38.

Farooqui, M. Y., H. Hou, G. Li, N. Machin, T. Neville, A. Pal, C. Shrivastva, Y. Wang, F. Yang, C. Yin, et al. (2009). “Evaluating volcanic reservoirs”. Oilfield Review 21.1, pp. 36–47.

Fossum, B. J., Schmidt, W. J., Jenkins, D. A., Bogatsky, V. L. & Rappoport, B. I. (2001). New frontiers for hydrocarbon production in the Timan–Pechora Basin, Russia. In: Downey, M. W., Threet, J. C. & Morgans, W. A. (eds) Petroleum Provinces of the Twenty-first Century. American Association of Petroleum Geologists, Tulsa, OK, Memoirs, 74, 259–279.

Gabrielsen R.H., Færseth R.R., Jensen L.N., Kalheim J.E. & Riis F. (1990). Structural elements of the Norwegian continental shelf, part 1, the Barents Sea region. Norwegian Petroleum Directorate Bulletin 6. Stavanger: Norwegian Petroleum Directorate.

Gudlaugsson, S. T., Faleide, J. I., Johansen, S. E. & Breivik, A. J. (1998). Late Palaeozoic structural development of the South-western Barents Sea. Marine and Petroleum Geology, 15, 73–102.

Harland, W.B., 1973.Mesozoic geology of Svalbard. In: Pitcher,M.G. (Ed.), Second International Symposium on Arctic Geology, 1–4 February (1971), San Francisco, California, USA.

Harland W.B. (1997). The geology of Svalbard. London: Geological Society.

Harland W.B. & Wright N.J.R. (1979). Alternative hypothesis for the pre-Carboniferous evolution of Svalbard. Norsk Polarinstitutt Skrifter 167, 89–117.

Henriksen, E., Bjornseth, H.M., Hals, T.K., Heide, T., Kiryukhina, T., Klovjan, O.S., Larssen, G.B., Ryseth, A.E., Ronning, K., Sollid, K. & Stoupakova, A. (2011): Chapter 17 Uplift and erosion of the greater Barents Sea: impact on prospectivity and petroleum systems. Geological Society, London, Memoirs 35, 271–281.

Jerram, D.A. & Bryan, S.E. (2015). Plumbing systems of shallow level intrusive complexes. In: Breitkreuz, C.H. & Rocchi, S. (eds) Physical Geology of Shallow Magmatic Systems. Advances in Volcanology. Springer, Berlin, 1–22, http://doi.org/10.1007/11157_2015_8.

Johannessen E.P. & Steel R.J. (1992). Mid-Carboniferous extension and rift-infill sequence in the Billefjorden Trough, Svalbard. Norsk Geologisk Tidsskrift 72, 35–48.

Lecomte et al. (2016). 2(3)D convolution modelling of complete geological targets beyond – 1D convolution.

Magee, C., C. A.-L. Jackson, and N. Schofield (2014). "Diachronous sub-volcanic intrusion along deep-water margins: insights from the Irish Rockall Basin". Basin Research 26.1, pp. 85–105. issn: 0950091X. doi: 10.1111/bre.12044.

Magoon, L.B,and W. G. Dow, eds., (1994), The petroleum system—from source to trap: AAPG Memoir 60.

Maher Jr., H.D., (2001). Manifestations of the Cretaceous High Arctic Large Igneous Province in Svalbard. J. Geol. 109 (1), 91–104. http://dx.doi.org/10.1086/317960.

Nejbert, K., Krajewski, K.P., Dubińska, E., Pécskay, Z., (2011). Dolerites of Svalbard, northwest Barents Sea Shelf: age, tectonic setting and significance for geotectonic interpretation of the High-Arctic Large Igneous Province. Polar Res. 30 (7306), 1–24. http://dx.doi.org/10.3402/polar.v30i0.7306.

Nilsen, K. T., Henriksen, E. & Larssen, G. B. (1993). Exploration of the Late Palaeozoic carbonates in the southern Barents Sea – a seismic stratigraphic study. In: Vorren, T. O., Bergsager, E. et al. (eds) Arctic Geology and Petroleum Potential. Elsevier, Amsterdam/Norwegian Petroleum Society, Trondheim, Special Publications, 2,393–402.

Nøttvedt, A., Livbjerg, F., Midbøe, P.S., Rasmussen, E., (1993a). Hydrocarbon potential of the Central Spitsbergen Basin. In: Vorren, T.O., Bergsager, E., Dahl-Stamnes, Ø.A., Holter, E., Johansen, B., Lie, E., Lund, T.B. (Eds.), Arctic Geology and Petroleum Potential. Elsevier, Amsterdam, pp. 333–361.

Nøttvedt, A., Cecchi, M., Gjelberg, J.G., Kristensen, S.E., Lønøy, A., Rasmussen, A., Rasmussen, E., Skott, P.H., Veen, P.M.v, (1993b). Svalbard–Barents Sea correlation: a short review. In: Vorren, T.O., Bergsager, E., Dahl-Stamnes, Ø.A., Holter, E., Johansen, B., Lie, E., Lund, T.B. (Eds.),

Planke, S., T. Rasmussen, S. S. Rey, and R. Myklebust (2005). "Seismic characteristics and distribution of volcanic intrusions and hydrothermal vent complexes in the Vøring and Møre basins". Petroleum Geology: North-West Europe and Global Perspectives – Proceedings of the 6th Petroleum Geology Conference. Geological Society of London, pp. 833–844. isbn: 1-86239-164-5. doi: 10.1144/0060833.

Planke, S., H. Svensen, R. Myklebust, S. Bannister, B. Manton, and L. Lorenz (2014). “Geophysics and Remote Sensing”. Advances in Volcanology. Berlin and Heidelberg: Springer Berlin Heidelberg. doi: 10.1007/11157_2014_6.

Polteau, S., A. Mazzini, O. Galland, S. Planke, and A. Malthe-Sørenssen (2008). “Saucershaped intrusions: Occurrences, emplacement and implications”. Earth and Planetary Science Letters 266.1-2, pp. 195–204. issn: 0012821X. doi: 10.1016/j.epsl.2007.11.015.

Polteau, S., Bart W.H. Hendriks, B., Planke, S., Ganerød, M., Fernando Corfu, F., Inge Faleide J. I., Midtkandal, I., S. Svensen, H., Myklebust, R. (2016). The Early Cretaceous Barents Sea Sill Complex: Distribution, 40Ar/39Ar geochronology, and implications for carbon gas formation

Rodriguez Monreal, F., H. J. Villar, R. Baudino, D. Delpino, and S. Zencich (2009). “Modeling an atypical petroleum system: A case study of hydrocarbon generation, migration and accumulation related to igneous intrusions in the Neuquen Basin, Argentina”. Marine and Petroleum Geology 26.4, pp. 590–605. issn: 02648172. doi: 10.1016/j.marpetgeo.2009.01.005.

Saunders, G. (2014). “The development and application of a workflow for photogrammetric analysis of landslides”. PhD thesis. Oslo: University of Oslo. url: https://www.duo.uio.no/handle/10852/42338.

Schofield, N., S. Holford, J. Millett, D. Brown, D. Jolley, S. Passey, D. Muirhead, C. Grove, C. Magee, J. Murray, M. Hole, C. Jackson, and C. Stevenson (2015). “Regional Magma Plumbing and emplacement mechanisms of the Faroe-Shetland Sill Complex: Implications for magma transport and petroleum systems within sedimentary basins”. Basin Research, n/a. issn: 0950091X. doi: 10.1111/bre.12164.

Senger, K., Roy, S., Braathen, A., Buckley, S.J., Balum, K., Gernigon, L., Mjelde, R., Noormets, R., Ogata, K., Olaussen, S., Planke, S., Ruud, B.O. & Tveranger, J. (2013): Geometries of doleritic intrusions in central Spitsbergen, Svalbard: an integrated study of an onshore-offshore magmatic province with implications for CO2 sequestration. Norwegian Journal of Geology, Vol 93, pp. 143–166. Trondheim 2013, ISSN 029-196X.

Senger, K., Planke, S., Polteau, S., Ogata, K., Svensen, H.: Sill emplacement and contact metamorphism in a siliciclastic reservoir on Svalbard, Arctic Norway. Norwegian Journal of Geology, Vol 94, pp. 155–169. Trondheim (2014). ISSN 029-196X.

Senger, K., S. J. Buckley, L. Chevallier, Å. Fagereng, O. Galland, T. H. Kurz, K. Ogata, S. Planke, and J. Tveranger (2015). “Fracturing of doleritic intrusions and associated contact zones: Implications for fluid flow in volcanic basins”. Journal of African Earth Sciences 102, pp. 70–85.

Senger, K., Millett, J., Planke, S., Ogata, K., Haug Eide, C., Festoy, M., Galland, O., Jerram, D., (2017) Effects of igneous intrusions on the petroleum system: a review. DOI 10.3997/1365-2397.2017011

Smith, D.G., Harland, W.B., Hughes, N.F., Pickton, C.A.G., (1976). The geology of Kong Karls Land, Svalbard. Geol. Mag. 113 (3), 193–232.

Steel, R.J., Worsley, D., (1984). Svalbard's post-Caledonian strata — an atlas of sedimentational patterns and paleogeographic evolution. In: Spencer, A.M. (Ed.), Petroleum Geology of the North European Margin. Graham & Trotman, London, pp. 109–135.

Stemmerik L. & Worsley D. (1995). Permian history of the Barents Shelf area. In P.A. Scholle et al. (eds.): Permian of northern Pangaea. Vol. 2. Sedimentary basins and economic resources. Pp. 81–97. Berlin: Springer.

Stemmerik L. & Worsley D. (2005). 30 years on—Arctic Upper Palaeozoic stratigraphy, depositional evolution and hydrocarbon prospectivity. Norwegian Journal of Geology 85, 151–168.

Witte, J., M. Bonora, C. Carbone, and O. Oncken (2012). “Fracture evolution in oil producing sills of the Rio Grande Valley, northern Neuquén Basin, Argentina”. AAPG Bulletin 96.7, pp. 1253–1277. issn: 0149-1423. doi: 10.1306/10181110152.

Worsley D., Aga O.J., Dalland A., Elverhøi A. & Thon A. (1986). The geological history of Svalbard—evolution of an Arctic archipelago. Stavanger: Statoil.

Worsley, D. (2008). The post-Caledonian development of Svalbard and the western Barents Sea. Polar Research, 27, 298–317.

Appendix 1: Intrusion analysis results

Intrusion ID	Area [km2]	Easting	Northing	Length exposed [m]	Elevation Base [m]	Elevation Top [m]	Max Thickness [m]	Dyke/Sill
0	0,14	589571	8701895	4547	349,36	418,05	68,69	Sill
1	1,96	590279	8701538	8537	269,45	422,13	152,68	Sill
2	0,02	589767	8703360	829	346,33	358,18	11,85	Sill
3	0,09	573740	8703382	1490	378,33	449,47	71,14	Sill
4	0,21	583319	8702914	7070	172,23	253,28	81,05	Sill
5	0,06	583760	8703501	2046	224,28	270,30	46,02	Sill
6	0,02	538751	8704566	542	604,77	624,59	19,83	Sill
7	0,06	589755	8704464	2440	316,06	414,27	98,20	Sill
8	0,44	573871	8704655	2960	310,52	495,13	184,61	Sill
10	0,04	589600	8705260	1223	341,91	388,69	46,78	Sill
11	0,01	538308	8705522	968	658,18	671,82	13,64	Sill
12	0,06	589158	8705602	1496	349,89	402,34	52,45	Sill
13	0,04	573112	8706706	849	476,17	530,17	53,99	Sill
14	0,02	481405	8706876	1103	366,95	402,30	35,36	Sill
15	0,08	576729	8706976	1949	347,98	410,17	62,19	Sill
16	0,03	480970	8707303	933	156,63	316,35	159,72	Dyke
17	0,03	576211	8707575	989	374,88	423,61	48,73	Sill
18	0,03	479783	8707738	1281	246,38	292,57	46,20	Sill
19	0,27	531492	8707492	2247	1,46	44,60	43,13	Sill
20	0,04	481073	8708942	1593	353,72	557,63	203,92	Dyke
21	0,17	527190	8709067	1931	0,45	17,92	17,47	Sill
22	0,48	531435	8708545	4845	5,62	229,80	224,19	Sill
23	0,02	527831	8709452	610	0,31	7,04	6,73	Sill
25	0,9	530223	8708949	11798	0,15	61,80	61,65	Sill
26	0,29	526836	8709528	2878	0,11	16,74	16,63	Sill
27	0,01	574899	8709995	424	467,55	476,31	8,76	Sill
28	0,01	514548	8710336	398	26,16	34,43	8,26	Sill
29	0,03	482978	8710298	1348	91,92	172,49	80,57	Sill
30	0,04	573962	8711439	1268	465,90	538,75	72,85	Sill
32	0,03	586929	8711890	840	417,04	469,97	52,93	Sill
33	0,1	514641	8710971	5724	34,47	171,11	136,65	Sill
34	0,08	582882	8711963	1587	368,42	395,28	26,85	Sill
35	0,02	519607	8712191	1538	14,08	41,56	27,48	Sill
38	0,09	587505	8712724	2156	305,26	388,04	82,78	Sill
39	0,04	586187	8713162	1479	405,75	464,97	59,23	Sill
40	0,02	518734	8713314	862	105,32	206,02	100,70	Dyke

Intrusion ID	Area [km2]	Easting	Northing	Length exposed [m]	Elevation Base [m]	Elevation Top [m]	Max Thickness [m]	Dyke/Sill
42	0,01	462511	8713474	388	348,58	412,14	63,56	Dyke
43	0,01	464893	8713568	585	570,10	631,60	61,50	Dyke
44	0,01	465127	8713632	458	464,21	501,08	36,87	Sill
45	0,01	577957	8713638	330	494,56	507,97	13,42	Sill
46	0,48	518357	8712333	6200	206,80	340,43	133,62	Sill
47	0,08	578249	8713600	1724	377,80	519,00	141,20	Sill
48	0,03	464859	8713848	1583	433,66	590,79	157,14	Dyke
49	0,24	579167	8713610	4284	311,68	517,06	205,37	Sill
50	0,02	464491	8714047	631	470,04	562,53	92,49	Sill
51	0,07	482672	8713800	2301	120,45	637,64	517,19	Dyke
52	0,07	516961	8713880	2636	282,66	319,63	36,97	Sill
53	0,62	585640	8713999	8577	227,97	421,59	193,62	Sill
54	0,05	483031	8714029	2075	115,95	485,09	369,14	Dyke
56	0,03	481737	8714334	1489	186,50	427,80	241,30	Dyke
57	0,02	519744	8714655	971	313,56	359,66	46,10	Sill
58	0,5	512951	8714401	4352	407,27	465,81	58,54	Sill
59	0,17	520579	8714109	7468	94,92	260,95	166,03	Sill
60	0,01	464724	8733686	931	672,67	757,00	84,33	Dyke
61	0,15	591336	8733667	1785	121,50	142,51	21,00	Sill
62	0,03	589801	8733808	611	419,39	482,53	63,14	Sill
63	0,1	590106	8734331	1319	412,88	493,05	80,18	Sill
64	0,01	499525	8734396	852	712,72	750,71	38,00	Sill
65	0,11	499891	8733613	5638	504,05	710,94	206,89	Sill
66	1,85	502166	8733463	8251	349,48	552,48	203,01	Sill
67	0,82	592265	8734710	3600	327,58	427,04	99,45	Sill
68	0,01	512726	8735386	348	587,60	600,59	12,99	Sill
69	0,05	513049	8735339	1643	646,69	702,13	55,44	Sill
70	0,02	512547	8735567	800	622,26	682,50	60,24	Sill
72	0,07	591103	8735943	1612	416,08	444,90	28,82	Sill
73	0,13	512930	8735901	3574	622,91	764,55	141,64	Sill
74	0,13	592820	8736017	1541	295,49	393,48	97,99	Sill
75	0,06	497622	8736505	935	631,56	775,47	143,91	Sill
76	0,28	501219	8737833	8607	528,26	746,46	218,20	Sill
77	0,03	498404	8738358	657	737,15	787,73	50,58	Sill
78	0,02	498310	8739086	542	862,35	911,58	49,22	Sill
79	0,07	497133	8739026	1841	556,56	701,91	145,36	Sill
80	0,05	499635	8742545	1693	726,43	776,83	50,40	Sill

Intrusion ID	Area [km2]	Easting	Northing	Length exposed [m]	Elevation Base [m]	Elevation Top [m]	Max Thickness [m]	Dyke/Sill
81	0,24	501572	8742298	6361	670,57	832,06	161,49	Sill
83	0,01	533560	8760836	789	71,35	138,81	67,46	Dyke
84	0,01	533399	8760941	842	76,31	134,51	58,20	Dyke
85	0,04	542236	8525853	1130	259,78	443,21	183,44	Sill
86	0,01	541332	8528212	439	404,07	438,87	34,80	Sill
87	0,02	540752	8529715	661	609,39	759,38	149,99	Dyke
88	0,01	540540	8530092	563	575,40	780,83	205,43	Dyke
89	0,04	540232	8531353	1079	452,36	732,39	280,03	Dyke
90	0,01	539046	8534147	303	474,12	519,29	45,17	Sill
91	0,02	538283	8535719	853	527,81	660,55	132,74	Dyke
92	0,06	537742	8537008	1874	516,16	825,06	308,90	Dyke
94	0,02	533219	8543893	590	8,06	19,02	10,96	Sill
95	0,03	518499	8550102	1478	139,08	222,73	83,66	Sill
96	0,01	518410	8550396	857	202,38	244,40	42,02	Sill
97	0,02	519787	8550609	957	223,22	306,79	83,57	Sill
98	0,01	520752	8550842	824	492,13	545,07	52,94	Dyke
99	0,01	520234	8550889	863	446,59	475,81	29,22	Sill
102	0,03	511363	8551922	1123	456,90	572,01	115,11	Sill
103	0,01	508402	8551935	431	163,69	165,90	2,21	Sill
104	0,03	510373	8551967	1432	326,38	437,84	111,46	Sill
105	0,05	509358	8551990	2385	287,52	491,57	204,06	Sill
106	0,09	504974	8552190	5862	30,99	493,99	463,00	Dyke
107	0,03	512654	8552214	990	400,88	415,26	14,38	Sill
108	0,02	507661	8552477	1315	339,87	538,92	199,05	Dyke
109	0,01	509325	8553057	371	471,68	557,02	85,33	Dyke
110	0,01	500859	8558425	304	0,00	3,31	3,31	Sill
111	0,01	500977	8558401	425	0,00	3,65	3,65	Sill
112	0,02	501024	8558930	1036	2,52	11,83	9,31	Sill
113	0,01	485662	8568325	552	2,04	3,08	1,03	Sill
114	0,01	485457	8568753	465	0,69	1,84	1,15	Sill
124	0,01	484200	8582360	537	97,56	102,32	4,76	Sill
125	0,02	523261	8583054	1223	415,20	582,15	166,95	Dyke
126	0,02	516079	8586893	709	610,08	770,69	160,61	Dyke
128	0,03	509909	8588984	1371	862,90	957,13	94,23	Sill
129	0,12	509993	8588593	3575	724,47	1101,35	376,88	Sill
130	0,03	509611	8590206	1326	765,98	863,49	97,51	Sill
131	0,02	509470	8590736	1089	673,88	805,15	131,27	Dyke

Intrusion ID	Area [km2]	Easting	Northing	Length exposed [m]	Elevation Base [m]	Elevation Top [m]	Max Thickness [m]	Dyke/Sill
132	0,05	508574	8594091	1488	636,04	924,85	288,80	Dyke
133	0,06	508579	8594435	2229	679,38	991,57	312,19	Dyke
134	0,01	507631	8595246	841	652,37	724,84	72,47	Dyke
135	0,03	503622	8598673	1316	567,05	832,01	264,96	Dyke
136	0,05	503695	8598841	2179	509,22	865,92	356,70	Dyke
137	0,19	501221	8600803	6457	707,87	888,54	180,67	Sill
138	0,02	501593	8603630	907	549,53	772,95	223,41	Dyke
139	0,08	501238	8603613	2312	576,78	1184,45	607,67	Dyke
140	0,02	494310	8604649	887	0,00	4,67	4,67	Sill
141	0,02	500657	8604997	968	635,87	847,78	211,91	Dyke
142	0,05	494318	8605297	1721	1,74	28,99	27,25	Sill
143	0,06	500031	8607368	2174	22,49	431,61	409,11	Dyke
144	0,02	497602	8615042	1012	5,49	16,43	10,94	Sill
145	0,1	498508	8616118	3419	7,59	308,38	300,79	Sill
146	0,03	497671	8616912	1092	227,50	386,77	159,27	Dyke
147	0,02	496871	8617032	910	63,56	139,64	76,08	Sill
148	0,04	497528	8617539	1450	151,48	380,13	228,64	Dyke
149	0,07	495102	8618951	3176	0,00	262,41	262,41	Sill
150	0,03	495825	8619620	1093	481,22	634,60	153,39	Dyke
151	0,03	494439	8619955	1181	2,18	357,09	354,91	Dyke
152	0,23	495378	8619227	7572	9,93	490,55	480,63	Sill
153	0,03	496180	8621044	1280	1,48	328,88	327,39	Dyke
154	0,02	492770	8626060	829	10,62	25,69	15,07	Sill
155	0,01	492049	8626599	488	0,00	5,41	5,41	Sill
156	0,02	486754	8631553	1071	146,64	174,34	27,71	Sill
157	0,02	487170	8631572	1693	5,81	195,97	190,16	Dyke
158	0,07	487357	8631980	3253	9,65	427,26	417,62	Dyke
160	0,06	484070	8633638	3437	173,24	276,23	102,99	Sill
161	0,18	484780	8634304	3711	413,20	725,40	312,20	Sill
162	0,01	481489	8634721	321	16,49	20,64	4,15	Sill
163	0,01	481480	8634920	435	23,79	28,66	4,88	Sill
164	0,02	484130	8634975	856	350,63	480,36	129,73	Dyke
165	0,17	484660	8633122	11242	152,66	373,42	220,76	Sill
166	0,03	483981	8635870	1188	234,06	326,36	92,30	Sill
167	0,09	483086	8635422	4826	32,24	262,41	230,16	Sill
168	0,04	482064	8636981	2145	38,88	67,30	28,42	Sill
169	0,37	483785	8637831	11063	97,67	424,27	326,60	Sill

Intrusion ID	Area [km2]	Easting	Northing	Length exposed [m]	Elevation Base [m]	Elevation Top [m]	Max Thickness [m]	Dyke/Sill
170	0,13	482170	8640575	7060	51,69	128,61	76,92	Sill
171	0,16	480067	8641523	6298	134,29	413,05	278,76	Sill
172	0,01	478856	8644047	402	412,88	458,80	45,92	Sill
175	0,48	476104	8652803	6974	58,98	505,61	446,63	Sill
177	0,1	580105	8656955	1767	3,59	18,56	14,96	Sill
178	1,04	580163	8655983	12585	0,00	28,11	28,11	Sill
179	0,03	475032	8660182	1526	78,26	102,99	24,73	Sill
180	0,01	475020	8660481	778	60,87	77,76	16,89	Sill
181	1,07	579501	8658947	10591	0,00	67,19	67,19	Sill
182	0,27	577772	8661652	6671	68,87	132,31	63,45	Sill
183	0,32	478745	8659680	13160	45,64	346,70	301,05	Sill
184	0,14	576704	8663164	3827	150,84	253,61	102,76	Sill
185	0,02	472693	8664724	1041	29,73	65,64	35,91	Sill
186	0,38	474116	8662855	19046	58,70	209,31	150,61	Sill
187	0,03	472302	8665103	968	15,39	36,33	20,94	Sill
188	0,01	474161	8667689	364	301,07	308,95	7,88	Sill
189	0,08	473725	8668420	3406	0,96	306,18	305,22	Sill
190	0,06	581967	8670134	1126	167,36	187,25	19,89	Sill
191	0,02	581729	8670806	486	180,76	198,20	17,44	Sill
192	0,03	582477	8670858	735	187,86	190,20	2,34	Sill
193	0,05	582041	8670761	1197	182,77	188,40	5,63	Sill
194	0,03	582136	8670943	796	189,91	194,48	4,57	Sill
195	0,05	582352	8671139	906	194,92	198,53	3,61	Sill
196	0,01	591633	8673024	438	68,17	75,49	7,32	Sill
197	0,04	591945	8673037	703	71,54	90,22	18,67	Sill
198	0,13	592424	8673084	2512	55,53	100,60	45,07	Sill
199	0,01	591448	8673459	384	111,89	121,72	9,83	Sill
200	0,03	591269	8673403	685	134,32	155,26	20,95	Sill
201	0,03	591755	8673429	891	79,24	91,50	12,26	Sill
202	2,65	580748	8672294	19300	116,70	293,52	176,82	Sill
203	0,09	589383	8675489	1915	51,69	96,88	45,19	Sill
204	0,08	588845	8675894	1299	76,25	127,82	51,57	Sill
205	0,02	589293	8675928	519	78,74	84,76	6,02	Sill
206	0,02	588497	8676105	497	133,23	156,68	23,45	Sill
207	0,15	589525	8676246	1552	44,46	86,62	42,16	Sill
208	1,12	590978	8675712	12185	36,89	125,40	88,51	Sill
209	0,02	588058	8676776	476	257,08	270,83	13,76	Sill

Intrusion ID	Area [km2]	Easting	Northing	Length exposed [m]	Elevation Base [m]	Elevation Top [m]	Max Thickness [m]	Dyke/Sill
210	0,05	587683	8676822	867	278,41	323,83	45,43	Sill
211	0,01	585306	8676933	368	142,13	146,65	4,52	Sill
212	0,14	589410	8676885	1461	67,73	109,74	42,01	Sill
213	0,01	585721	8677157	363	146,83	152,58	5,75	Sill
214	0,01	585010	8678204	345	174,60	183,30	8,70	Sill
215	0,01	586176	8678256	471	123,74	130,37	6,63	Sill
216	0,03	586198	8678527	824	126,30	140,33	14,03	Sill
217	0,02	586557	8678571	510	119,65	126,72	7,07	Sill
218	0,6	587430	8678634	4044	116,38	172,77	56,39	Sill
219	0,13	586187	8678918	1887	119,56	147,08	27,52	Sill
220	5,26	579263	8677488	14560	280,72	391,91	111,19	Sill
221	0,91	588902	8678755	13864	34,32	149,79	115,47	Sill
222	2,11	584233	8680481	9788	203,91	338,34	134,44	Sill
223	0,13	567773	8682610	3154	337,63	441,95	104,32	Sill
224	0,04	567104	8683070	1357	209,24	338,12	128,88	Sill
225	0,03	455779	8683682	929	0,67	3,52	2,85	Sill
227	0,03	589688	8685683	721	209,73	220,58	10,85	Sill
228	0,03	590154	8685794	1110	235,52	264,59	29,07	Sill
229	0,01	589894	8685878	367	222,30	228,94	6,64	Sill
230	0,03	590620	8685918	925	254,33	269,06	14,73	Sill
231	0,01	589826	8685987	371	212,03	218,50	6,47	Sill
232	0,04	586902	8685889	1034	331,19	346,11	14,91	Sill
233	0,04	579153	8685993	1675	321,87	387,68	65,82	Sill
234	0,03	589212	8686288	589	224,37	239,51	15,14	Sill
235	0,03	454239	8686389	660	22,39	24,30	1,91	Sill
236	0,08	589570	8686310	1120	209,24	229,06	19,82	Sill
237	0,07	589826	8686312	1260	208,74	216,22	7,48	Sill
238	0,03	590157	8686641	716	213,29	215,38	2,09	Sill
239	0,05	589991	8686966	856	217,38	234,27	16,89	Sill
240	0,03	589755	8687182	691	246,02	261,56	15,55	Sill
241	0,05	590705	8687166	859	213,06	233,57	20,52	Sill
242	0,08	591281	8687179	1027	201,73	211,62	9,89	Sill
244	0,06	567215	8688503	2036	494,55	553,44	58,89	Sill
245	0,01	566423	8688767	452	346,72	430,11	83,39	Dyke
246	1	565026	8685945	18104	110,73	298,68	187,95	Sill
247	0,03	465592	8688900	885	217,43	282,30	64,87	Sill
248	5,52	588991	8686795	36511	114,77	335,00	220,23	Sill

Intrusion ID	Area [km2]	Easting	Northing	Length exposed [m]	Elevation Base [m]	Elevation Top [m]	Max Thickness [m]	Dyke/Sill
250	0,21	568744	8688882	6883	336,81	472,99	136,18	Sill
251	0,02	574791	8689642	495	579,06	613,37	34,32	Sill
252	0,06	573899	8689789	2297	577,22	642,32	65,10	Sill
253	0,05	465325	8689483	2005	204,13	338,10	133,98	Sill
254	0,1	570400	8689380	4444	316,00	418,50	102,50	Sill
255	0,29	572107	8689573	7957	351,39	753,80	402,41	Sill
256	0,04	537740	8692113	1688	474,96	509,10	34,14	Sill
257	0,1	535700	8692068	4105	289,35	321,44	32,09	Sill
258	0,19	588819	8693261	2589	5,10	44,33	39,23	Sill
259	0,04	574832	8693746	1152	525,75	590,22	64,46	Sill
260	0,03	530947	8693711	983	171,20	213,40	42,20	Sill
261	0,11	561475	8693686	3066	391,41	651,73	260,32	Sill
262	0,02	555565	8693988	1290	395,09	439,28	44,19	Sill
263	0,02	530901	8694026	1024	182,55	260,51	77,96	Sill
264	0,12	574032	8694106	1426	596,32	664,63	68,31	Sill
265	0,34	533209	8693055	11999	183,32	497,53	314,21	Sill
267	0,03	528364	8694395	1525	105,33	192,78	87,45	Sill
268	0,01	533154	8694503	290	411,89	420,84	8,94	Sill
269	0,03	555962	8694696	1615	480,06	484,79	4,73	Sill
270	0,02	528282	8694660	800	127,75	242,39	114,64	Dyke
271	0,12	529551	8695048	1348	69,70	78,94	9,23	Sill
272	0,51	585454	8694660	4169	357,23	449,82	92,59	Sill
273	0,03	451292	8695183	814	7,31	12,99	5,68	Sill
274	0,15	555597	8693320	8711	264,49	483,62	219,13	Sill
275	0,34	583204	8695202	2417	436,57	477,81	41,23	Sill
276	0,01	531239	8695596	274	451,53	455,29	3,75	Sill
277	0,11	529589	8695539	1291	72,95	82,41	9,46	Sill
281	0,04	528056	8695770	1534	220,59	297,37	76,78	Sill
282	0,41	531736	8695161	11104	368,45	481,34	112,89	Sill
283	0,01	525846	8696466	547	212,59	267,44	54,85	Dyke
284	0,16	579880	8696302	4204	511,95	552,60	40,64	Sill
285	0,03	568028	8696794	997	471,43	550,50	79,07	Sill
286	0,02	574531	8697022	1057	599,44	625,80	26,36	Sill
287	0,03	567385	8697671	1244	572,13	633,64	61,50	Sill
288	0,04	523770	8697769	1138	89,25	159,28	70,02	Sill
289	0,05	523377	8697994	1210	15,99	44,85	28,86	Sill
290	1,83	530099	8696046	37226	0,00	419,73	419,73	Sill

Intrusion ID	Area [km2]	Easting	Northing	Length exposed [m]	Elevation Base [m]	Elevation Top [m]	Max Thickness [m]	Dyke/Sill
293	0,36	524102	8698459	3018	1,56	125,74	124,18	Sill
294	0,04	574602	8698627	1859	620,41	685,40	64,99	Sill
296	0,01	574534	8699087	485	559,28	588,01	28,73	Sill
297	0,65	525616	8698844	3860	0,00	70,09	70,09	Sill
298	0,03	574680	8699262	722	458,91	518,69	59,78	Sill
299	8,28	566632	8695060	47866	408,68	800,93	392,24	Sill
300	0,01	576850	8699418	284	584,23	605,12	20,89	Sill
301	0,02	578072	8700073	647	571,77	592,92	21,15	Sill
302	0,21	589075	8699359	4149	42,49	160,35	117,86	Sill
303	0,27	589362	8700672	2077	319,86	374,19	54,33	Sill
304	0,77	591654	8699951	5038	0,00	20,87	20,87	Sill
305	0,23	574617	8701117	2292	378,69	526,46	147,76	Sill
306	0,23	588324	8700711	3272	127,02	217,83	90,81	Sill
308	0,07	591143	8702366	1580	40,64	72,16	31,51	Sill
309	0,04	482999	8715107	1564	358,77	588,18	229,41	Dyke
310	0,09	483369	8714928	3497	77,72	591,91	514,19	Dyke
311	0,06	519214	8715538	2721	238,93	303,96	65,04	Sill
312	9,92	513118	8711696	22120	1,67	616,47	614,81	Sill
313	0,44	586290	8715594	8341	58,57	241,06	182,49	Sill
315	0,07	513859	8715726	3683	296,17	353,18	57,01	Sill
316	0,01	482992	8716613	436	192,21	214,43	22,21	Sill
317	0,2	508855	8716232	1969	163,08	244,49	81,41	Sill
319	0,02	482409	8716528	960	316,33	435,16	118,83	Dyke
320	0,45	517532	8715483	11227	288,73	529,96	241,23	Sill
322	0,03	466388	8717009	1035	615,53	672,28	56,75	Sill
323	0,01	511618	8717151	434	283,07	304,94	21,87	Sill
324	0,07	462276	8716659	2753	240,28	643,68	403,40	Dyke
325	0,82	512428	8716403	9854	207,77	601,60	393,83	Sill
326	0,08	463230	8716797	3396	288,39	678,32	389,92	Sill
327	0,01	462681	8717557	460	411,45	427,14	15,69	Sill
330	0,15	520328	8717228	2893	582,76	663,30	80,54	Sill
332	0,05	466496	8717714	2074	431,26	609,44	178,18	Sill
333	0,05	520755	8717429	3127	409,02	487,62	78,60	Sill
334	0,04	513693	8717898	978	491,37	544,71	53,33	Sill
335	0,05	482168	8717631	2240	293,19	570,83	277,64	Dyke
336	0,01	467591	8718037	553	618,30	682,83	64,54	Dyke
337	0,38	580240	8717879	4871	462,57	628,02	165,45	Sill

Intrusion ID	Area [km2]	Easting	Northing	Length exposed [m]	Elevation Base [m]	Elevation Top [m]	Max Thickness [m]	Dyke/Sill
338	0,01	462732	8718177	1088	298,06	375,95	77,89	Dyke
339	0,02	467474	8718279	820	508,44	701,63	193,19	Dyke
340	0,77	511147	8717262	14607	202,88	405,99	203,11	Sill
341	0,05	516802	8717942	2502	556,67	636,14	79,47	Sill
342	0,47	581502	8717652	8813	374,81	557,42	182,61	Sill
343	0,1	482452	8717878	3531	164,69	392,69	228,01	Sill
344	0,02	481714	8718434	1042	229,90	425,19	195,29	Dyke
345	0,17	578909	8718441	1942	584,31	665,38	81,07	Sill
346	0,07	517595	8718495	2562	595,62	679,87	84,25	Sill
347	0,33	513065	8718563	4238	407,47	507,84	100,37	Sill
348	1,86	519734	8716573	21320	231,76	655,83	424,07	Sill
349	0,01	513389	8719118	396	435,87	452,72	16,85	Sill
350	0,03	580207	8719249	678	442,42	508,63	66,21	Sill
351	0,08	466159	8719044	4658	411,86	828,57	416,71	Dyke
352	0,04	513582	8719401	902	437,88	514,60	76,72	Sill
353	0,08	581612	8719463	1400	333,89	386,09	52,20	Sill
354	0,1	518068	8719435	2089	518,98	631,83	112,85	Sill
355	0,02	572086	8719580	1018	482,95	507,17	24,23	Sill
356	0,05	461386	8719451	1715	0,00	134,23	134,23	Sill
357	0,01	462083	8719739	820	80,69	149,38	68,69	Dyke
358	0,04	467694	8719782	1590	572,28	671,90	99,62	Sill
359	0,35	512437	8719926	2829	399,75	503,92	104,17	Sill
360	0,01	579053	8720396	415	439,43	462,57	23,13	Sill
361	0,02	578162	8720418	668	558,29	593,38	35,10	Sill
362	0,01	578774	8720461	412	502,32	523,49	21,17	Sill
364	0,01	467083	8720524	441	547,40	629,46	82,06	Dyke
365	0,03	466859	8720572	1228	538,72	650,01	111,29	Sill
366	0,02	467289	8720559	813	577,06	754,21	177,15	Dyke
367	0,92	514083	8720281	6050	467,11	654,63	187,51	Sill
369	2,92	508312	8718825	34211	199,49	603,04	403,55	Sill
370	0,04	462593	8721176	1514	32,04	130,88	98,84	Sill
371	0,62	515449	8720934	3305	412,69	662,20	249,52	Sill
372	0,02	577541	8721238	999	618,11	646,11	28,00	Sill
373	0,18	573123	8721493	3373	498,10	533,78	35,68	Sill
374	0,05	573728	8721998	847	447,37	483,95	36,58	Sill
375	0,07	584155	8722137	1238	399,41	456,32	56,91	Sill
377	0,1	573861	8722432	1519	363,60	474,58	110,98	Sill

Intrusion ID	Area [km2]	Easting	Northing	Length exposed [m]	Elevation Base [m]	Elevation Top [m]	Max Thickness [m]	Dyke/Sill
378	0,04	466729	8723121	1675	308,91	468,69	159,78	Dyke
379	0,03	584009	8723083	1029	375,13	416,77	41,64	Sill
380	0,02	583071	8723103	918	472,52	497,46	24,94	Sill
381	0,02	465828	8723229	849	212,34	403,40	191,06	Dyke
382	0,01	575916	8723450	701	547,83	569,55	21,72	Sill
383	0,04	583833	8723508	1164	359,60	418,21	58,61	Sill
384	0,08	583205	8723758	1578	358,54	461,12	102,58	Sill
385	0,16	580833	8723668	2592	393,59	539,95	146,37	Sill
386	0,03	575863	8724303	1096	543,37	586,82	43,45	Sill
389	0,06	579355	8724568	2272	361,57	445,40	83,83	Sill
390	0,09	483951	8724627	1911	167,44	346,93	179,49	Sill
391	0,03	466277	8724912	1230	338,10	436,51	98,41	Sill
394	0,02	485001	8725164	746	88,30	135,84	47,54	Sill
395	0,2	578481	8725525	2506	323,58	420,12	96,54	Sill
396	0,01	577634	8725651	403	317,35	348,10	30,75	Sill
397	0,44	575683	8725268	4422	314,10	569,11	255,01	Sill
398	0,2	482814	8724449	6668	208,12	316,95	108,83	Sill
399	0,06	576873	8725617	1470	364,10	480,05	115,95	Sill
400	0,02	484849	8726034	752	90,56	105,40	14,85	Sill
401	0,03	489448	8726391	1000	3,74	16,14	12,41	Sill
402	0,63	485200	8726909	4283	115,60	396,60	280,99	Sill
403	0,1	482410	8727569	3003	633,42	835,96	202,54	Sill
404	0,01	485428	8727949	432	528,78	545,94	17,16	Sill
405	0,02	487534	8727984	583	391,58	438,41	46,83	Sill
406	0,07	488835	8727561	3111	104,33	195,23	90,90	Sill
407	0,05	467234	8728167	1112	426,92	657,28	230,35	Sill
408	0,04	464224	8728284	1548	214,96	362,33	147,37	Sill
409	0,01	479779	8728676	621	634,74	690,26	55,52	Dyke
410	0,05	465146	8728691	2080	334,79	550,18	215,39	Sill
411	0,04	487274	8728863	1575	163,44	312,78	149,34	Sill
412	0,09	482154	8728999	1595	718,54	868,64	150,10	Sill
414	0,08	479355	8728862	2768	369,40	723,33	353,93	Sill
415	0,01	465402	8729374	570	458,45	502,30	43,85	Sill
416	0,04	478770	8729890	1950	411,63	842,10	430,47	Dyke
417	0,02	470948	8730194	788	657,86	760,61	102,75	Dyke
418	0,05	487025	8730253	1912	165,27	429,26	263,99	Dyke
419	0,05	467505	8730241	1827	581,80	682,64	100,83	Sill

Intrusion ID	Area [km2]	Easting	Northing	Length exposed [m]	Elevation Base [m]	Elevation Top [m]	Max Thickness [m]	Dyke/Sill
421	2,88	496351	8729166	11953	0,00	96,50	96,50	Sill
422	0,02	487887	8730546	845	121,57	128,59	7,02	Sill
423	0,01	470175	8730710	567	743,16	799,91	56,74	Dyke
424	0,06	487109	8730795	2030	202,13	412,00	209,88	Sill
425	0,01	478237	8731263	364	978,06	1010,92	32,86	Sill
426	0,1	602204	8731364	3173	124,47	171,21	46,74	Sill
427	0,05	602305	8731486	2527	185,69	239,00	53,31	Sill
428	0,11	464003	8731324	3545	492,93	781,88	288,95	Sill
430	0,01	577892	8732200	355	373,07	380,15	7,09	Sill
432	0,03	464911	8732141	1021	761,17	906,29	145,12	Sill
434	0,51	602455	8732121	3040	417,55	450,75	33,20	Sill
440	0,07	577072	8732682	1725	408,01	434,43	26,42	Sill
441	0,09	486382	8732480	3190	124,08	194,66	70,57	Sill
442	0,05	484635	8733226	1691	254,58	279,74	25,17	Sill
443	0,36	500837	8732433	7864	394,73	569,51	174,78	Sill
444	0,01	463491	8733419	671	512,28	595,60	83,32	Dyke
446	0,01	464313	8733656	401	789,68	838,58	48,90	Dyke
447	0,6	591881	8819253	4582	0,00	14,70	14,70	Sill
448	0,08	592487	8816364	1266	0,00	17,45	17,45	Sill
449	0,06	586929	8837966	1056	0,00	12,69	12,69	Sill
450	0,23	584497	8837284	2813	0,00	35,90	35,90	Sill
451	0,04	593127	8823893	951	0,46	3,85	3,39	Sill
452	0,08	592102	8813837	1154	0,00	16,53	16,53	Sill
453	0,03	597648	8801897	686	0,26	21,26	21,00	Sill
455	0,04	599434	8801080	948	0,00	10,05	10,05	Sill
456	0,3	588520	8813125	3120	0,00	29,57	29,57	Sill
457	0,35	590053	8812829	3248	0,00	18,74	18,74	Sill
458	0,01	590859	8813186	390	0,26	6,91	6,65	Sill
459	0,04	607059	8805411	1287	0,00	5,18	5,18	Sill
460	0,09	608257	8804688	1303	0,00	10,98	10,98	Sill
462	0,12	602701	8802439	1563	0,00	31,60	31,60	Sill
468	0,02	599704	8799081	578	0,00	15,67	15,67	Sill
469	0,17	599097	8799121	1791	0,00	32,59	32,59	Sill
470	0,33	598145	8799030	3489	0,00	27,37	27,37	Sill
471	0,03	602144	8799658	1365	0,00	29,80	29,80	Sill
472	0,01	581575	8833264	343	0,00	2,24	2,24	Sill
473	0,02	581793	8833175	481	0,00	7,32	7,32	Sill

Intrusion ID	Area [km2]	Easting	Northing	Length exposed [m]	Elevation Base [m]	Elevation Top [m]	Max Thickness [m]	Dyke/Sill
478	0,11	632744	8681770	1845	0,00	2,00	2,00	Sill
480	0,32	632088	8682021	3095	0,00	1,00	1,00	Sill
484	1,16	634887	8674024	11978	0,00	109,25	109,25	Sill
485	0,31	635044	8677916	14797	89,56	236,81	147,25	Sill
486	0,23	637654	8671872	15149	145,25	315,75	170,50	Sill
488	0,07	533691	8876002	1208	0,00	13,69	13,69	Sill
489	0,04	534732	8869625	991	0,00	9,86	9,86	Sill
490	0,01	543216	8864285	571	375,59	380,54	4,95	Sill
491	0,03	542855	8864639	956	360,53	372,72	12,19	Sill
492	0,03	542149	8865249	1057	273,35	313,91	40,57	Sill
493	0,09	541378	8865860	2853	164,34	291,04	126,70	Sill
494	0,46	537991	8869569	14287	8,80	339,10	330,30	Sill
495	1,31	565278	8840320	20089	0,00	379,59	379,59	Sill
497	0,02	567110	8839623	937	8,32	104,65	96,33	Sill
498	0,4	567714	8839120	4071	0,00	88,20	88,20	Sill
499	0,12	574759	8839311	1572	0,00	16,34	16,34	Sill
501	0,12	568000	8838363	2333	90,80	255,32	164,52	Sill
502	0,14	568561	8838197	2012	0,00	172,76	172,76	Sill
504	0,36	564541	8837250	3641	384,23	437,86	53,63	Sill
505	0,39	570430	8836952	5548	0,00	178,62	178,62	Sill
506	0,02	569808	8836779	650	253,20	262,69	9,49	Sill
507	0,04	565167	8836172	1118	418,06	441,38	23,32	Sill
508	0,08	572449	8835327	4758	0,00	7,63	7,63	Sill
510	0,03	570333	8835670	834	334,21	371,41	37,21	Sill
511	0,04	562922	8835107	3025	212,18	266,51	54,33	Sill
512	0,01	564661	8835566	551	445,26	450,73	5,47	Sill
514	0,1	568424	8835120	2037	359,69	425,67	65,98	Sill
515	0,03	563190	8835262	640	349,58	373,51	23,94	Sill
516	0,1	564188	8834880	2534	434,18	468,51	34,33	Sill
517	0,02	569839	8834566	1055	322,20	360,02	37,83	Sill
518	0,69	575597	8833918	4354	0,00	31,17	31,17	Sill
519	0,02	565260	8834316	1322	464,35	518,27	53,92	Sill
520	0,01	562812	8834326	1749	182,93	200,32	17,39	Sill
522	1,36	574561	8833198	7890	0,00	122,53	122,53	Sill
523	0,16	579291	8834042	2064	0,00	25,68	25,68	Sill
526	0,1	565719	8833972	2019	486,23	566,86	80,63	Sill
528	0,01	565843	8833803	877	489,23	504,98	15,74	Sill

Intrusion ID	Area [km2]	Easting	Northing	Length exposed [m]	Elevation Base [m]	Elevation Top [m]	Max Thickness [m]	Dyke/Sill
529	0,03	564905	8833254	2644	250,42	298,45	48,03	Sill
530	0,09	568908	8833470	2063	374,16	438,63	64,48	Sill
531	0,02	566242	8833481	772	539,04	542,42	3,38	Sill
535	0,05	566294	8833108	925	519,39	547,88	28,49	Sill
536	0,03	566079	8832899	1116	485,33	515,81	30,47	Sill
537	0,01	566770	8832858	336	523,35	528,25	4,90	Sill
538	0,12	571503	8832342	1818	335,03	395,31	60,28	Sill
539	0,01	562594	8832466	1798	176,59	207,43	30,84	Sill
540	0,02	570783	8832147	746	391,35	410,67	19,31	Sill
541	0,84	562812	8830809	11322	320,29	490,25	169,96	Sill
542	0,01	562174	8831612	1296	209,60	215,50	5,90	Sill
543	0,04	563403	8831565	2759	285,42	356,21	70,78	Sill
544	0,01	571876	8831533	582	362,77	384,90	22,13	Sill
545	0,01	562425	8831462	363	338,92	355,41	16,49	Sill
546	0,1	572146	8831056	1668	328,20	395,81	67,61	Sill
548	0,06	562305	8830151	5022	257,13	355,30	98,18	Sill
550	0,01	571116	8831056	709	441,03	447,76	6,73	Sill
551	0,2	563368	8830621	2425	346,34	420,09	73,75	Sill
552	0,02	571649	8830976	903	394,21	429,08	34,88	Sill
553	0,07	565280	8830723	2366	453,28	486,45	33,17	Sill
556	0,04	570521	8830697	1578	456,84	505,78	48,94	Sill
557	0,04	564119	8830300	753	346,93	403,18	56,25	Sill
558	0,01	562178	8829131	451	235,68	255,95	20,27	Sill
559	0,02	562707	8829022	660	399,04	454,09	55,05	Sill
560	2,12	562706	8823153	19308	112,15	257,24	145,09	Sill
561	0,02	562696	8828070	980	517,70	526,27	8,58	Sill
562	0,71	563400	8824790	14154	308,26	524,22	215,96	Sill
563	0,01	572225	8827120	1216	221,64	246,64	25,00	Sill
564	0,03	571592	8825871	3010	274,02	335,93	61,91	Sill
565	0,01	570863	8826074	375	372,02	385,95	13,93	Sill
566	0,5	569801	8825587	5925	400,76	467,91	67,15	Sill
567	0,1	565453	8825144	2010	403,33	449,87	46,54	Sill
568	0,01	571042	8825231	670	293,62	294,80	1,18	Sill
569	0,1	565387	8824777	3273	352,53	421,71	69,18	Sill
570	0,13	570231	8824556	6338	178,47	253,58	75,11	Sill
571	0,23	554395	8822737	7509	536,38	702,94	166,56	Sill
573	0,37	554893	8823001	4961	531,44	642,46	111,02	Sill

Intrusion ID	Area [km2]	Easting	Northing	Length exposed [m]	Elevation Base [m]	Elevation Top [m]	Max Thickness [m]	Dyke/Sill
574	0,03	568834	8823541	1370	169,13	184,80	15,67	Sill
575	0,12	568364	8823005	2161	168,08	178,95	10,87	Sill
576	0,23	561742	8821084	5149	8,25	58,29	50,03	Sill
577	0,23	566803	8822303	6391	161,64	214,52	52,88	Sill
578	0,83	555012	8820742	5949	626,16	735,04	108,88	Sill
579	0,57	566325	8820521	5103	242,21	311,29	69,08	Sill
581	0,01	574853	8820467	496	380,64	423,27	42,64	Sill
582	0,27	576638	8820000	2808	339,80	434,05	94,26	Sill
583	6,21	563011	8817023	27316	7,69	309,32	301,64	Sill
584	0,96	577919	8818745	7755	275,37	444,48	169,11	Sill
585	0,03	575264	8820048	880	292,38	355,43	63,05	Sill
587	0,03	565522	8819585	736	195,96	218,18	22,21	Sill
590	0,8	554738	8818383	10228	618,23	748,90	130,66	Sill
593	0,01	565110	8818807	482	142,83	187,90	45,07	Sill
594	0,39	565362	8817380	7763	173,91	321,44	147,53	Sill
595	0,03	575694	8817785	875	378,77	408,72	29,95	Sill
597	0,29	576912	8817196	3299	303,58	407,04	103,46	Sill
599	0,09	576009	8817253	1502	290,15	354,89	64,74	Sill
601	1,66	552238	8815587	13997	665,92	784,01	118,09	Sill
602	0,02	553627	8816977	994	606,00	669,61	63,61	Sill
604	0,05	564700	8816195	992	201,01	230,19	29,18	Sill
605	0,01	576808	8815704	897	226,82	235,01	8,18	Sill
606	0,37	563990	8815157	3890	196,91	434,65	237,74	Sill
607	0,02	553573	8815624	757	656,05	712,93	56,88	Sill
608	0,08	562327	8815303	2207	97,91	114,89	16,98	Sill
610	0,01	563772	8815216	727	319,02	320,41	1,39	Sill
611	0,1	563366	8813736	2294	362,28	471,94	109,66	Sill
612	0,03	575132	8814111	691	279,28	311,61	32,34	Sill
613	0,11	575815	8813674	1430	260,76	318,81	58,05	Sill
614	0,07	574520	8813275	1919	419,34	484,14	64,80	Sill
615	0,11	563850	8813097	1388	451,59	476,09	24,50	Sill
618	0,02	577631	8812539	1048	284,99	323,26	38,27	Sill
619	0,05	560648	8811308	2628	275,77	337,47	61,70	Sill
620	0,16	574159	8811501	2067	498,67	540,15	41,47	Sill
621	0,02	574577	8811650	749	504,75	520,87	16,12	Sill
622	0,08	578726	8811190	2141	218,09	254,90	36,81	Sill
629	0,02	560072	8810488	1254	280,24	327,10	46,86	Sill

Intrusion ID	Area [km2]	Easting	Northing	Length exposed [m]	Elevation Base [m]	Elevation Top [m]	Max Thickness [m]	Dyke/Sill
630	0,01	560768	8810544	371	553,79	572,51	18,72	Sill
632	0,02	578749	8810426	644	201,74	241,97	40,23	Sill
636	0,13	578614	8809792	1679	137,94	246,82	108,88	Sill
640	0,09	560062	8809082	4018	559,63	605,63	46,00	Sill
641	0,54	557018	8809560	5029	364,73	526,20	161,47	Sill
643	0,02	575302	8809528	797	298,18	327,85	29,67	Sill
644	0,01	575652	8809602	451	375,81	381,65	5,84	Sill
650	0,02	574239	8809276	623	324,00	348,39	24,39	Sill
651	0,04	576945	8809068	1210	336,18	388,25	52,07	Sill
652	0,01	574356	8809143	485	316,42	349,04	32,62	Sill
653	0,02	576000	8809122	583	360,36	367,86	7,51	Sill
655	0,05	574549	8808961	939	275,30	345,87	70,56	Sill
656	0,07	578290	8808909	1529	180,59	252,30	71,71	Sill
657	0,1	557051	8808153	6129	353,85	488,62	134,77	Sill
658	0,01	556298	8808745	1256	493,93	511,78	17,85	Sill
659	0,04	576539	8808777	904	317,56	344,42	26,86	Sill
661	0,21	577477	8808468	3115	240,30	292,85	52,55	Sill
662	0,12	578161	8808542	1947	203,24	247,08	43,84	Sill
663	0,02	560825	8808482	758	583,08	592,53	9,45	Sill
664	0,01	556266	8808226	683	511,43	523,56	12,13	Sill
665	0,15	574763	8807960	2132	251,67	375,58	123,91	Sill
667	0,34	559127	8807502	4460	455,37	544,79	89,43	Sill
668	0,03	575180	8807854	693	241,12	310,27	69,15	Sill
669	0,04	559632	8807782	1239	488,29	539,66	51,37	Sill
671	0,02	575492	8807667	635	255,03	306,32	51,29	Sill
672	0,01	575781	8807480	515	253,18	269,30	16,11	Sill
673	0,16	576197	8807274	2954	200,15	373,40	173,25	Sill
674	0,04	556390	8807004	2468	471,72	540,14	68,42	Sill
675	0,07	559568	8807209	1353	523,42	553,79	30,37	Sill
676	0,06	576922	8806957	1288	177,85	256,49	78,64	Sill
677	0,05	576375	8806953	1309	287,21	330,53	43,33	Sill
678	0,02	575949	8806932	635	365,88	376,07	10,19	Sill
679	0,2	576544	8806608	5030	175,39	387,94	212,56	Sill
680	0,04	577308	8806482	972	158,41	201,52	43,11	Sill
681	0,02	577079	8806523	562	212,62	229,75	17,14	Sill
683	0,14	577636	8806299	2092	138,04	197,53	59,49	Sill
687	0,19	577079	8805757	3921	194,58	248,19	53,61	Sill

Intrusion ID	Area [km2]	Easting	Northing	Length exposed [m]	Elevation Base [m]	Elevation Top [m]	Max Thickness [m]	Dyke/Sill
689	0,27	577673	8805499	4072	131,19	191,02	59,83	Sill
691	0,01	557951	8805801	430	521,52	536,73	15,21	Sill
693	0,04	569695	8805543	2003	492,33	541,93	49,60	Sill
694	0,01	557871	8805457	298	544,42	548,06	3,64	Sill
695	0,04	556043	8805214	1224	479,61	542,60	62,98	Sill
696	0,03	557791	8805064	971	550,54	577,33	26,80	Sill
697	0,02	570379	8805118	985	477,01	529,09	52,08	Sill
698	0,06	555797	8804715	1126	536,32	607,81	71,49	Sill
699	0,07	557481	8804007	1536	594,38	628,73	34,35	Sill
703	0,33	571769	8803308	3714	399,94	474,25	74,31	Sill
705	0,01	565376	8803554	637	595,80	619,73	23,93	Sill
706	0,01	557643	8803420	574	634,75	641,21	6,46	Sill
707	0,03	557987	8803176	898	665,45	678,98	13,54	Sill
709	0,06	558336	8803136	1236	686,41	733,83	47,42	Sill
710	0,04	565895	8803081	1299	557,97	599,04	41,07	Sill
711	0,04	566273	8802722	968	516,02	587,12	71,10	Sill
716	0,33	564492	8801176	5109	719,74	783,25	63,51	Sill
719	0,09	564012	8799829	1599	725,61	766,95	41,34	Sill
720	0,01	591290	8799659	471	0,00	8,00	8,00	Sill
721	0,02	563346	8799183	650	735,27	756,03	20,75	Sill
722	2,98	592450	8798375	10672	0,00	87,79	87,79	Sill
723	0,07	578200	8798592	1474	279,06	324,41	45,35	Sill
724	0,01	578698	8798523	481	283,28	292,91	9,63	Sill
725	0,02	562753	8798398	625	718,03	740,43	22,40	Sill
726	0,01	577533	8798359	982	322,23	355,24	33,00	Sill
727	0,01	577087	8798087	505	404,12	426,29	22,17	Sill
728	0,89	561265	8797499	7744	745,48	832,21	86,73	Sill
729	0,11	571313	8796875	1451	523,48	559,35	35,88	Sill
731	0,03	560200	8796782	1131	720,24	818,20	97,96	Sill
732	0,02	560460	8796525	675	718,22	810,23	92,01	Sill
735	0,02	560768	8796229	582	709,94	799,09	89,15	Sill
736	0,72	560104	8795615	9099	698,97	854,90	155,93	Sill
737	0,35	559159	8794437	3155	695,66	834,04	138,38	Sill
739	0,04	558479	8794292	892	841,06	851,33	10,27	Sill
740	0,07	558730	8794052	1063	783,16	828,96	45,81	Sill
741	0,4	557785	8793282	3158	765,75	845,40	79,66	Sill
742	0,12	563779	8792259	1721	689,13	749,72	60,59	Sill

Intrusion ID	Area [km2]	Easting	Northing	Length exposed [m]	Elevation Base [m]	Elevation Top [m]	Max Thickness [m]	Dyke/Sill
743	0,11	562378	8791934	2313	570,26	659,34	89,08	Sill
746	0,02	564987	8791411	668	724,15	739,33	15,18	Sill
747	0,07	566853	8787513	1716	767,22	853,09	85,87	Sill
748	0,07	568189	8783180	1336	831,02	889,47	58,45	Sill
749	0,29	587860	8782634	3522	364,38	497,65	133,27	Sill
750	0,02	565539	8782090	545	781,40	811,19	29,79	Sill
751	1,06	566833	8781255	6043	752,14	830,93	78,79	Sill
752	0,09	587627	8781541	1155	279,96	397,73	117,77	Sill
754	0,2	587484	8780654	3648	269,24	429,09	159,84	Sill
758	0,24	587671	8779543	3096	351,32	447,33	96,01	Sill
761	0,05	588301	8779321	1005	349,22	458,36	109,13	Sill
762	0,54	571100	8778700	3237	656,29	751,71	95,42	Sill
763	0,22	588699	8778490	2031	374,30	485,78	111,48	Sill
764	0,49	569630	8776636	7978	565,14	731,74	166,60	Sill
765	0,51	587702	8776815	5471	421,01	493,73	72,72	Sill
766	0,17	588141	8775941	1733	419,57	481,09	61,52	Sill
767	0,03	577615	8774454	803	800,12	824,54	24,42	Sill
768	0,89	588048	8772835	10768	316,50	523,52	207,02	Sill
769	0,03	577666	8773884	706	783,38	805,79	22,41	Sill
770	0,57	579167	8773417	4950	565,42	753,84	188,43	Sill
771	0,01	573230	8773478	1089	513,16	529,21	16,05	Sill
772	0,04	573657	8772975	1773	631,32	650,10	18,78	Sill
773	0,01	571992	8772917	1294	503,85	517,49	13,64	Sill
777	0,07	579275	8772270	1170	553,51	589,45	35,93	Sill
779	0,01	581284	8772356	578	623,00	650,94	27,94	Sill
780	0,03	579014	8772170	1399	597,02	710,75	113,74	Sill
781	0,07	580709	8771789	3562	615,40	679,32	63,91	Sill
782	0,03	581921	8771931	1597	570,00	618,07	48,07	Sill
783	0,52	581107	8770203	7931	527,37	702,22	174,86	Sill
785	0,01	580053	8769173	401	608,61	625,32	16,71	Sill
786	0,03	580048	8769096	943	634,55	727,54	93,00	Sill
787	0,04	579180	8768947	1243	745,68	774,55	28,87	Sill
788	0,1	580389	8768633	1876	611,65	691,95	80,30	Sill
789	0,01	578484	8768030	464	710,82	760,04	49,23	Sill
791	0,01	581988	8767853	434	713,40	739,62	26,23	Sill
792	0,01	579680	8767355	452	747,07	773,54	26,47	Sill
793	0,06	579753	8767046	1356	808,70	845,37	36,67	Sill

Intrusion ID	Area [km2]	Easting	Northing	Length exposed [m]	Elevation Base [m]	Elevation Top [m]	Max Thickness [m]	Dyke/Sill
794	0,03	579807	8766522	965	842,10	852,96	10,85	Sill
795	0,03	579078	8766457	1044	819,20	852,06	32,85	Sill
797	0,08	583517	8757064	1159	613,26	635,33	22,07	Sill
798	0,01	583606	8756696	567	631,63	635,84	4,21	Sill
799	0,01	560285	8790165	436	698,18	705,76	7,59	Sill
800	0,3	621229	8852819	3656	303,25	350,75	47,50	Sill
801	4,8	618153	8851497	11339	240,69	363,00	122,31	Sill
802	1,01	624360	8851893	3819	303,75	354,94	51,19	Sill
804	3,41	595224	8849954	18085	0,00	25,00	25,00	Sill
809	0,34	593911	8849116	3978	0,00	12,81	12,81	Sill
810	0,33	614377	8848816	2797	347,00	354,00	7,00	Sill
811	0,35	612888	8848329	2904	280,69	317,00	36,31	Sill
812	0,73	612901	8845332	4169	275,94	341,19	65,25	Sill
813	0,45	616947	8844131	4407	200,94	244,56	43,63	Sill
815	0,01	617783	8844138	350	217,44	224,31	6,88	Sill
816	1,46	603781	8843086	7689	211,91	264,72	52,81	Sill
817	0,66	599423	8843155	3130	203,84	268,92	65,08	Sill
818	8,74	595634	8840924	16206	135,84	255,48	119,63	Sill
819	0,57	599489	8841437	3583	250,85	284,38	33,53	Sill
821	1,76	599584	8839185	7295	244,57	292,98	48,41	Sill
822	2,96	611814	8837482	6775	170,28	339,42	169,14	Sill
823	1,99	600546	8835966	9205	221,60	309,17	87,57	Sill
824	0,4	624106	8835221	2877	190,31	308,00	117,69	Sill
825	0,01	610688	8835143	387	277,70	292,31	14,61	Sill
826	0,3	622936	8834546	2799	247,31	345,75	98,44	Sill
827	4,37	599107	8833655	14966	134,12	254,21	120,09	Sill
828	0,01	610913	8834840	539	282,28	290,11	7,83	Sill
829	0,01	611082	8834675	361	256,72	280,75	24,03	Sill
831	0,01	622477	8834489	316	267,80	284,34	16,54	Sill
832	0,01	601353	8834456	464	236,39	240,46	4,08	Sill
833	0,32	611604	8833896	3384	170,15	321,47	151,32	Sill
834	0,01	632629	8834295	349	302,31	306,56	4,25	Sill
835	0,28	632544	8833955	2458	284,25	318,94	34,69	Sill
838	0,05	600996	8833614	1428	187,36	204,81	17,45	Sill
839	1,82	602013	8829612	14497	5,27	244,22	238,95	Sill
840	1,7	617147	8830733	5508	228,38	310,94	82,56	Sill
841	1,28	616107	8829461	8755	157,38	237,16	79,79	Sill

Intrusion ID	Area [km2]	Easting	Northing	Length exposed [m]	Elevation Base [m]	Elevation Top [m]	Max Thickness [m]	Dyke/Sill
842	0,16	615592	8828610	4202	201,51	234,90	33,39	Sill
843	0,6	614700	8827461	11410	117,20	271,86	154,66	Sill
844	0,05	615971	8828263	1295	256,80	269,41	12,61	Sill
845	0,01	616292	8827893	516	258,91	267,06	8,15	Sill
846	0,15	604459	8827243	2125	91,28	124,83	33,55	Sill
847	0,01	616176	8827318	686	254,97	260,37	5,40	Sill
848	0,45	615981	8826461	5376	92,22	280,58	188,36	Sill
849	1,53	606176	8826009	14898	21,64	270,78	249,15	Sill
850	2,87	637631	8825422	10965	164,50	254,00	89,50	Sill
851	0,22	617033	8825727	3492	215,85	264,01	48,16	Sill
853	0,07	616929	8825287	2880	162,10	194,16	32,06	Sill
854	0,4	609158	8824562	6688	7,49	144,92	137,43	Sill
855	0,01	617209	8823621	363	42,63	47,99	5,36	Sill
856	0,01	617486	8823440	645	71,88	77,21	5,33	Sill
857	0,18	618392	8822428	3446	98,65	185,21	86,56	Sill
858	4,06	593461	8821290	16682	0,00	48,29	48,29	Sill
859	0,25	621585	8817773	2731	179,19	205,13	25,94	Sill
860	0,15	622608	8817204	3517	104,50	207,50	103,00	Sill
861	0,02	621030	8816695	1320	56,00	92,81	36,81	Sill
862	0,02	621150	8816626	1301	43,06	51,94	8,88	Sill
863	0,15	620167	8816476	4900	19,00	66,00	47,00	Sill
865	0,86	615719	8813931	7520	0,00	26,05	26,05	Sill
867	0,14	619004	8811833	1597	0,00	9,54	9,54	Sill
868	1,22	597664	8806921	6424	0,00	42,49	42,49	Sill
869	0,01	601748	8806715	376	0,53	6,91	6,38	Sill
870	0,01	621852	8853794	823	294,13	303,44	9,31	Sill
871	0,4	626514	8811580	4615	0,00	41,33	41,33	Sill
872	16,58	600395	8814541	116178	0,00	188,57	188,57	Sill
873	0,04	624272	8817215	1089	146,75	165,69	18,94	Sill
874	1,04	625214	8817371	12270	42,44	186,00	143,56	Sill
875	2,2	626191	8809333	13068	0,00	39,97	39,97	Sill
876	0,24	595154	8807397	2760	0,00	36,20	36,20	Sill
877	0,43	592458	8808764	2875	0,00	40,99	40,99	Sill
878	0,37	593947	8809382	3059	0,00	25,34	25,34	Sill
879	0,01	593580	8809822	411	0,24	2,04	1,80	Sill
881	0,19	592704	8807801	2497	0,67	11,55	10,88	Sill
882	0,6	586101	8808751	3839	0,00	21,79	21,79	Sill

Intrusion ID	Area [km2]	Easting	Northing	Length exposed [m]	Elevation Base [m]	Elevation Top [m]	Max Thickness [m]	Dyke/Sill
883	0,91	586592	8837293	4705	0,00	87,84	87,84	Sill
884	1,8	635430	8826529	7393	146,25	258,00	111,75	Sill
885	0,12	636368	8824670	2072	97,50	153,75	56,25	Sill
886	0,91	636339	8822189	4099	64,25	141,00	76,75	Sill
887	0,33	639198	8824353	2191	108,25	202,38	94,13	Sill
888	1,27	607047	8802508	9785	0,00	33,21	33,21	Sill
889	15,46	604307	8803579	57616	0,00	74,45	74,45	Sill